UNIVERSIDAD COMPLUTENSE DE MADRID

FACULTAD DE CIENCIAS FÍSICAS
Departamento de Física de la Tierra, Astronomía y Astrofísica I
(Geofísica y Meteorología) (Astronomía y Geodesia)

TESIS DOCTORAL

Afternoon and evening transitions in the atmospheric boundary layer: observational and numerical analysis

Análisis observacional y numérico de las transiciones vespertinas en la capa límite atmosférica

MEMORIA PARA OPTAR AL GRADO DE DOCTOR

PRESENTADA POR

Mariano Sastre Marugán

Director
Carlos Yagüe Anguís

Madrid, 2016

Universidad Complutense de Madrid

Facultad de Ciencias Físicas

Departamento de Física de la Tierra, Astronomía y Astrofísica I

(Geofísica y Meteorología)

AFTERNOON AND EVENING TRANSITIONS IN THE ATMOSPHERIC BOUNDARY LAYER: OBSERVATIONAL AND NUMERICAL ANALYSIS

ANÁLISIS OBSERVACIONAL Y NUMÉRICO DE LAS TRANSICIONES VESPERTINAS EN LA CAPA LÍMITE ATMOSFÉRICA

Memoria para optar al grado de Doctor presentada por

Mariano Sastre Marugán

Director: Carlos Yagüe Anguís

Madrid, 2015

Este trabajo ha sido financiado por una beca para la formación de personal investigador de la Universidad Complutense de Madrid (Becas Complutense predoctorales en España, código BE45/10; Estancias breves, código EB47/11), así como por un contrato asociado al proyecto de investigación CGL2012-37416-C04-02 del Plan Nacional del Ministerio de Economía y Competitividad (Gobierno de España). Además, parte de las actividades relacionadas con esta tesis han recibido apoyo económico directo de los proyectos nacionales CGL2009-12797-C03-03 y CGL2011-13477-E, el grupo de Micrometeorología y Variabilidad Climática de la Universidad Complutense (Santander-UCM; referencias GR35/10-A y GR3/14) y la Universidad Paul Sabatier (Francia). Parte de las simulaciones de este trabajo se llevaron a cabo en EOLO, el clúster científico de alto rendimiento para computación científica del Campus de Excelencia Internacional de Moncloa (Cambio Global y Nuevas Energías), financiado por el Gobierno de España. Una etapa inicial del periodo predoctoral fue financiada a través de una ayuda para formación de personal investigador del CIEMAT. La campaña BLLAST fue posible gracias a la contribución y financiación de varias instituciones, así como la participación de todos los grupos de investigación que estuvieron involucrados.

This work has been funded through a research fellowship FPI-UCM (BE45/10 and EB47/11), as well as a contract associated to project CGL2012-37416-C04-02 (Spanish Government). Additional financial support for some of the activities related to this PhD was directly obtained from national research projects CGL2009-12797-C03-03 and CGL2011-13477-E, the research group *Micrometeorología y Variabilidad Climática* (Santander-UCM; references GR35/10-A y GR3/14) and *Université Paul Sabatier* (France). Part of the computations of this work were performed in EOLO, the HPC of Climate Change of the International Campus of Excellence of Moncloa, funded by the Spanish Government. Initial predoctoral financial support was provided by a CIEMAT grant. BLLAST field experiment was made possible thanks to the contribution of several institutions and supports, as well as the participation of all the research groups involved.

A Nati

A Evi, Paco y Asunción

Agradecimientos

Es casi imposible poner por escrito tanto como quiero agradecer, así que quizá quede sólo en un esbozo. Disculpas de antemano por todo lo que quede en el tintero.

Primeramente, gracias a Carlos Yagüe, mi director. Por los conocimientos transmitidos, por el tiempo dedicado, por el espíritu crítico, por la confianza y apoyo, por las facilidades dadas. Aprecio mucho también que me hayas dado la posibilidad de introducirme en el ámbito de las medidas experimentales, y que siempre cuentes conmigo para los proyectos que surgen. Pero además, gracias por las buenas conversaciones, por transmitir optimismo y ver siempre el lado positivo en las dificultades. Es increíble la cantidad de cosas que se pueden aprender cerca de ti. Sencillamente, un lujo trabajar contigo.

Han sido muy importantes durante este tiempo los compañeros de Meteo, con todas las actividades compartidas y el día a día. Semanas de la ciencia, PIE, congresos, predicción TORREMETEO, o simplemente la reunión a la hora de comer. Gracias Elsa, Teresa, Cristina, Encarna. Gracias Belén por ser ejemplo en la lucha constante por dignificar la investigación, y por ver en cada situación una oportunidad en vez de un problema. Gracias, compañeros doctorandos. Los que ya terminasteis: Blanca, Álvaro, Marta Á., Marta M.; a los que aún os queda algún año más: Jesús, Rober, Julián; los que lleváis aquí menos tiempo: Ade, Antonio, Jon; a este último, junto con Zamo, gracias también porque con vuestros trabajos de máster aprendí enseñando. Y los que estáis ahora acabando casi al tiempo que yo: Íñigo, Cahlo, Jorge y Javi. Gracias por compartir no solo la llegada a meta, sino también el trayecto desde el principio. Además, Cahlo, tu ayuda, comentarios y sugerencias a este trabajo han supuesto siempre mejoras y por ello estoy muy agradecido. Gracias a las chicas de Geo: Beatriz, María, Izarra, Marta R., Diana; da gusto teneros por compañeras. También a Coumba e Ibrahima, visitantes muy queridos. Gracias al resto del departamento, a Salva y Lucía, tantas veces resolviendo problemas, y al equipo de dirección, tanto al actual como al anterior.

Recuerdo con cariño a los compañeros con los que compartí el edificio 23 del CIEMAT hace unos años: Paco, Alfonso, Arantxa, Pedro, Curro, José Luis, José Manuel, Beatriz, Juan Carlos, Lourdes, Begoña, Manolo, Esther, Alberto, Reinares y Fátima. Gracias a todos.

The BLLAST campaign meant a great opportunity to learn, begin collaborations with international research groups and meet wonderful people. I am very grateful to the BLLAST community. Marie, Fabienne and David are especially acknowledged. Thanks to the modelling group too.

Gracias a Javier Peláez y a José Luis Casanova por facilitar el acceso al CIBA y sus datos. Agradezco también la ayuda, en numerosos momentos del doctorado, de Samuel, Francisco Salamanca, Jorge Navarro y Goyo. Thanks Wayne Angevine also for self-spinup advice, and Jessica Busse for sending your PhD thesis to me.

My stay in Wageningen was a very nice period. Thank you very much, Gert-Jan, for the time you spent with me discussing there (and the collaboration afterwards), always pointing out good ideas, helping me to improve my work. Thanks Jordi for your tips, talks and meetings. I appreciated a lot the company of the PhD students, who shared both working hours and amusement time: Michał, Eduardo, Daniëlle, Joel, Marina, Natalie, Huug, Anneke, Ivar, Denica, Marie, Bram, Miranda and Henk. Thanks to all the other MAQ staff, especially to Oscar, Kees and Caroline. Thanks also to Anna, Nikos, Nick, Ioulia, Justine, Paula, Luis, Emilio, Enrique and Grego. Thank you all. You made me feel at home.

Gracias a mis amigos de Segovia: Javi, Charo, Juan, Chema, Bárbara, Isa, Carola, Etuka, Miriam, Sandra. Gracias a los demás amigos y compañeros de la facultad: Édgar, Rubén Pedro, Joserra, y tantos otros, incluidos los vinculados a EMOTAMZOR.

Gracias también a todo lector de esta tesis, porque los libros se escriben para ser leídos.

Y los más importantes: gracias a mi familia por vuestro cariño, apoyo y comprensión.

Contents

Summary

Introduction

This PhD thesis focuses on the study of the physical processes occurring in the atmospheric boundary layer (ABL) during the transition from a convective, well-mixed diurnal situation, to a nocturnal stable one: the afternoon and evening transition. This is a challenging topic mainly due to the confluence of weak and frequently opposite forcings. Furthermore, the micrometeorological conditions in this time frame may play a crucial role in diverse and relevant events, such as fog onset and growth, the development of frost or health hazards linked to air quality. For these reasons, the interest in this area of research is currently increasing, and field experiments are designed to better understand the afternoon and evening transition processes.

Objectives

Improving the understanding of the ABL afternoon and evening transition is the general objective of this thesis. This includes several sub-objectives:

- To characterize the phenomenology of the ABL afternoon and evening transition, identifying patterns in the typical events which occur during this period.
- To study the role of those characteristic events, elucidating their influence in the development of a stable nocturnal boundary layer.

- To deep into the evolution of the time and spatial scales involved along the afternoon and evening transition events.
- To find out the importance of different modelling aspects for this transition, in order to achieve a better understanding of them and to improve the performance of mesoscale numerical models during this time frame.
- To study the differences in the physical processes during the transition regarding the observational site and the season of the year.

Methodology

Two approaches are used in this thesis: study the transition through observations and considering numerical simulations from a meteorological mesoscale model.

On the one hand, the observational measurements were gathered at two experimental sites with different features, here referred as CIBA and BLLAST. The former is located in Spain, whereas the latter in France, and it is named after the field campaign which took place at that site in 2011. It is remarkable that the BLLAST site is significantly more heterogeneous and humid than the CIBA site.

The mathematical treatment of these data includes Reynolds decomposition of instantaneous measurements, obtaining an average value and turbulent perturbation. Next, eddy-covariance analysis with 5-minutes averaging is employed. Besides, two spectral techniques are applied to high resolution data: a Multi-Resolution Flux Decomposition (MRFD) to sonic anemometers measurements, and wavelet analysis to microbarometers data. Additionally, for part of the study the transitions with significant synoptic forcing are not considered in order to focus on the micrometeorological effects. Furthermore, local sunset is mostly used as the timing reference ($t = 0$ h) for easiness of comparison.

On the other hand, numerical simulations of the transition are performed with the Weather Research and Forecasting (WRF) model. This is a non-hydrostatic mesoscale model designed for both research and operational applications, which has been earlier employed to successfully simulate other phenomena, like radiation fog events, sea breezes or gravity waves. For this thesis, the Advanced Research WRF (ARW) core is used, working with version 3.4.1 or 3.5 depending on the experiment. Analogously, WRF is fed either with NCEP or ECMWF initial and boundary conditions.

Results

The principal findings of this thesis are structured in four groups of results:

- Observational characterization. This first approach is performed in two ways: on the one hand, characterizing individual case studies with sonic anemometer and microbarometers measurements (BLLAST), and on the other hand, doing a statistical analysis of a three-months dataset of continuous measurements (CIBA). Besides, the latter allows defining a classification of the transitions at CIBA in three different kinds, according to the values of wind speed, temperature inversion and turbulence threshold.
- Comparison BLLAST-CIBA. Measurements from these two locations over two months are considered for site-to-site comparison. The similarities and differences in the average evolution of atmospheric variables are addressed, as well as in wind distributions. Moreover, an experiment with WRF to test the influence of soil moisture on evening transitions is performed for an individual case from each site.
- WRF experiments. Three kinds of experiments are performed in order to investigate the model ability to represent the transitional processes:

i) to test the sensitivity of the model to the Planetary Boundary Layer (PBL) scheme and the Land Surface Model (LSM); ii) to study the influence of varying the number of domains and the domain size; iii) to study the effect of initializing soil temperature and moisture using a self-spinup method. For all these experiments, simulations are validated with observations from two transitions of the BLLAST field campaign.

- Seasonal comparison. Using measurements from six years at CIBA, differences and similarities in the transitional processes depending on the time of the year are studied. For this analysis, the particulate matter concentrations are also considered, linking their average evolution to atmospheric variables.

Conclusions

The main conclusions of this thesis are summarized as:

- During the transition, there is an average qualitative evolution of most of the ABL variables, regardless of the observational site.
- The main differences from one to another site involve absolute values, time lags and katabatic wind occurrence.
- Soil and air humidity affect decisively the whole transition, showing an important interaction with turbulence. This influence is particularly noticeable before sunset, and not only close to the ground, but also at upper levels.
- Turbulence developing at night corresponds to smaller time scales than afternoon turbulence.
- Along the transition, WRF simulations show more sensitivity to changes in the LSM scheme for a fixed PBL than opposite.

- Simulations with the combination of relatively simple PBL and LSM schemes in WRF globally provide good results, often closer to observations than other more sophisticated setups.
- Using one-domain simulations provides good results rather than increasing the number of nested domains for the afternoon and evening transition numerical experiments.
- On a seasonal basis, the specific humidity evolution is significantly more site-dependent than other variables, considering both the average evolution and its variability.

Resumen

Introducción

En esta tesis doctoral se estudian los procesos físicos que tienen lugar en la capa límite atmosférica (CLA) durante la transición desde una situación diurna, convectiva y bien mezclada, a una situación de estabilidad nocturna: la transición vespertina. Este tema supone un reto por tratarse de un periodo temporal en el que confluyen forzamientos débiles y habitualmente de signos opuestos. Las condiciones micrometerológicas durante dicha transición pueden influir de manera decisiva, entre otros procesos, sobre la formación y el desarrollo de nieblas, heladas o situaciones de alerta por contaminación atmosférica, hechos todos de gran relevancia. Por ello, esta área de investigación está ganando interés, diseñándose campañas experimentales de medidas para mejorar el conocimiento actual sobre los procesos de la transición vespertina.

Objetivos

Contribuir a mejorar el conocimiento de esta transición en la CLA es el objetivo fundamental de esta tesis. Esto incluye varios sub-objetivos:

- Caracterizar los fenómenos de la transición, identificando patrones en los eventos más relevantes que ocurren durante la misma.
- Estudiar el papel de dichos eventos y explicar su influencia en el posterior desarrollo de la capa límite estable nocturna.
- Profundizar en la evolución de escalas espaciales y temporales involucradas durante la transición vespertina.

- Investigar la importancia de diferentes aspectos de la modelización de esta transición, para así entenderlos mejor y proponer mejoras a la hora de simular la transición vespertina.
- Estudiar las diferencias en los procesos de transición vespertina según las características del sitio de observación, y también dependiendo de la estación del año.

Metodología

Se usan dos enfoques: observacional y mediante simulaciones numéricas. Las observaciones corresponden a dos localizaciones experimentales: CIBA (España) y BLLAST (Francia). Esta última es denominada así en la tesis debido a que ahí tuvo lugar una campaña homónima en el año 2011. La diferencia fundamental entre ambos sitios es que la zona de BLLAST es mucho más húmeda y heterogénea que CIBA.

El tratamiento matemático de estos datos incluye la descomposición de Reynolds, expresando las medidas instantáneas de una variable como suma de un valor medio y una perturbación. A continuación, se usa un análisis *eddy-covariance* con un promediado de 5 minutos. Además, se utilizan dos técnicas espectrales para el tratamiento de datos de alta resolución: la descomposición del flujo multi-resolución (datos de anemómetros sónicos), y el análisis *wavelet* (datos de microbarómetros). También, en parte del estudio no se consideran las transiciones con forzamiento sinóptico importante, para centrar la atención en los efectos micrometeorológicos. Y para facilitar la comparación entre días distintos se usa frecuentemente la hora de la puesta de sol como referencia temporal (t = 0 h).

Por otra parte, se simula la transición vespertina con WRF, un modelo meteorológico mesoescalar no hidrostático diseñado para uso tanto en investigación como operativo. WRF ha sido empleado anteriormente para simular fenómenos como nieblas de radiación, brisas marinas u ondas

de gravedad. En esta tesis se trabaja con el módulo de investigación WRF-ARW, particularmente con la versión 3.4.1 o 3.5, dependiendo del experimento. Como condiciones iniciales y de contorno se usan datos del reanálisis de NCEP o de ECMWF.

Resultados

Los resultados se presentan en cuatro grupos:

- Caracterización observacional. Este primer enfoque se desarrolla de dos formas: caracterización individual (casos de estudio) con medidas de anemómetros sónicos y microbarómetros (BLLAST), y análisis estadístico de una base de datos de tres meses de medidas de forma continuada (CIBA). Además, esto último permite realizar una clasificación de las transiciones en CIBA, definiendo tres categorías según los valores de viento, inversión de temperatura y umbrales de turbulencia alcanzados.
- Comparación BLLAST-CIBA. La comparación se realiza usando medidas experimentales de ambos sitios durante dos meses. Se muestran las diferencias y semejanzas en la evolución promedio de variables atmosféricas, y se analiza la distinta distribución de los vientos. También se evalúa la influencia de la humedad del suelo durante la transición mediante un experimento con WRF, usando un día de cada sitio experimental.
- Experimentos con WRF. Se realizan tres tipos de experimentos para investigar la capacidad del modelo para representar los procesos durante la transición: i) evaluar la sensibilidad del modelo a los esquemas de capa límite (*PBL*) y suelo (*LSM*); ii) estudiar la influencia de variar el número de dominios que se emplean en la simulación, y el tamaño de los mismos; iii) estudiar el efecto de inicializar la humedad y temperatura del suelo con un método de auto-inicialización. Estas

simulaciones son validadas con observaciones de dos transiciones correspondientes a la campaña BLLAST.

- Comparativa estacional. Con seis años consecutivos de medidas en CIBA, se estudian las diferencias y semejanzas en la transición vespertina según la época del año. Además, se considera la evolución promedio de la concentración de partículas y su relación con otras variables.

Conclusiones

Las principales conclusiones obtenidas se resumen en:

- La evolución cualitativa promedio de la mayoría de las variables de la ABL es independiente del sitio observacional.
- Las diferencias más relevantes entre un sitio y otro corresponden a valores absolutos, desfases temporales y frecuencia de vientos catabáticos.
- La humedad del suelo y del aire influyen de forma decisiva sobre toda la transición a través de su interacción con la turbulencia. Este efecto es más acusado antes de la puesta de sol, y se manifiesta no solo junto al suelo sino también en niveles superiores.
- La turbulencia que se desarrolla por la noche corresponde a escalas temporales menores que la de la tarde.
- Las simulaciones de WRF tienen mayor sensibilidad a cambios en el esquema de *LSM* que en el de *PBL*.
- Simulaciones de WRF usando una combinación relativamente sencilla de *LSM* y *PBL* proporcionan buenos resultados globales, con frecuencia más próximos a las observaciones que otras configuraciones más sofisticadas.

- Simulando la transición vespertina, usar un único dominio da mejores resultados que incrementar el número de dominios anidados.
- La evolución de la humedad específica del aire en las transiciones es más dependiente del sitio y de la estación del año que las demás variables atmosféricas estudiadas, tanto en evolución promedio como en variabilidad.

1. Introduction and objectives

1.1 The atmospheric boundary layer

An initial concept of boundary layer in a fluid flow is thought to have been introduced in the early 1870s by William Froude (1810–1879), while studying the frictional resistance of a thin flat plate when towed in still water. The term is found in the literature a few decades later in a study by Prandtl (1904), who showed that in a fluid flow with a solid body as an obstacle, two regions can be distinguished: a thin one close to the body, where friction plays a major role, and the remaining region where friction is neglectable (Sorbjan, 1989). Similarly, nowadays the boundary layer of a fluid is considered as the layer of fluid in the immediate vicinity of a bounding material surface, and where viscosity effects can be noticed. This means that the mentioned surface has an influence on the flow to modify its characteristic features. As a border region, abrupt changes in the fluid properties may take place here, being this fact mathematically represented by the boundary conditions associated to the equations which represent the flow. Considering the particular case of the terrestrial atmosphere, for such fluid it is the Earth's surface which acts as the bounding surface. Hence, the planetary or atmospheric boundary layer (ABL) can be seen as the bottom layer of the troposphere, directly influenced by the underlying surface. Actually, through the ABL take place the surface–atmosphere interactions, connecting a lot of biological, hydrologic, and atmospheric processes (Moene and van Dam, 2014). Above the ABL, the rest of the troposphere is called the free atmosphere, whose name reminds that it is not tied to the surface. Indeed, within the free atmosphere the effect of the

Earth's surface friction is negligible and the air can often be treated as an ideal fluid.

Several definitions of the ABL from different authors can be considered, all of which help to specify what the meaning of this Earth's surface influence is. Most of these definitions depend on which of the ABL features they focus on, e.g., the typical time scale (one hour or less) of response to a surface forcing (Stull, 1988), the surface influence on vertical profiles of temperature (André and Mahrt, 1982) or wind speed (Clarke, 1970), or the predominance of turbulence therein (Arya, 2001). An integration of these ABL definitions could be carried out by considering it as the region in which the wind, temperature, moisture and atmospheric constituents change from the large atmospheric scales to their conditions in the biosphere (Vilà-Guerau de Arellano et al., 2015). All these features are usually referred to the ABL over land, but a marine ABL can be also defined over water masses like a sea or an ocean, often requiring particular considerations, as for example in Carrillo et al. (2015). In this thesis, the studies are focused on the ABL over land.

Turbulence is very characteristic of the ABL (Wyngaard, 2010), and is directly related to non-linearity interactions. It can be pictured considering the chaotic and irregular motions of a fluid flow, whose high diffusivity favours the mixing of the flow properties, and involve a wide range of temporal and spatial scales (Nieuwstadt and Duynkerke, 1996). ABL turbulence can be classified in two categories, depending on its origin: mechanical (from shear production) and convective (from buoyancy production). On the one hand, mechanical turbulence results of an airflow over a surface with obstacles, and its intensity is determined by the surface roughness, the wind speed or the atmospheric stability (van de Boer, 2015). On the other hand, convective turbulence is due to radiative heating from the Earth's surface to the adjacent air parcels, which become lighter and consequently rise (thermals); oppositely, relatively cold and heavy air

sinks. The agents involved in a turbulent flow are swirls, named eddies, whose typical scales are very variable, from some millimetres to even a few kilometres (Garratt, 1992). The large eddies eventually break up, giving rise to smaller eddies. The former eddy's energy is divided into the latter smaller eddies that stemmed from it. This process, called inertial cascade, may actually occur to these smaller eddies, originating even smaller eddies, and so on, transferring energy from the large scales of the motion to smaller ones. However, there is a limit: when it is reached a sufficiently small length scale such that the viscosity of the fluid can effectively dissipate the kinetic energy into internal energy. All these processes describing turbulence were theoretically stated by Kolmogorov (1941a,b).

Another remarkable aspect of the ABL is that its height is significantly variable in time and space: it can range from tens of meters in strongly statically stable situations, to several kilometres (Kaimal and Finnigan, 1994) in convective conditions, especially over deserts (Holtslag and Boville, 1993). This is partly related to the eddies size. Furthermore, as calculating the ABL height can be done through different approaches (Vogelezang and Holtslag, 1996), choosing an appropriate one in each case is essential for accurate atmospheric modelling.

Many meteorological phenomena are very closely related to or occur within the ABL. To name some of them, cumulus and stratocumulus clouds (Angevine, 2008) can form within the top portion of a humid ABL; radiation fogs (Fitzjarrald and Lala, 1989) develop at the bottom of a stable boundary layer, where also gravity waves can be detected (Eymard and Weill, 1979; Román-Cascón et al., 2015a), sometimes interacting with turbulence (Román-Cascón et al., 2015b; Sun et al., 2015a,b). Moreover, magnitudes like energy, momentum or scalars (including mass, water vapour and aerosols) are exchanged between the ABL and the Earth's surface. This is directly linked to a significant fact: within the ABL take place a great amount of life-related processes and particularly it is where

human activities are most frequently developed. At least for this reason, it is worth studying the ABL structure and properties. A deeper comprehension of the mechanisms governing the physical processes in the ABL helps to improve life quality, by for example providing better forecasting conditions in numerical weather prediction (Baklanov et al., 2011) and climate modelling (Holtslag, 2006). This is important for aspects so diverse and relevant such as agricultural techniques optimization (Kelvin, 2011), the dispersion of pollutants (Seibert et al., 2000) or a safer aircraft landing and takeoff (Blay-Carreras, 2014). Related to the aviation activities, it is worth reminding the ABL importance, even for the characterization of events in which larger atmospheric scales may play a predominant role, such as an episode of great ash concentration in the atmosphere due to a volcanic eruption (Revuelta et al., 2012). For these situations, an accurate dynamic and thermodynamic representation of the ABL contributes to a better understanding and prediction of the local aerosol concentrations. Moreover, as many climate and weather prediction models do not represent boundary-layer processes realistically (Teixeira et al., 2008; Holtslag et al., 2013), they would greatly benefit from advances in ABL research. And additionally, enhancing our knowledge of the Earth's ABL would be indirectly helpful in other fields of research like aerosols characterization (Fernández-Gálvez et al., 2013) or planetary sciences, to improve the characterization of the ABL in other planets, for example, Mars (Martínez et al., 2009, 2011, 2013, 2014; Petrosyan et al., 2011).

1.2 Transitional processes in the ABL: the evening transition

With fair weather conditions (mainly associated to weak synoptic forcings) and over land, the ABL presents a very remarkable diurnal cycle (Figure 1.1). During daytime, a mixed layer of strong turbulence progressively grows in depth, capped by a statically stable entrainment

zone of intermittent turbulence: this is the convective ABL. Then, around sunset, turbulence decays leaving a residual layer in place of the convective mixed layer. At night, the bottom of the residual layer is transformed into a statically stable layer due to the contact with the radiatively cooled surface.

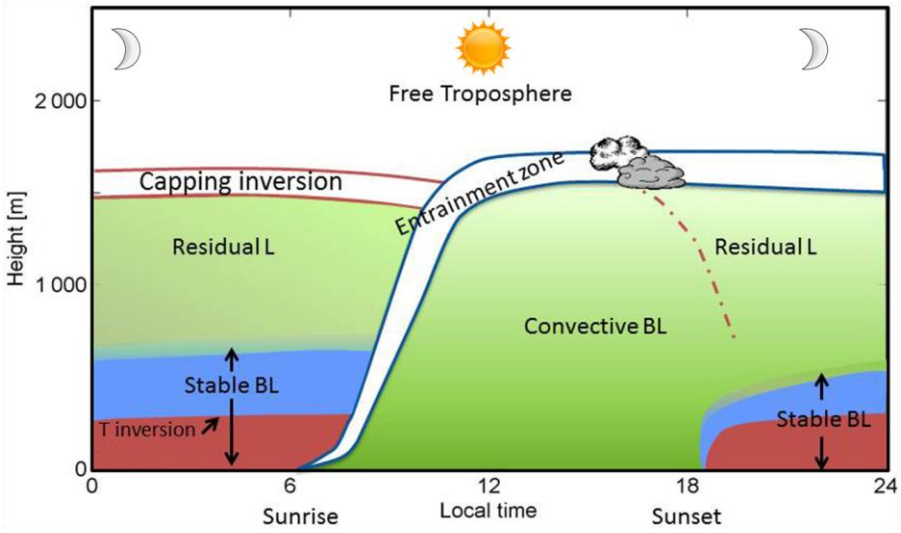

Figure 1.1. Schematic representation of the ABL diurnal cycle over land for a typical clear convective day. Adapted from Stull (1988) and Collaud Coen et al. (2014).

This is the stable ABL, typical of clear nights. Sometimes, over the residual layer, a capping inversion appears. So globally, the solar diurnal cycle is mainly controlling the evolution of the ABL physical properties, especially with weak synoptic forcing conditions, e.g. through the small-scale processes producing turbulence in the lower atmosphere. Some of these processes are not well understood, particularly when related to the transitions in the ABL. Actually, transitional boundary layers can be observed at very different locations which includes over land, along coastal regions, and beneath cloud boundaries (Angevine, 2008), being atmospheric turbulence common to all of them. Specifically, this thesis is focused on the phenomena occurring in the transition, over land, from the

daytime convective boundary layer to the nighttime stable boundary layer: the so-called afternoon or evening transition (Nadeau et al., 2011). Similarly as with its analogous the morning transition (Lenschow et al., 1979; Angevine et al., 2001; Lapworth, 2006, 2015), several key times are considered indicators of the evening transition: the astronomical sunset, the reversal of the surface heat flux, and the onset of a stable boundary layer. During the afternoon, the solar energy received at the Earth's surface starts to decrease, turbulence weakens and the afternoon transition starts (Sorbjan, 2007). This transition ends when the heat flux becomes negative (Nadeau et al., 2011). Acevedo and Fitzjarrald (2001) use the term early evening transition to study the period around sunset, when the residual layer of the ABL becomes decoupled from the surface layer, pointing out this decoupling is responsible for increases in the near-surface mixing ratio. For the evening transition, the definitions are usually linked to the onset of negative surface heat flux (Caughey et al., 1979; Beare et al., 2006). Nonetheless, it can be delimited according to wind speed deceleration and wind direction rotation (Mahrt, 1981). Lothon et al. (2014) consider that an appropriate definition for the evening transition is the period of time between the zero surface sensible heat flux and the establishment of the nocturnal stable layer, with quasi-steady depth.

1.3 Motivation and objectives

As it has been shown, the distinction between afternoon transition, early evening transition and evening transition may vary depending on the authors. In spite of those discrepancies, all the authors agree that these transitional processes around sunset play a substantial role in practical meteorological issues. There are studies where the relevance of the ABL evening transition is specifically revealed for the onset and growth of fog (Fitzjarrald and Lala, 1989; Román-Cascón et al., 2015c), the development of frost or freezing conditions (Bonin et al., 2013), the vertical transport of

tropospheric ozone (Klein et al., 2014) or the establishment of health hazards related to air quality (Pardyjak et al., 2009), to mention a few of them. Additionally, a better understanding of ABL afternoon and evening transition is important for model development and improving forecasts for several other applications, such as wind-energy production (Peña et al., 2015) or convective storm initiation (Lothon and Lenschow, 2010). In this thesis, the term most often employed will be the evening transition, but most of the characteristics associated to the afternoon transition are often included in the study as well.

Previous observational studies on the afternoon and evening transition focused on the surface buoyancy flux decrease (Grimsdell and Angevine, 2002) and the turbulent kinetic energy (TKE) decay (Grant, 1997), which begins in the vicinity of the boundary-layer top and eventually descends to near-surface levels (Darbieu et al., 2015). Furthermore, Blay-Carreras et al. (2014a) found a delay between the buoyancy flux crossover and the change in sign of the local gradient of the virtual potential temperature during the transition, concluding that this might be a site-dependent phenomenon. Continuing this study on countergradient heat fluxes, Jensen et al. (2015) compared observations at two sites with similar large-scale forcing, finding that the differing behaviour is primarily due to site-to-site subsurface thermal differences. On the other hand, the effect of the terrain has been investigated (Lapworth and Claxton, 2010), including for example, in the framework of the African Monsoon Multidisciplinary Analysis (AMMA) experiment, the study of soil humidity influence on both the surface fluxes and the entrainment on the top of the ABL in West Africa (Lothon el al., 2008; Lohou et al., 2010, 2014). Besides, Lapworth (2003) and Brazel et al. (2005) discussed the influence of surface cooling on the wind field along the transition. In this context, katabatic winds are found to play a role in the development of the stable boundary layer during the evening transition (Papadopoulos and Helmis, 1999). Additionally, the development of low-

level jets and wave-turbulence interactions (Sun et al., 2015b) may produce elevated turbulence during this time period, which is usually decoupled from the surface turbulence associated with wind shear (Viana et al., 2012; Mahrt, 2014). Thus, different atmospheric variables or events are employed in the study of the transition. Regarding the timing of the transition, there is not a systematic methodology but a few studies take sunset as their principal temporal reference (Busse and Knupp, 2012; Wingo and Knupp, 2015; Sandeep et al., 2015).

In this context, some research projects have included the understanding of these transitional processes among their objectives (LeMone et al., 2000; Doran et al., 2002; Poulos et al., 2002), and specific field experiments for afternoon and evening transitions have been conducted at various locations (Beyrich and Mengelkamp, 2006; Bonin et al., 2013; Fernando et al., 2013; Lothon et al., 2014).

Other approaches to the comprehension of the transitional ABL processes have been performed, including theoretical considerations (Fernando et al., 2004) eventually tested with experimental data too. In addition, attempts have been made to address this issue by means of numerical models, particularly large eddy simulations (LES): Nieuwstadt and Brost (1986) studied turbulence decay associated with a sudden cessation of the sensible heat flux, and Sorbjan (1997) presented results on how convective turbulence declines, showing that TKE decay is governed by two scales. More recently, Blay-Carreras et al. (2014b) analysed a case study, focusing on the residual layer and the presence of subsidence in the convective boundary-layer evolution. Using mixed-layer theory as well as LES, Pietersen et al. (2015) studied large-scale influence in the development of the convective boundary layer. Other works, like Edwards et al. (2014), addressed the effect of radiation at night and during the morning transition, and the evening transition modelling has been applied to theoretical and practical dispersion purposes too (Taylor et al., 2014).

Focusing on the exchange of species, both the morning and the evening transition are found to be relevant (Vilà-Guerau de Arellano et al., 2004; Casso-Torralba et al., 2008; Ouwersloot et al., 2012), but mesoscale numerical models fail to predict transition periods accurately (Lee et al. 2007). For example, Xie et al. (2013) found that latent heat flux was overestimated, whereas Svensson et al. (2011) showed that several models underestimated the wind speed decrease around sunset, as well as discrepancies with vertical temperature profiles observations during the transition. Globally, transition periods are replete with small space-time scale phenomena, like non-equilibrium turbulence, flow instabilities and gravity currents, so that their inclusion as subgrid phenomena is imperative if the transition predictions by mesoscale models are to be improved (Fernando et al., 2013).

Considering all these previous studies, there is a need for research combining experiments and numerical simulations in order to better model these transitional periods, to identify weaknesses, and to provide solutions thereto. This thesis tries to provide this two-way approach to the evening transition issue: observational and numerical. Then, the main objectives of the thesis are:

- To characterize the phenomenology of the atmospheric boundary layer evening transition, looking for patterns in the typical events which occur during this period and their timing.

- To study the role of those characteristic events, elucidating their influence in the development of a stable nocturnal boundary layer.

- To deep into the evolution of the time and spatial scales involved along the afternoon and evening transition events.

- To find out the importance of different modelling aspects for this transition, in order to collaborate to a better understanding of them and to improve the performance of mesoscale numerical models during this time frame.

- To study the differences in the physical processes during the transition regarding the observational site and the season of the year, including the relationships between the variables.

1.4 Thesis outline

The thesis is structured as follows. After the introduction in the current chapter, in Chapter 2 we discuss the two experimental sites whose measurements are used in the studies of this thesis. Field campaign and instrumentation details are also given. Afterwards, Chapter 3 focuses on the methods considered for the data treatment as well as details on the mesoscale meteorological model employed to perform the numerical simulations of this thesis. The next chapters correspond to the main results. In Chapter 4, some characteristic events of the evening transition are explained through case studies, as well as a statistical analysis. Results from a comparison of the evening transition at the two experimental sites are detailed in Chapter 5, including a couple of experiments with numerical simulations. The study with simulations is extended in Chapter 6, where experiments on different model settings are evaluated. Then, a seasonal analysis with an experimental dataset of six years is shown in Chapter 7. The differences and similarities in the transitional processes depending on the time of the year are studied, including the concentration of particulate matter. Finally, a summary of the thesis is presented in Chapter 8, showing

the main conclusions obtained, and with an outlook to future work and open lines of research.

2. Observations: experimental sites, data and field campaigns

Data employed for this thesis were gathered at two different observational sites. On the one hand, the Research Centre for the Lower Atmosphere, known by its Spanish acronym CIBA (Yagüe et al., 2009), and located in Valladolid (Spain). On the other hand, the Centre for Atmospheric Research (*Centre de Recherches Atmosphériques*, CRA), placed in the area of Lannemezan (France). The latter is actually the location of the Boundary Layer Late Afternoon and Sunset Turbulence (BLLAST) field campaign (Lothon et al., 2014). Henceforth, these two sites are referred as the CIBA site and the BLLAST site, respectively (Figure 2.1). Both of them are locations with permanent meteorological instrumentation deployed, and have hosted experimental field campaigns on boundary-layer meteorology related topics. In the current chapter, these sites are described focusing especially on the instrumentation and the data used for this thesis, providing also some results from the most recent experimental field campaigns.

Most of the contents of this chapter are based on these two publications:
- Yagüe, C., Sastre, M., Maqueda, G., Viana, S., Ramos, D. and Vindel, J. M.: CIBA2008, an experimental campaign on the atmospheric boundary layer: preliminary nocturnal results, *Física de la Tierra*, 21, 13–26, 2009.
- Lothon, M. and coauthors: The BLLAST field experiment: Boundary-Layer Late Afternoon and Sunset Turbulence, *Atmospheric Chemistry and Physics*, 14, 10931–10960, 2014.

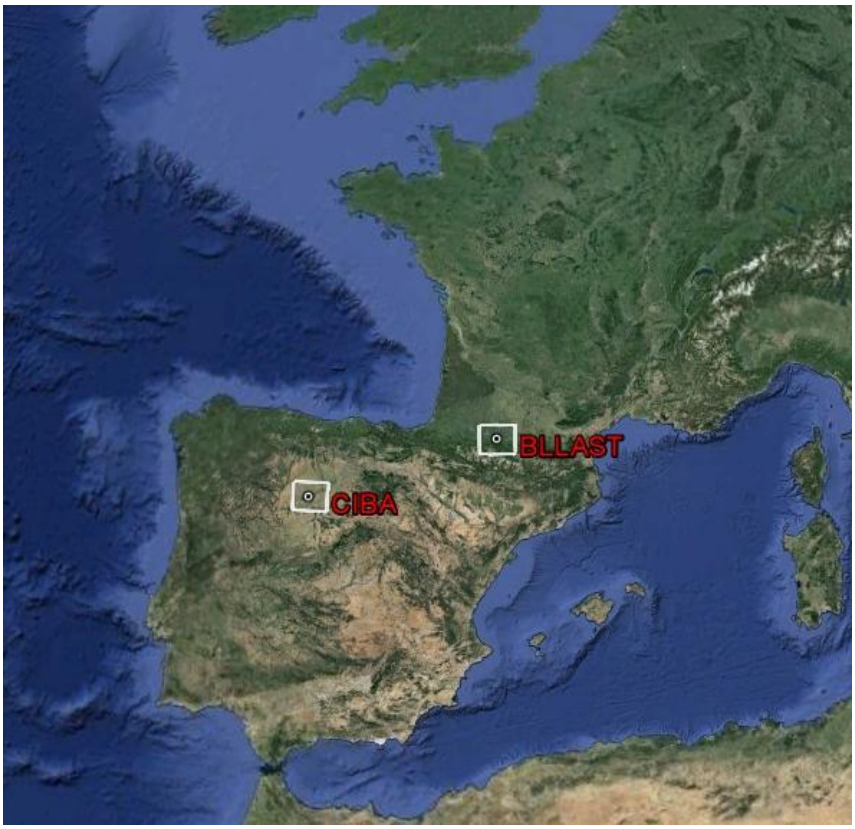

Figure 2.1. Location of the two experimental sites: CIBA and BLLAST. Adapted from Google Earth images.

2.1 CIBA site

The CIBA site (41º 49' N, 4º 56' W; 840 m above sea level, a.s.l.) is located in the northern Iberian plateau. There are four mountain systems that surround this plateau: Cantabrian Range (to the north), Iberian System (east), Central System (south) and Galician Massif (north-west), none being closer than 150 km. CIBA's location comprises a quite plain and homogeneous terrain (Figure 2.2). However, there are occasional gentle slopes (Cuxart et al., 2000; Yagüe et al., 2007), the most relevant one being from the north-east to the south-west direction (1:1660). Therefore, this is a preferred direction for katabatic events. This is usually a dry location

(435 mm year^{-1} as mean annual precipitation, according to Agencia Estatal de Meteorología and Instituto de Meteorologia, 2011), especially in summer, and the site is surrounded by crop fields and some pasture and shrub areas.

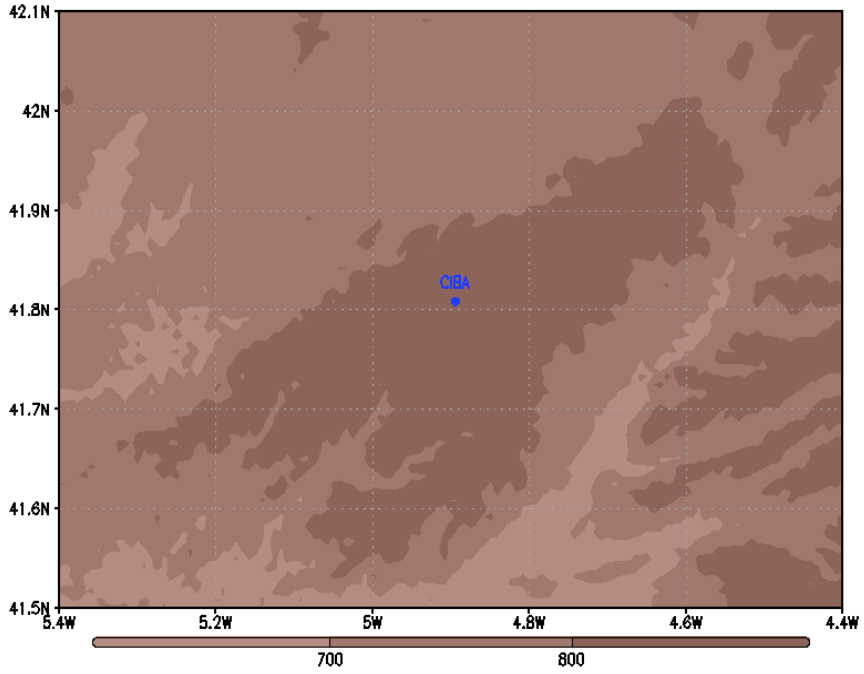

Figure 2.2. Terrain altitude of CIBA surroundings.

During the last two decades several field campaigns were conducted at CIBA, named SABLES98 (Cuxart et al., 2000), SABLES2006 (Yagüe et al., 2007), CIBA2008 (Yagüe et al., 2009). All of them were mainly focused on nocturnal and stable ABL. For this thesis, CIBA data from the period 2008-2013 are analysed, focusing especially on summer 2009. The permanent instrumentation set-up at CIBA has been regularly updated (Cuxart et al., 2000; Viana et al., 2009; Yagüe et al., 2009; Román-Cascón et al., 2015c). Measurements considered for this thesis mostly correspond to devices deployed in a 10-m meteorological mast:

- a sonic anemometer (METEK USA-1) at 10 m above ground level (a.g.l.), sampling with a very high temporal resolution (20 Hz)
- cup anemometers and vanes at 1.5 and 10 m a.g.l. (1 Hz)
- thermo-hygrometers at 1.5 and 10 m a.g.l. (1 Hz)

Additionally, a GRIMM 365 monitor at surface (around 1 m a.g.l.), registers particulate matter (PM) concentrations. It provides 1 data every 6 seconds. These measurements are based on an optical method, and classified according to the equivalent particle radius: smaller than 10 μm (PM10), 2.5 μm (PM2.5) and 1μm (PM1).

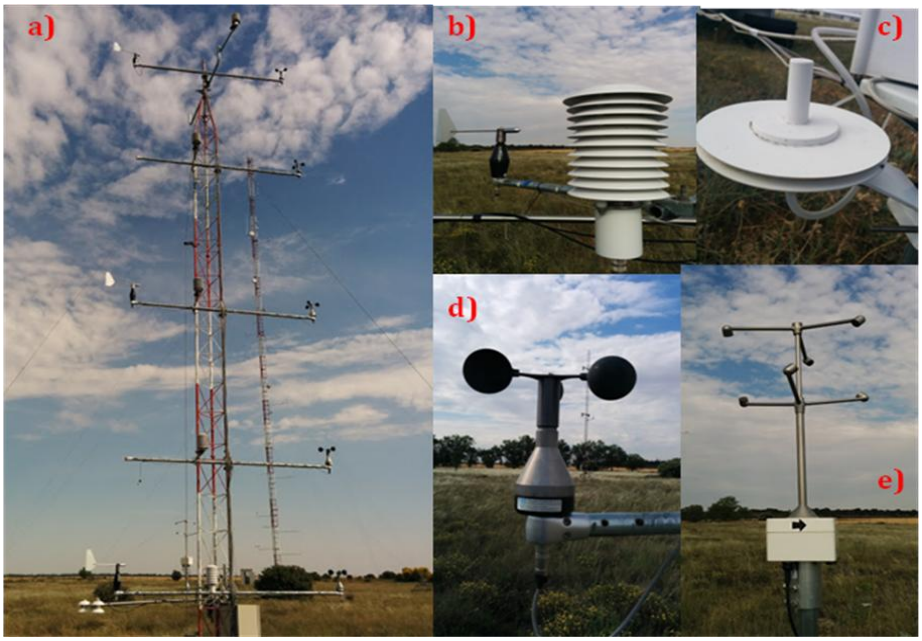

Figure 2.3. Some of the meteorological equipment at CIBA: a) instrumented 10-m mast (background: 100-m meteorological tower); b) thermo-hygrometer and vane; c) static pressure port, linked to one microbarometer in order to avoid contamination from wind speed; d) cup anemometer; e) sonic anemometer.

Data from other devices at different heights in the 10-m mast and from additional permanent instrumentation at CIBA are occasionally used as

complementary information. This includes, at surface, a RASS- SODAR and three microbarometers (PAROSCIENTIFIC) deployed at a nearly 200m side triangular array, as well as an equipped 100-m meteorological tower (San José et al., 1985; Yagüe and Cano, 1994), which has, among others, microbarometers at 3 levels (20, 50 and 100m). Pictures of some of these instruments are shown in Figure 2.3.

2.2 BLLAST site

The BLLAST site (43º 7' N, 0º 21' E; 600 m a.s.l.) is located on the Lannemezan plateau. This plateau, with an area of approximately 200 km^2, is a quite heterogeneous, and located a few kilometres north of the Pyrenees foothills, around 45 km away from the highest peaks in the Spanish border. The plateau has an average height of around 600 m a.s.l. (Figure 2.4).

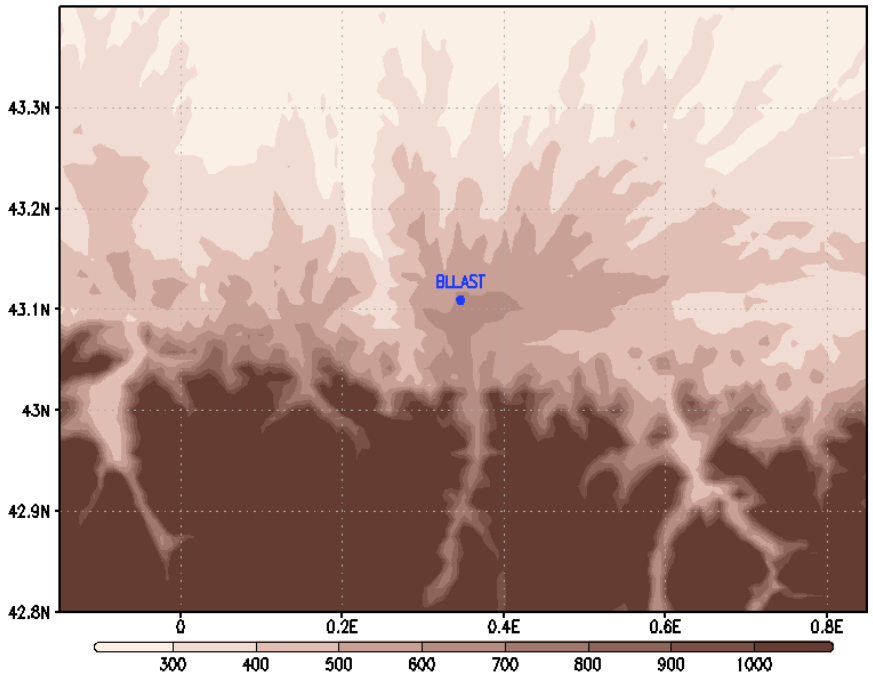

Figure 2.4. Terrain altitude of BLLAST surroundings.

The neighbouring surface is covered by considerably heterogeneous vegetation: grassland, meadows, crops, moor and forest; moreover, urban and industrial areas can be found in the surroundings as well (Figure 2.5).

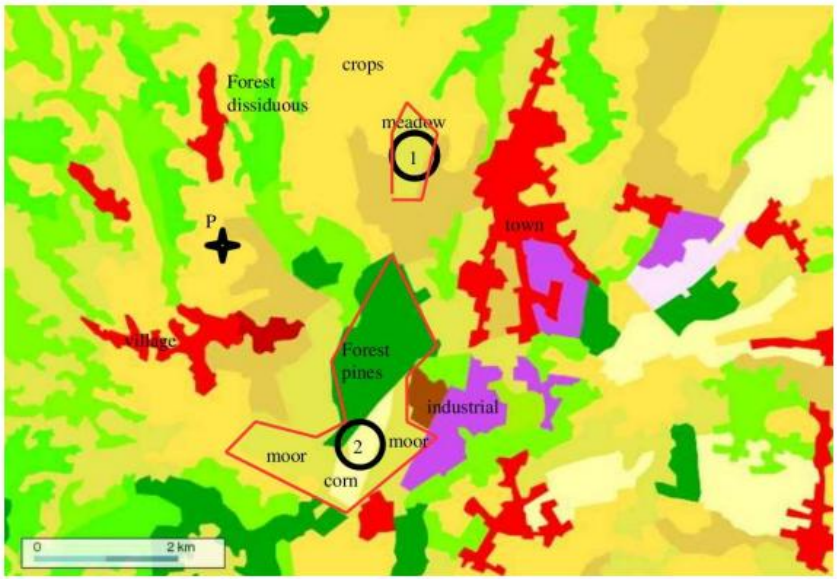

Figure 2.5. Land use of the BLLAST site and its surroundings, based on CORINE land cover. Super-sites are marked with circles and a cross. From: BLLAST experimental planning (courtesy of Marie Lothon).

The Boundary Layer Late Afternoon and Sunset Turbulence (BLLAST) field experiment (Lothon et al. 2014) took place from 14 June to 8 July 2011, with the participation of more than 20 research institutions from 9 different countries. The campaign was specifically designed for the study of the afternoon and evening transition, willing to obtain a wide set of reliable observations, to better understand the physical processes that control the transition, and to study its role on mesoscale and turbulent-scale motions. Moreover, during the field campaign innovative measurement systems were also tested, including new miniaturized sensors

and a new technique for frequent radiosoundings (Legain et al., 2013), and a flux-footprint model (van de Boer et al., 2013) was tested.

Three main areas, named as super-sites (Figure 2.5), were defined, each one focused on an objective for the transition: to analyse the vertical structure of the low troposphere; to study the effect of terrain heterogeneity; and to study the atmospheric circulations. Additional to the permanent instrumentation at the BLLAST site, a dense array of meteorological platforms was employed over different surface types: full-size aircrafts (Saïd et al., 2005; Gioli et al., 2006), remotely piloted aircrafts (Martin et al., 2011; Reuder et al., 2012), remote-sensing instruments, radiosoundings, tethered balloons (Canut et al., 2014), surface flux stations and various meteorological towers. A few pictures from the BLLAST campaign instrumentation can be found in Figure 2.6.

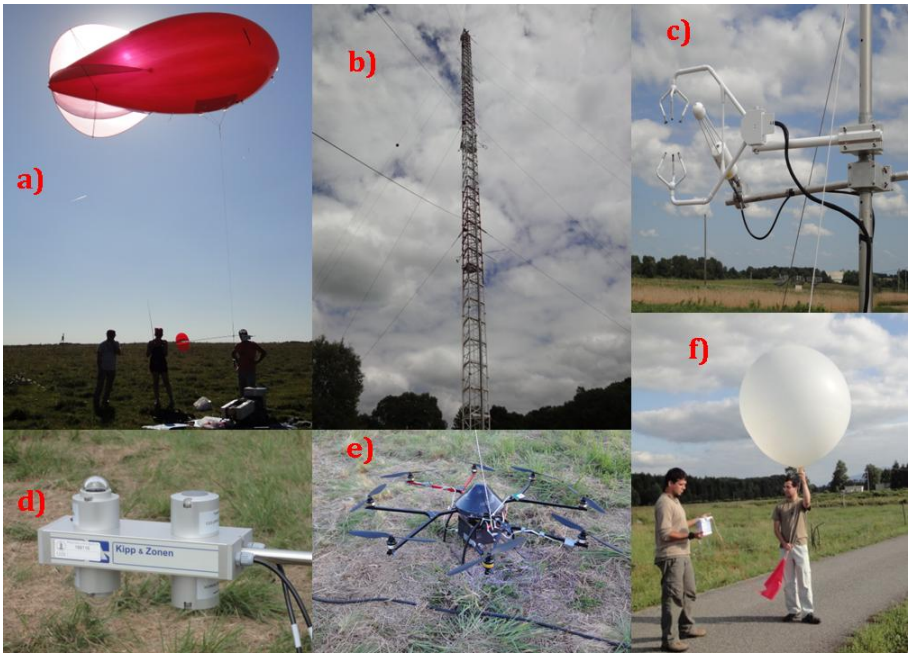

Figure 2.6. Some of the meteorological equipment at BLLAST: a) tethered balloon; b) 60-m instrumented tower; c) eddy correlation system (sonic anemometer and LICOR); d) radiometer; e) octocopter (remotely piloted aircraft); f) free radiosounding to be launched.

In particular, as one sub-objective of the BLLAST campaign was to study the influence of terrain heterogeneity, several sub-sites over various vegetation types, denoted as surface sub-sites, were instrumented with comparable devices with the aim of providing a thorough description of the surface fluxes (Table 2.1).

Table 2.1. Surface sub-sites instrumentation used.

Sub-site	Sampling frequency (Hz)	Height (m a.g.l)
Edge, wheat and grass sites	20	0.5 - 3
Microscale site	20	2
Moor site	20	2
Corn site	20	6
Forest site	10	22 - 30

In this thesis, data from the months of June and July 2011 are used, which correspond to the whole experimental field campaign plus several extra weeks, when some non-permanent instrumentation still stayed at the BLLAST site. Particularly, the data come from:

- 3 microbarometers (PAROSCIENTIFIC) deployed at surface (around 1 m a.g.l.) in a triangular structure with a separation of approximately 150 m, sampling at a rate of 2 Hz, which allowed a resolution of 0.002 hPa for the absolute pressure,
- a sonic anemometer (METEK USA-1, as in CIBA) on a small mast, at 2.4 m a.g.l., sampling at 20 Hz,

- cup anemometers, wind vanes and thermo-hygrometers (0.1 Hz) deployed at various levels (2, 15, 30 45, 60 m a.g.l.) in a 60-m tower,
- eddy-covariance devices from surface sub-sites (Table 2.1),
- free radiosoundings (MODEM and GRAW).

Globally, the ABL was probed with continuous observations, and in addition, intensive observational periods (IOPs) were designed for days with a common pattern of fair weather and lacking strong synoptic forcing. In these days, supplementary measurements from midday until sunset were performed. There was a total number of 12 IOPs during the field campaign (see Lothon et al., 2014 for further details on IOPs features).

Now, the main characteristics of IOP4 (24 June) and IOP5 (25 June) will be briefly explained, as data from these two IOPs will be used in the subsequent Chapter 4 and Chapter 6 of this thesis. Additionally, the characteristics for another day which was not IOP (29 June) will be explained too, as it is also analysed in Chapter 4. Regarding geopotential height in 500-hPa level (Figure 2.7), IOP4 was a day where a ridge over southwest Europe developed. That issue, together with the influence of a nearby high-pressure structure at surface, meant mainly stability. The clouds, present in the initial hours, moved to the east leaving mostly clear skies. Regarding the wind direction, a shift was observed, turning from east to south-west during the transition period. As in this case the next IOP was a consecutive day, IOP5 presented similar synoptic conditions, with a reinforced ridge in higher levels and a high pressure at surface over the BLLAST area (Figure 2.8). However, a significant difference was found, compared to IOP4: in IOP5 an intrusion of very warm air from higher tropospheric levels takes place, affecting the ABL growth and leaving its maximum around 600 m, significantly smaller than the value of the

previous day (1000 m). Moreover, the surface temperature values were affected, being this day the beginning of a heat wave.

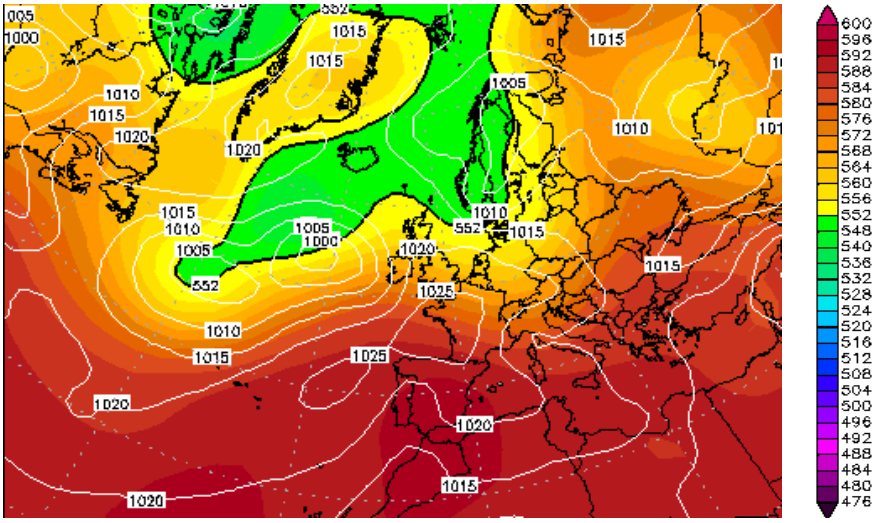

Figure 2.7. Synoptic situation for 24 June 2011 (12 UTC): geopotential height (gpdm) at the level of 500 hPa (contours) and pressure (hPa) at sea level (white lines). Obtained from www.wetterzentrale.de (NCEP reanalysis data).

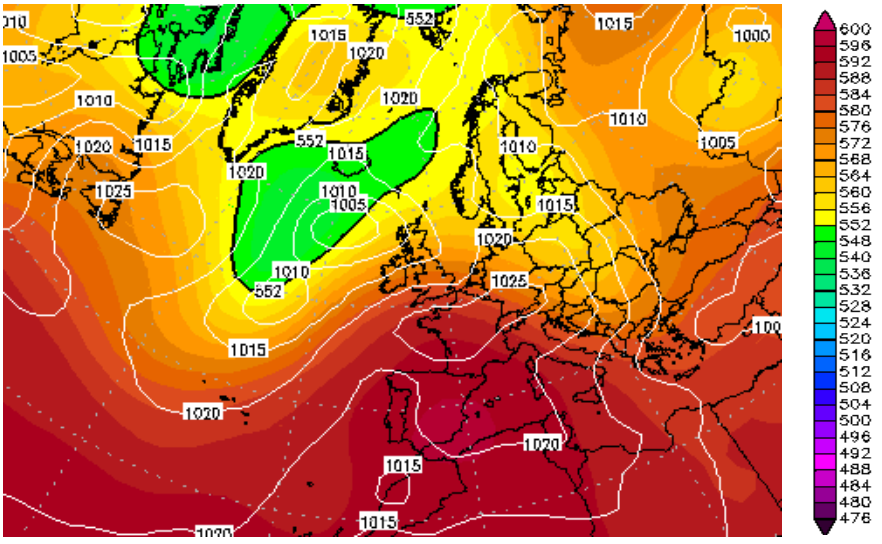

Figure 2.8. Same as Fig. 2.7 for 25 June 2011.

On the contrary, 29 June 2011 was not an IOP during the BLLAST campaign, as its synoptic situation was very different from the previous two days explained. It presented instability due to the influence of a trough in the geopotential height at the level of 500 hPa (Figure 2.9), and northerly wind was predominant. This synoptic situation led to a cloudy day with rainfall until around 16:00 UTC, which induced high relative humidity values near surface, even before sunset. This issue affected the processes of the evening transition, as will be exposed in Chapter 4.

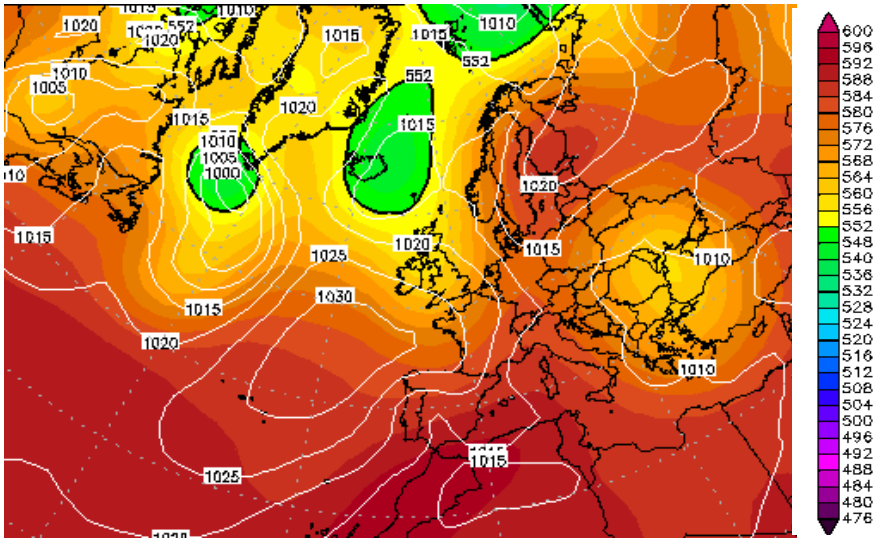

Figure 2.9. Same as Fig. 2.7 for 29 June 2011.

A wider description of the BLLAST project, with many details on the experimental field campaign, participants, data and other related issues can be found on the website: http://bllast.sedoo.fr/.

2.3 Summary of sites differences

There are several differences between these two experimental sites. First, the geographical situation: CIBA is farther south and at a higher

elevation than BLLAST, thus affecting the incoming radiation, which differs from one site to the other depending on the season. Moreover, since the BLLAST site is closer to the mountains, their influence on atmospheric phenomena such as wave-like activity or katabatic winds is expected to be more significant. The proximity to the mountains results also in a more heterogeneous terrain altitude.

Second, the land use: the CIBA site is located in a more homogeneous area than the BLLAST site, which is a crucial factor influencing the variability of transition processes. This is consistent with a wider range in the magnitudes of micrometeorological variables at the BLLAST site compared with the CIBA site.

Third, climatology: the BLLAST site is much more humid than the CIBA site, in particular during the summer months, which will be compared in Chapter 5. For example, considering the months whose data are studied in Chapter 5, according to the climate summary of Météo-France, the mean monthly precipitation at the BLLAST site is 85 mm in June and 88 mm in July; whereas the 1971-2000 average of the CIBA site for July and August are 16 and 18 mm, respectively (Agencia Estatal de Meteorología and Instituto de Meteorologia, 2011). Additional to land use, these facts show that the soil moisture at BLLAST is significantly higher than at CIBA, directly influencing surface-atmosphere exchange.

3. Methodology

A description of the methods employed for calculations to obtain the main results of this thesis is now presented. These include both the experimental data treatment and the numerical simulations performed.

3.1 Data analysis

In micrometeorology, it is often required a detailed analysis of the small-scale fluctuations of the flow. With this aim, Reynolds decomposition (Reynolds, 1895) is used, splitting variables into mean and fluctuating portions. This implies that any variable associated to a flow (generically, x) can be expressed as the sum of an average value, which corresponds to the mean flow, and a turbulent perturbation:

$$x = \overline{x} + x', \qquad [3.1]$$

having these perturbations (x') an average equal to zero (Stull, 1988). This averaging can be done in different ways, but ideally it should be a statistical ensemble. For this thesis, the averaging is temporal, assuming the ergodic hypothesis can be applied. In this context it implies that if a turbulent flow is both statistically stationary in time and spatially homogeneous, its statistical temporal and spatial properties must be equivalent.

Sonic anemometer measurements are employed to obtain turbulent fluxes by using eddy-covariance methods (Foken, 2008; Aubinet et al.,

2012) with a 5-min mean, and the turbulence parameters friction velocity [equation 3.2], turbulent kinetic energy [3.3] and vertical sensible heat flux [3.4] are calculated:

$$u_* = \sqrt[4]{(-\overline{u'w'})^2 + (-\overline{v'w'})^2} \quad , \qquad [3.2]$$

$$e = \frac{1}{2}(\overline{u'^2} + \overline{v'^2} + \overline{w'^2}) \quad , \qquad [3.3]$$

$$H = \rho c_p \overline{\theta' w'} \quad , \qquad [3.4]$$

where u', v', w' and θ' are the turbulent perturbations of the wind components (u, v, w) and the potential temperature of the air (θ), respectively, ρ is the standard air density and c_p is the air specific heat at constant pressure.

As an indicator of the surface-based inversion strength at nighttime, the potential temperature difference ($\Delta\theta$) between selected levels of a meteorological tower is employed. These values are calculated considering the potential temperature definition, the ideal gases equation and the hydrostatic equation, obtaining:

$$\Delta\theta \approx \Delta T + \Gamma \Delta z = (T_{up} - T_{down}) + 0.0098\,(z_{up} - z_{down}) \,, \qquad [3.5]$$

with Γ the dry air adiabatic lapse rate; T_{up} and T_{down} the temperatures at the two vertical levels, named z_{up} and z_{down}, respectively. The 5-min means are applied to these data too.

3.2 Coordinate system rotation

The sonic anemometer data might require a correction in order to remove fake contributions to vertical fluxes calculations due to possible experimental misalignment between the vertical axis of the instrument

(Viana, 2011). The global idea of the correction consists mathematically in transforming the measurement coordinate system into a streamline coordinate system by applying a rotation to the original variables (*u, v, w*):

$$\begin{bmatrix} u_m \\ v_m \\ w_m \end{bmatrix} = \mathbf{A} \begin{bmatrix} u \\ v \\ w \end{bmatrix} \quad , \qquad [3.6]$$

being **A** the rotation matrix and u_m, v_m, w_m the modified variables, already expressed in a coordinate system totally aligned with the local vertical direction. The rotation matrix can be expressed as the combination of three rotations, considering each one of the main axes (Wilczac et al., 2001):

$$\mathbf{A} = \begin{bmatrix} \cos\gamma & -\sin\gamma & 0 \\ \sin\gamma & \cos\gamma & 0 \\ 0 & 0 & 1 \end{bmatrix} \begin{bmatrix} 1 & 0 & 0 \\ 0 & \cos\beta & -\sin\beta \\ 0 & \sin\beta & \cos\beta \end{bmatrix} \begin{bmatrix} \cos\alpha & 0 & \sin\alpha \\ 0 & 1 & 0 \\ -\sin\alpha & 0 & \cos\alpha \end{bmatrix}, \qquad [3.7]$$

with α, β and γ the rotation angles for each step, following the scheme of Figure 3.1.

Since the experimental sites considered for this thesis are both located at a plateau, it is found not necessary applying tilt corrections for steep mountainous terrain (Oldroyd et al., 2015), but rotations with a standard planar fit method (Wilczac et al., 2001) are used. This method is based on the following hypothesis: over a period of time long enough, the mean flow registered with the sonic anemometer occurs, on average, in a plane which is parallel to the surface. With a multiple linear regression of the mean components of the flow (original measurements), this plane can be obtained. Details on the calculations which follow to obtain the rotation matrix are exposed in Wilczac et al., (2001), and additional practical recommendations on the method are provided by Viana (2011).

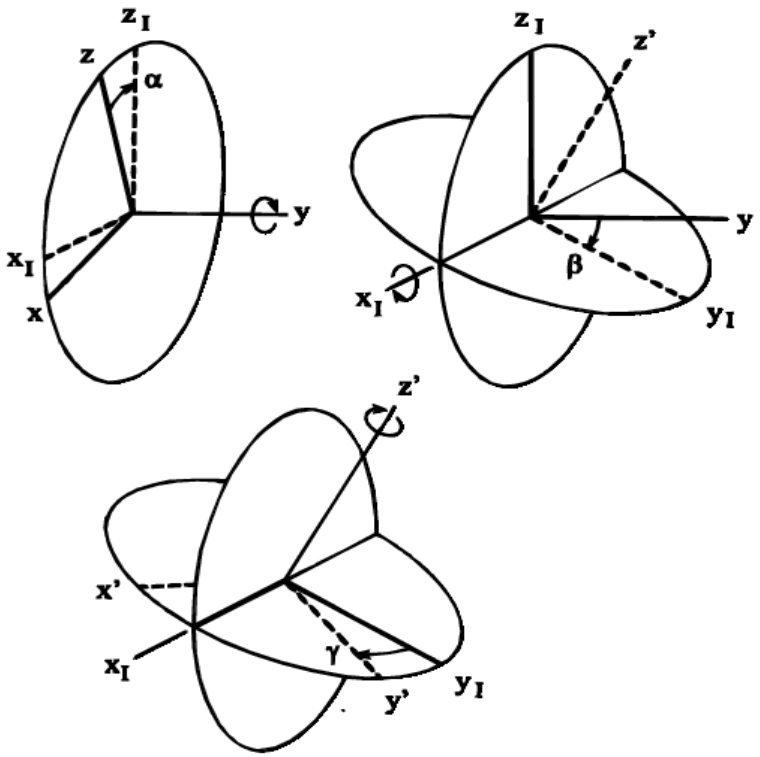

Figure 3.1. Rotation angles scheme, from an original coordinate system (x, y, z) to a final rotating coordinate system (x', y', z'), with the intermediate coordinate systems (x_I, y, z_I) and (x_I, y_I, z'). From: Wilczac et al. (2001).

3.3 Multi-resolution flux decomposition

It is worth analyzing physical processes along the transition time frame with a perspective on the spatial and time scales involved. For this purpose, a multi-resolution flux decomposition (MRFD) method is employed on sonic anemometer data. With this procedure, non-turbulent contributions can be identified and removed from the turbulent flux calculation, as far as possible. This tool became popular in the context of micrometeorology due to some studies on turbulence (Howell and Mahrt, 1997; Vickers and Mahrt, 2003). Besides, it has been employed, among others, to study the gap between the micro and the mesoscale (Voronovich

and Kiely, 2007; van den Kroonenberg and Bange, 2007; Viana et al., 2009, 2010) or to provide a new interpretation of the turbulence structure and exchange process of momentum in neutral and unstable stratification (Nilsson et al., 2014). The MRFD method is based on the Haar transform (Haar, 1910), which follows a simple subtraction of windowed, unweighted averages of decreasing length. It represents a simple orthogonal decomposition whose spectrum satisfies Reynolds averaging at every scale. This technique is applied to two temporal series of 2^N points equally spaced in time (Δt). The algorithm used in the calculations of this thesis is based on the one described by Vickers and Mahrt (2003) and Viana et al. (2010). The basic steps are as follows:

i) Calculate the covariance of the full series (two temporal series of 2^N points), yielding the total eddy-covariance flux. This is named as cumulative multi-resolution flux (CMRF) of the temporal scale $2^N\Delta t$ ($CMRF_N$).

ii) Both series are split up into two subseries of equal length. Then the respective averages are removed from them. The covariances of the resulting series yield the CMRF at the scale $2^{N-1}\Delta t$ ($CMRF_{N-1}$).

iii) Again, each subseries is divided into two parts and the respective averages are substracted. Now, the resulting covariances represent the CMRF at the scale $2^{N-2}\Delta t$ ($CMRF_{N-2}$), and so forth, up to the step with subseries with only two points ($CMRF_1$). A schematic representation of this iterative process is shown in Figure 3.2.

Focusing on the resulting series after each step, perturbations larger than the time scale associated with the length of the last averaging window applied are removed. Every $CMRF_n$ coefficient (with n = 1, …, N) can be seen as the average eddy-covariance flux of the whole couple of time series, for averaging windows of 2^n points. Consequently, the time series itself retains only fluctuations that are smaller than that specific scale $2^n\Delta t$.

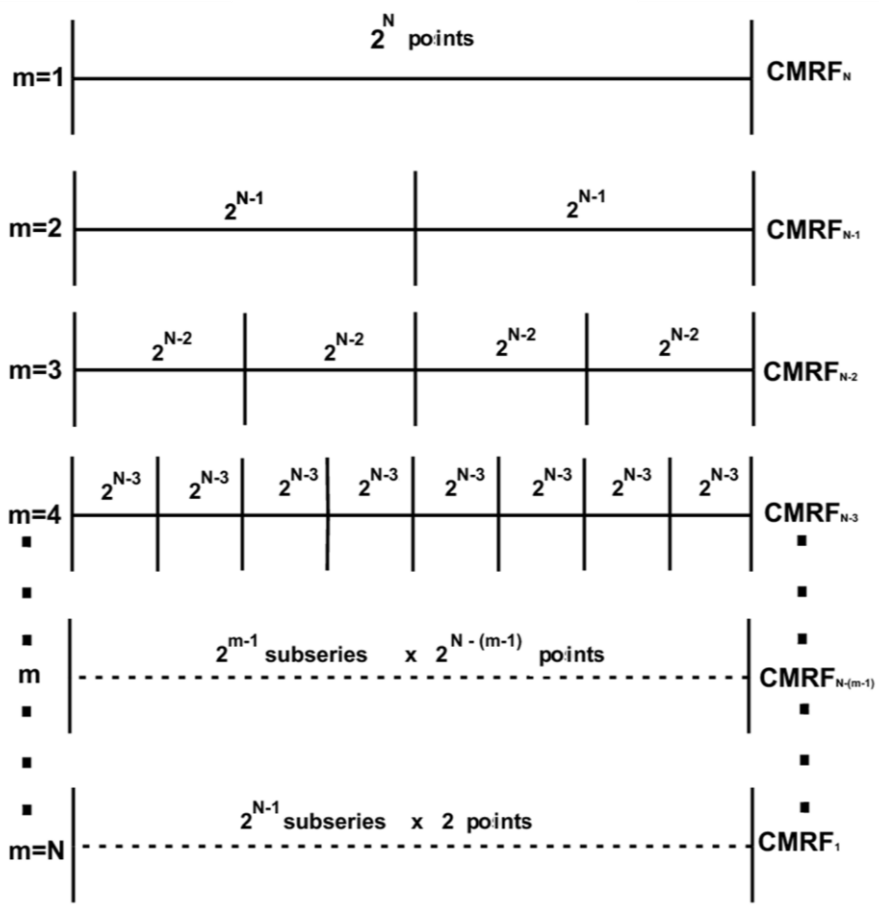

Figure 3.2. Schematic representation of the MRFD method for each one of the two original series of 2^N points, at every step (m). Adapted from Viana (2011).

Each iteration provides a value of the variance (or covariance, if both initial series are the same) of the partly filtered temporal series, so that the time series spectrum can be built by considering the differences between consecutive variances (or covariances), obtaining the multi-resolution flux cospectra (MRFC):

$$\mathrm{MRFC}_n = \mathrm{CMRF}_n - \mathrm{CMRF}_{n-1}, \qquad [3.8]$$

with n = 1, …, N.

Applying the method to two temporal series of different magnitudes (in this case, the wind vertical component, *w*, and the air temperature *T* or one of the wind horizontal components, *u* or *v*), the multi-resolution coefficients obtained at every step of the sequence are interpreted as contributions to the total flux from the structures of the corresponding time scales.

For this thesis, the calculations are performed with with $\Delta t = 0.05$ s, as far as the sampling frequency of the sonic anemometers is 20 Hz, and it is used N = 14. This makes the largest temporal window of 13.65 minutes.

3.4 Wavelet transform

The wavelet transform (WT) is a spectral tool which has similarities with the Fourier transform, but the WT uses a local decomposition of the time series, allowing an analysis varying the width of the spectral window, with fine temporal and spectral resolution. It can be used to analyse time series containing nonstationary power at many different frequencies (Daubechies, 1990; Torrence and Compo, 1998). For this reason, it has a wide range of applications in several fields of geophysics (Foufoula-Georgiou and Kumar, 1995), and in particular it has been applied to characterise coherent structures in turbulent flows (Farge, 1992) or wave-like events in the nocturnal ABL (Viana et al., 2009; Román-Cascón et al., 2015a,b). For this thesis, it is applied to near-surface atmospheric pressure time series, in order to determine the spectral energy distribution along the different temporal scales of the series, as well as the time evolution of this energy distribution.

Mathematically, the WT of a temporal series f(*t*) is defined as (Daubechies, 1992):

$$F_{s,\tau} = \int_{-\infty}^{\infty} f(t)\, \psi^{*}{}_{s,\tau}(t)\, dt\,, \qquad [3.9]$$

where $F_{s,\tau}$ represent the transform coefficients, s and τ are the scale and translation parameters, * indicates complex conjugate and $\psi_{s,\tau}(t)$ is the wavelet function, which is generated from a mother wavelet (Terradellas et al., 2001):

$$\psi_{s,\tau}(t) = \frac{1}{\sqrt{|s|}}\psi\left(\frac{t-\tau}{s}\right), \qquad [3.10]$$

with the normalization factor $\frac{1}{\sqrt{|s|}}$, and $\psi\left(\frac{t-\tau}{s}\right)$ the mother wavelet translated and scaled via τ and s. In principle, on a mother wavelet is only imposed one constrain named the admissibility condition, which requires (Farge, 1992):

$$C_\psi = \int_{-\infty}^{\infty} \frac{|\hat{\psi}(\omega)|}{\omega} d\omega < \infty, \qquad [3.11]$$

working in the frequencies space (ω) and with $\hat{\psi}(\omega)$ the Fourier transform of the mother wavelet $\psi(t)$.

Among all the existing possibilities of wavelet functions, here is chosen the Morlet wavelet (Morlet, 1981; Meyers et al., 1993). It uses a complex function consisting of a plane wave modulated by a Gaussian function and can be expressed as:

$$\psi(t) = e^{i\omega_0 t} e^{-t^2/2}, \qquad [3.12]$$

Besides, following Terradellas et al. (2001), to analyse the signal it is useful working with an energy related parameter, like the wavelet energy density per time and scale unit, which is defined as:

$$e_{s,\tau} = \frac{2}{s^2}\frac{|F_{s,\tau}|^2}{C_\psi}, \qquad [3.13]$$

where C_{ψ} is the normalizing factor from equation [3.11].

3.5 Numerical simulations: model features

The Weather Research and Forecasting (WRF) model (Skamarock and Klemp, 2008) has been chosen to perform ABL evening transition numerical simulations for this thesis, working with the Advanced Research WRF (ARW) core. This non-hydrostatic mesoscale model has been designed for both research and operational applications. Furthermore, it has been proved as a successful tool to simulate ABL phenomena, like radiation fog events (van der Velde et al., 2010; Román-Cascón et al., 2012; Steeneveld et al., 2015), sea breezes (Steele et al., 2013), gravity waves (Udina et al., 2013), stable ABL processes over snow (Sterk et al., 2013), atmospheric density currents (Soler et al., 2014) or the urban heat island effect (Salamanca et al., 2012; Theeuwes et al., 2014). For this thesis, WRF version 3.4.1 is mostly employed, but for some experiments version 3.5 is used instead. These two model versions were compared, for evening transition results, by Sastre et al. (2013), obtaining some differences for a few of the cases considered, but globally performing similarly. In this thesis, several tests are designed with some common configuration and varying other settings, depending on the specific aim of each simulation. Those settings which are not common will be subsequently detailed.

A wide range of physical schemes is provided by WRF. For example, the land-surface model (LSM) combines atmospheric information from the surface layer scheme with land-surface properties to evaluate the vertical transport done in the Planetary Boundary Layer (PBL) schemes (Borge et al., 2008). The surface processes represented by a generic LSM are illustrated in Figure 3.3.

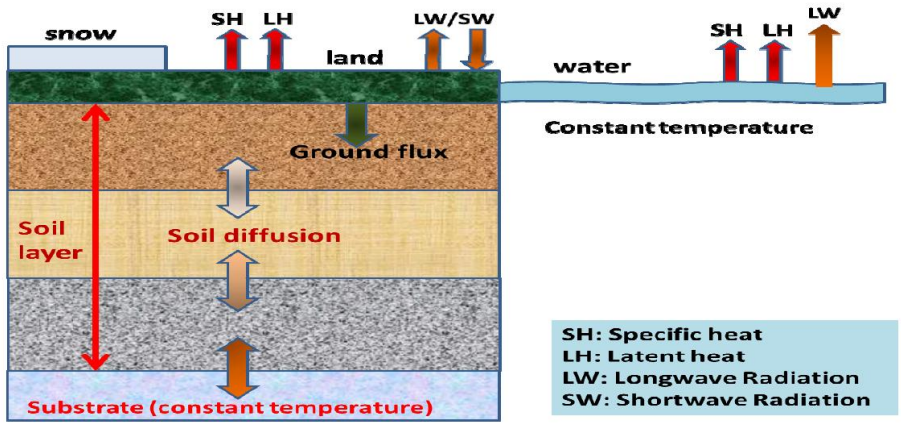

Figure 3.3. Scheme of surface processes represented by a generic LSM. From: Huang et al. (2014).

In this thesis, WRF experiments are performed with three different land-surface model (LSM) options: the 5-layer thermal diffusion scheme (here named as 5-layers), the unified Noah LSM (Noah) and the Rapid Update Cycle (RUC):

- The 5-layer thermal diffusion LSM (Dudhia, 1996) is based on the MM5 5-layer soil temperature model. It predicts ground temperature and soil temperature in 5 levels; these layers thicknesses are, from top to bottom: 1, 2, 4, 8, and 16 cm, and below the latter (at 32 cm) the temperature is fixed at a deep-layer average. The energy budget includes radiation, sensible and latent heat flux. Soil moisture is fixed with a landuse- and season-dependant constant value, and there are no explicit vegetation effects. This is the simplest of the three LSM considered for this work.
- The Noah LSM (Chen and Dudhia, 2001; Ek et al., 2003; Tewari et al., 2004) is a 4-layer soil temperature and moisture model with canopy moisture and snow cover prediction. The thickness of each layer from the ground surface to the bottom are 10, 30, 60, and 100 cm,

respectively, with a total soil depth of 2 m and the root zone in the upper 1 m of soil. Thus, the lower 1-m soil layer acts like a reservoir with. Evapotranspiration, soil drainage and runoff are included, with several vegetation categories, monthly vegetation fraction, and soil texture. This LSM provides sensible and latent heat fluxes to the PBL scheme and considers surface emissivity properties.

- The RUC (Smirnova et al., 1997, 2000; Benjamin et al., 2004) LSM has a multi-level soil model (6 as default) with higher resolution in the top part of soil domain (default: 0, 5, 20, 40, 160, 300 cm). Energy and moisture budgets are solved in a thin layer spanning the ground surface and including half of the top soil layer and half of the first atmospheric layer, with corresponding heat capacities and densities. Vegetation impact on evaporation is taken into account with canopy moisture being a prognostic variable and evapotranspiration parameters depending on any of the 11 soil texture classes available. Some of the prognostic variables provided are: soil temperature, volumetric liquid, frozen and total soil moisture contents, surface and sub-surface runoff, canopy moisture, evapotranspiration, latent, sensible and soil heat fluxes and skin temperature.

Regarding the PBL parametrization, three possibilities are considered in the experiments of this thesis: Yonsei University (YSU), Mellor-Yamada-Janjic (MYJ) and Quasi-Normal Scale Elimination (QNSE). A wide description of these PBL parametrizations is presented by Kleczek et al. (2014); here are explained their main characteristics:

- YSU scheme (Hong et al., 2006) is a first-order non-local turbulence closure. For unstable conditions, it applies a counter-gradient flux contribution to potential temperature and momentum in order to include the contribution of the large-scale eddies to the total flux. It has an explicit treatment of the entrainment layer at the ABL top, being the latter defined with a critical value of zero for the bulk

Richardson number. Therefore, there is a strong dependency on the buoyancy profile, in which the ABL top is defined at the maximum entrainment layer.

- MYJ (Mellor and Yamada, 1982; Janjić, 1994) is a local 1.5-order TKE closure scheme. Here the TKE production/dissipation equation is solved iteratively. Its prognostic equation for the potential temperature variance is omitted, and just the one for TKE is considered for the mean variables such as temperature, moisture and wind speed. An upper limit, which depends on the TKE as well as the buoyancy and shear of the driving flow, is imposed on the master length scale.
- QNSE (Sukoriansky et al., 2006) is also a local-1.5 order closure scheme, as it is based on MYJ. It has a prognostic TKE equation and is able to consider the spatial anisotropy of a turbulent flow. Additionally, this parametrization accounts for the combined effects of turbulence and waves. It is especially appropriate for stable ABL conditions.

Each one of these PBL parametrization works with a matching surface-layer scheme: the modified MM5 scheme (Jiménez et al., 2012) for YSU, the Janjic Eta Monin-Obukhov scheme (Janjic, 1996) for MYJ and the QNSE surface-layer scheme (Sukoriansky, 2008) for QNSE. A detailed description and comparison of these surface-layer parametrizations is provided by Liu et al. (2013). Other model features for this thesis are common to all the simulations here presented. This includes the land use, obtained from the United States Geological Survey (USGS) dataset, which provides 24 different categories (Wang et al., 2015a). Besides, 16 soil categories are considered by WRF. Regarding the vertical resolution, all the modelling tests are performed with 50 eta levels, 28 of them being located within the first kilometre of the troposphere, and 8 within the initial 100 metres. This choice provides a good resolution for the boundary

layer, the most interesting atmospheric region for the purpose of this thesis. Some other physical features correspond to the whole set of simulations, named: the rapid radiative transfer model (RRTM) for the longwave radiation (Mlawer et al., 1997), the Dudhia scheme (Dudhia, 1989) for the shortwave radiation, and the WRF single-moment 3-class (WSM3) microphysical scheme (Hong et al., 2004). More details about the model characteristics and options can be found in Skamarock et al. (2008) and Wang et al. (2015a).

Depending on the experiment, two different options are used for the initial and boundary conditions. On the one hand, some simulations are initialised with data from the European Centre for Medium-range Weather Forecasts (ECMWF) operational model, whose resolution is 0.25 degrees. On the other hand, we use the National Centers for Environmental Prediction (NCEP) reanalysis (Kalnay et al. 1996) too. These NCEP FNL (Final) Operational Global Analysis data used are on 1x1 degree grids. In both cases (ECMWF and NCEP), lateral boundary conditions are refreshed every 6 hours.

4. Characteristic phenomena of the ABL afternoon and evening transition: two observational approaches

An overview to the observations and phenomenology of the ABL evening transition is now presented. Two different approaches for experimental characterization are exposed. Firstly, the study of three individual cases, using mainly measurements from two types of high-frequency instruments, which provide very accurate records: a sonic anemometer and microbarometers. With the measurements provided by these devices, an analysis on the different scales involved and their evolution is performed, considering three cases from the BLLAST dataset: 24, 25 and 29 June 2011. Sensible heat flux and friction velocity are especially studied, as they are usually representative of the thermal and mechanical turbulence, respectively. In the second sub-section, the other experimental approach is presented. It consists of an analysis based on statistical calculations, considering a three-months dataset of observations from CIBA.

Part of the results presented in this chapter are published in: Sastre, M., Yagüe, C., Román-Cascón, C., Maqueda, G., Salamanca, F. and Viana, S.: Evening transitions of the atmospheric boundary layer: characterization, case studies and WRF simulations, Adv. Sci. Res., 8, 39–44, 2012.

4.1 Sonic anemometer and microbarometer characterization

Both 24 and 25 June 2011 were IOPs during the BLLAST campaign, mainly associated with large-scale stability and weak synoptic forcing; on the contrary, the third day selected for this section, 29 June 2011, was not an IOP. These three days are chosen here to study the afternoon and evening transition in a two-way comparison: two days with similar weak synoptic forcing but slight differences (like in wind speed), and a third one really different from the standard fair-weather transitions. In Chapter 2, a description of their respective synoptic situations was provided.

The evolution of the temperature at various levels close to the surface, the TKE and the wind speed are represented for each one of the three days (Figure 4.1, Figure 4.2 and Figure 4.3). For all of them, sunset took place at around 19:40 UTC. The stronger decay in temperature values closer to the surface is observed for 24 (Figure 4.1a) and 25 June (Figure 4.2a), favouring the development of a nocturnal surface-based temperature inversion. On the other hand, for 29 June (Figure 4.3a), the pre-sunset temperature evolution is quite plain for all the levels. It starts decaying just before sunset, but with a very similar intensity for all the levels, so that the nocturnal temperature inversion is not developing, or very weakly. The influence of the synoptic conditions makes 29 June not to have a transition in the temperature evolution in the same way as the other two days: wet soil due to rainfall and high relative humidity do not allow an intense surface cooling.

TKE presents differences of at least one order of magnitude between diurnal and nocturnal values for 24 and 25 June (Fig. 4.1b, Fig.4.2b), with a minimum around sunset (earlier for 24 June), and afterwards a recovery. Again, 29 June (Fig 4.3b) shows a pattern with nearly no turbulence decay. These values are oscillating, around 0.5 $m^2\ s^{-2}$ on average, with no clear distinction between nocturnal and diurnal ones.

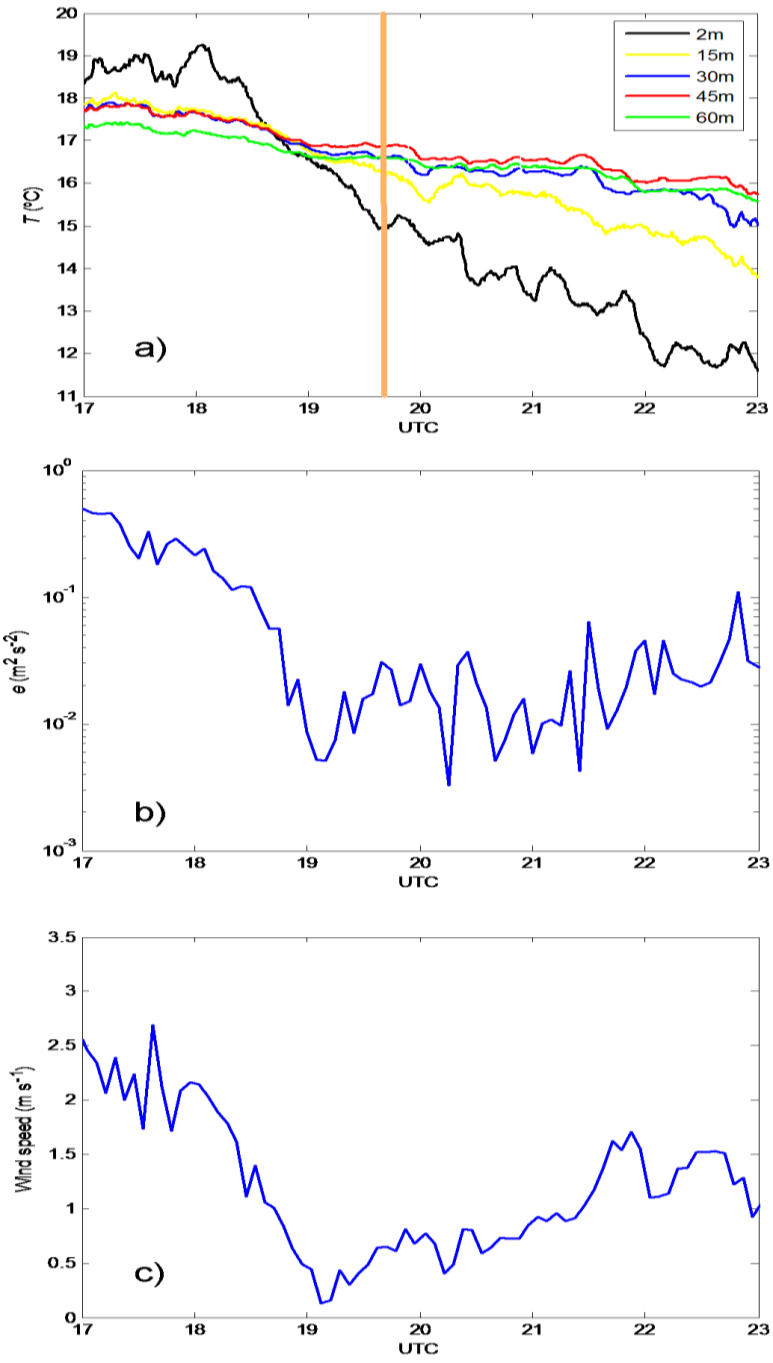

Figure 4.1. Time evolution for the 24 June 2011 transition of: a) temperature at various levels; b) TKE (log scale); c) wind speed. Vertical orange line indicates sunset.

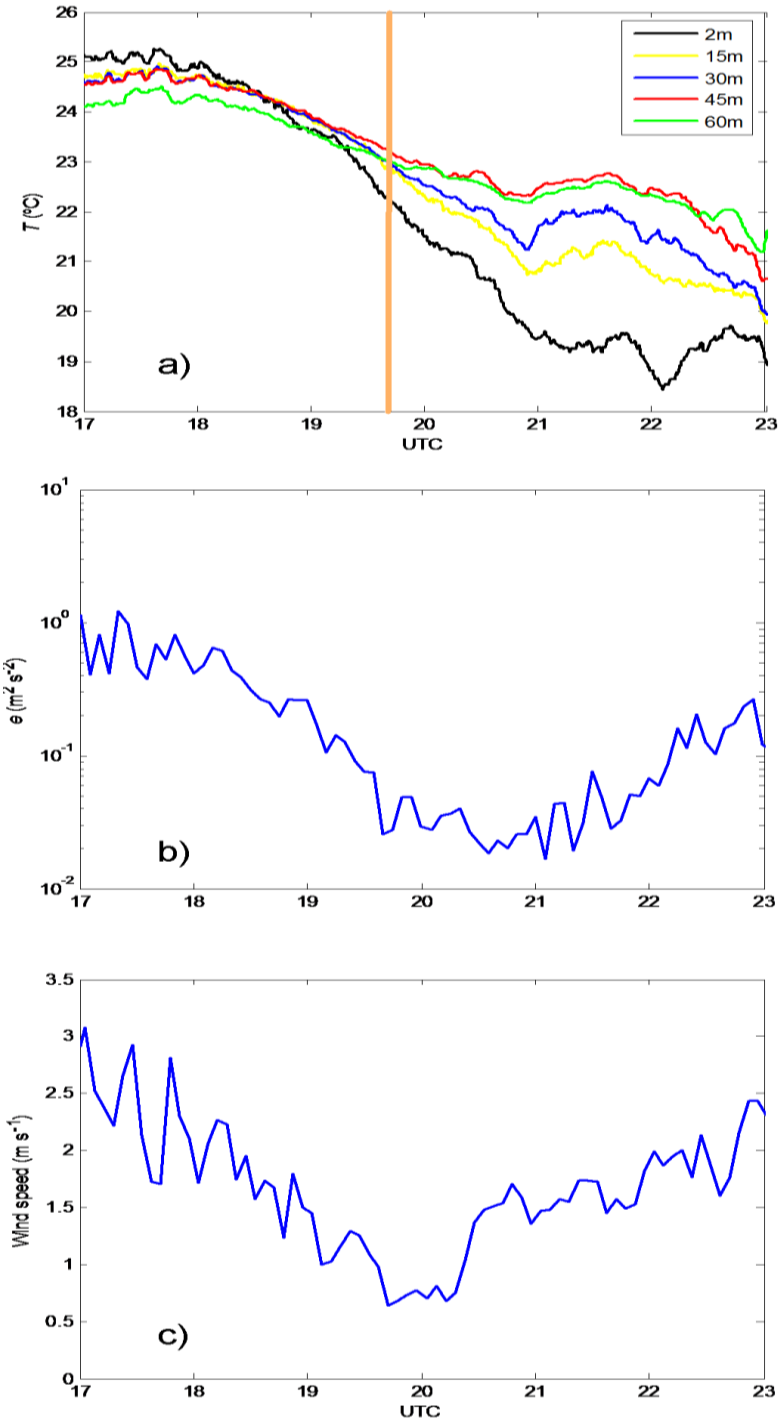

Figure 4.2. Same as Fig. 4.1 for 25 June 2011, with different axis limits in a) and b).

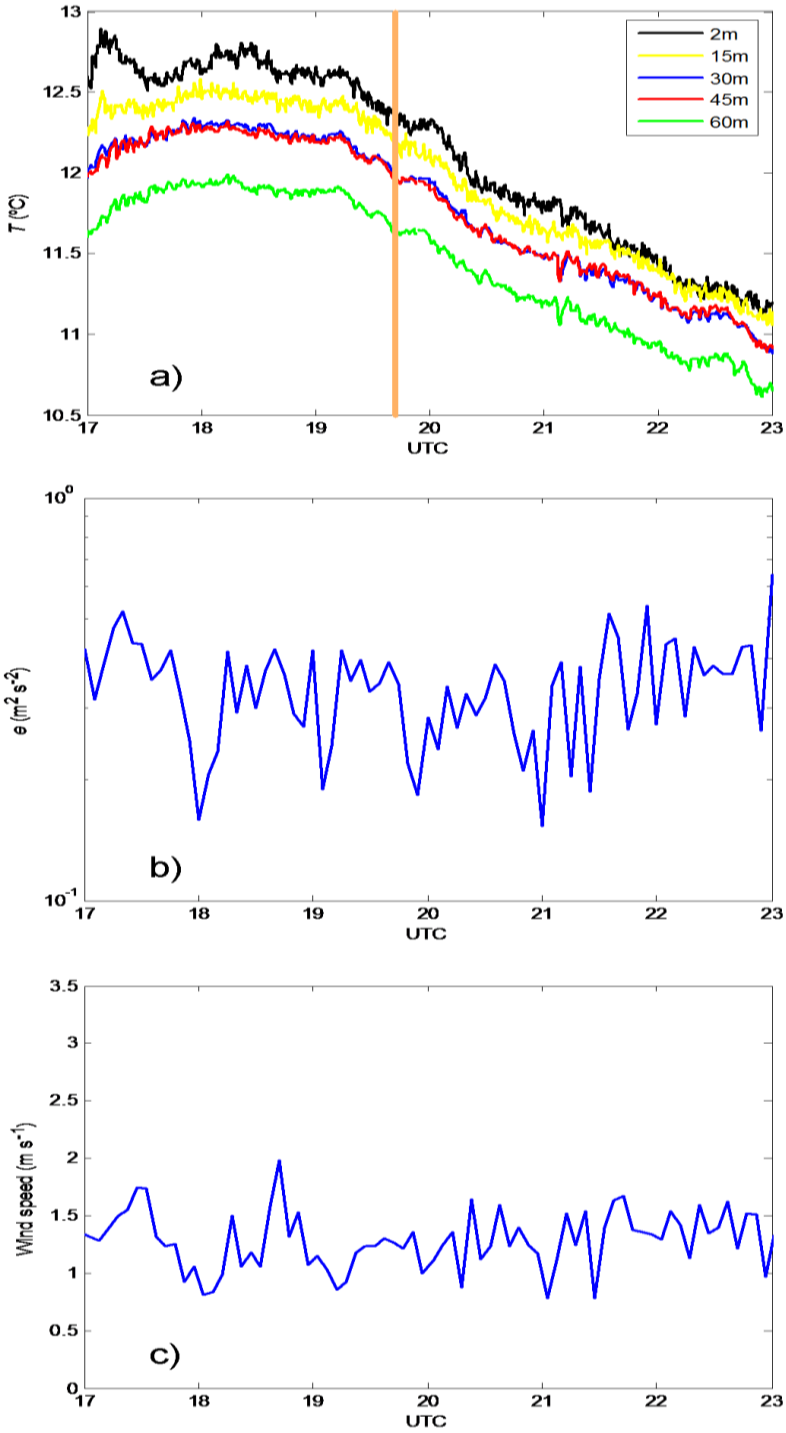

Figure 4.3. Same as Fig. 4.1 for 29 June 2011, with different axis limits in a) and b).

That is a significant difference compared with the other two days, whose values after sunset are at least one order of magnitude smaller than on 29 June. For the three days, similarities between the qualitative evolution of the wind speed and the TKE are found, showing the influence of the former on turbulence. However, quantitatively the wind speed reaches values not very different in the night period for the three days. So either a threshold in the wind minimum affects the turbulence, or there are other effects (possibly thermal related) for the nocturnal turbulence.

The multi-resolution technique (MRDF) is applied to the friction velocity (Figure 4.4), representing the contribution to this variable of different temporal scales involved (vertical axis) for a certain period of time (horizontal axis). In the vertical axis (logarithmic) scales from 0.1 seconds up to 14 minutes are represented, which includes the selected averaging time for eddy-covariance method (for these calculations, 5 minutes). This plot contains information on the contributing temporal scales at each time step. For 24 June (Fig. 4.4a), initially, when thermal turbulence is well developed (17-18 UTC), higher values correspond to processes of scales between 1 and 100 seconds. Later on, friction velocity decays and the most relevant scales correspond to two groups: over 100 seconds and between 1 and 10 seconds (around 19:30 UTC). Therefore, there is a change, not only in the absolute values of the friction velocity, but also in the predominant origin of these contributions. So the transition to the nocturnal boundary layer leads to the generation of a gap between different scales contributing to turbulent parameters, but these are integrated together when using eddy-covariance fluxes calculation.

The process of narrowing in the principal contributing time scales can be observed for 25 June (Fig. 4.4b) too. In this case it occurs progressively and for a longer time than on 24 June, in accordance with the TKE decay (Fig. 4.2b).

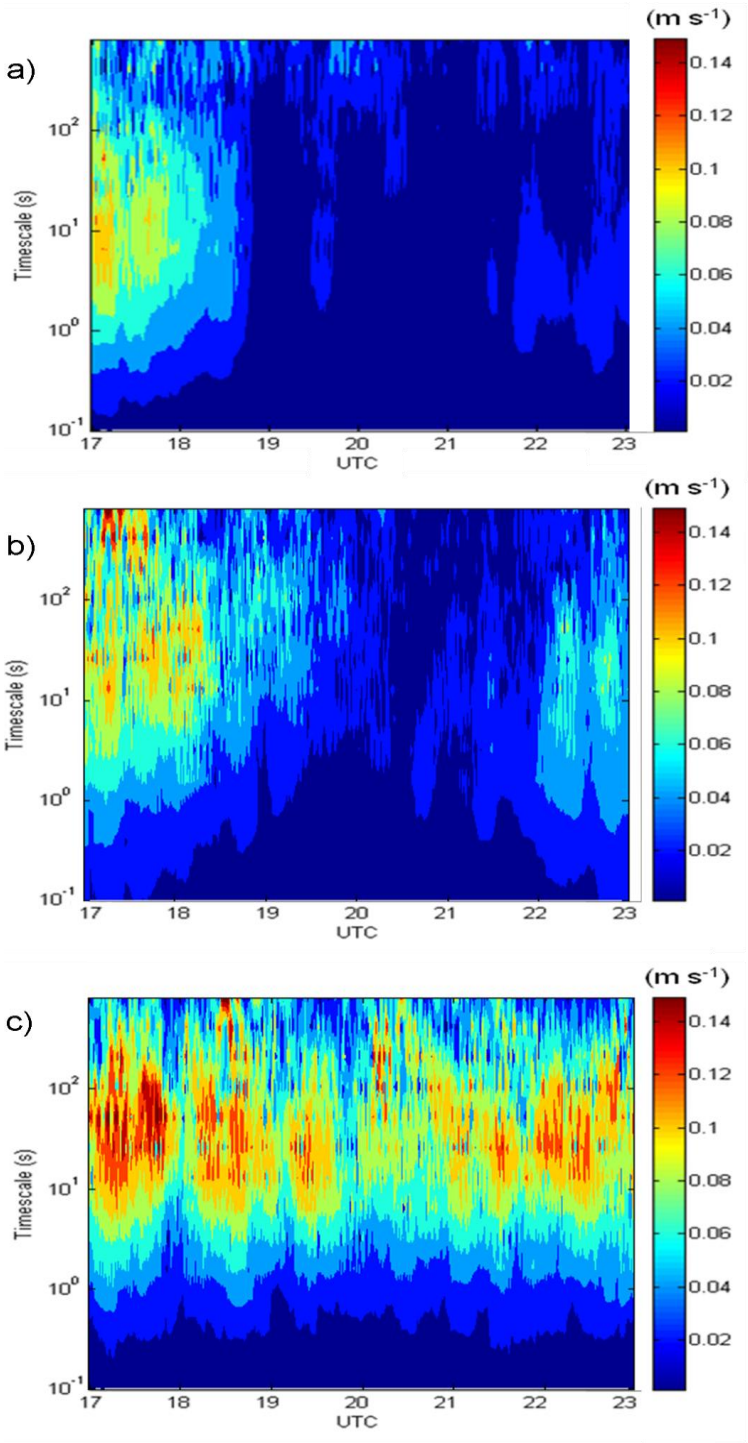

Figure 4.4. Friction velocity (m s^{-1}) MRFD for: a) 24 June, b) 25 June, c) 29 June.

At 17:30 UTC two are the most important temporal scales: one around 10 s and the other one of nearly 300 s. Then, between 19:30 and 20:00 UTC the main relative contributions come from only one scale, which is around 100 s. Nonetheless, for 29 June (Fig. 4.4c), the contributing scales are mostly the same for the whole period: there is not an evolution as clear as in the other two cases. The most relevant contributions correspond to physical processes of temporal scales between 10 and 100 s. Around sunset, a shift, linked to the suppression of the solar energy income, can be observed. Small contributions at all the scales can be found perhaps only for very narrow times: around 18:00 UTC and 19:00 UTC. As a whole, the absolute values are very homogeneous during the whole period represented. For comparison, the friction velocity evolution for each day, calculated with the eddy-covariance method, is shown in Figure 4.5. This complements the information provided by MRFD.

The MRFD technique has a potential use to separate turbulent and non-turbulent scales by identifying the gap between them, in order to calculate more accurately turbulent fluxes through the eddy-covariance method. A moving threshold, instead of a fixed value (5 minutes for Figure 4.5) could be employed for these calculations, making as small as possible the non-turbulent contributions to vertical fluxes. An example of this situation for 24 June (Fig. 4.4a) could be around 22:30 UTC, when scales between 10 and 100 seconds reach very low values, which could indicate that the separating gap has shifted to these scales. At this time, in Figure 4.5a there might be contributions of larger (non-turbulent) scales. There is also a temporal coincidence between the friction velocity minimum values (Figure 4.5a) and near zero contributions for all the scales for friction velocity MRFD (Figure 4.4a), for example, at 19:00 or 21:00 UTC. A similar effect is found for 25 June at 20:00 UTC (Fig. 4.4b and Fig 4.5b): the friction velocity MRFD values in practically all the scales represented are really small, with minimum values for the eddy-covariance calculations. The oscillating pattern for 29 June is observed in Fig. 4.4c and Fig. 4.5c.

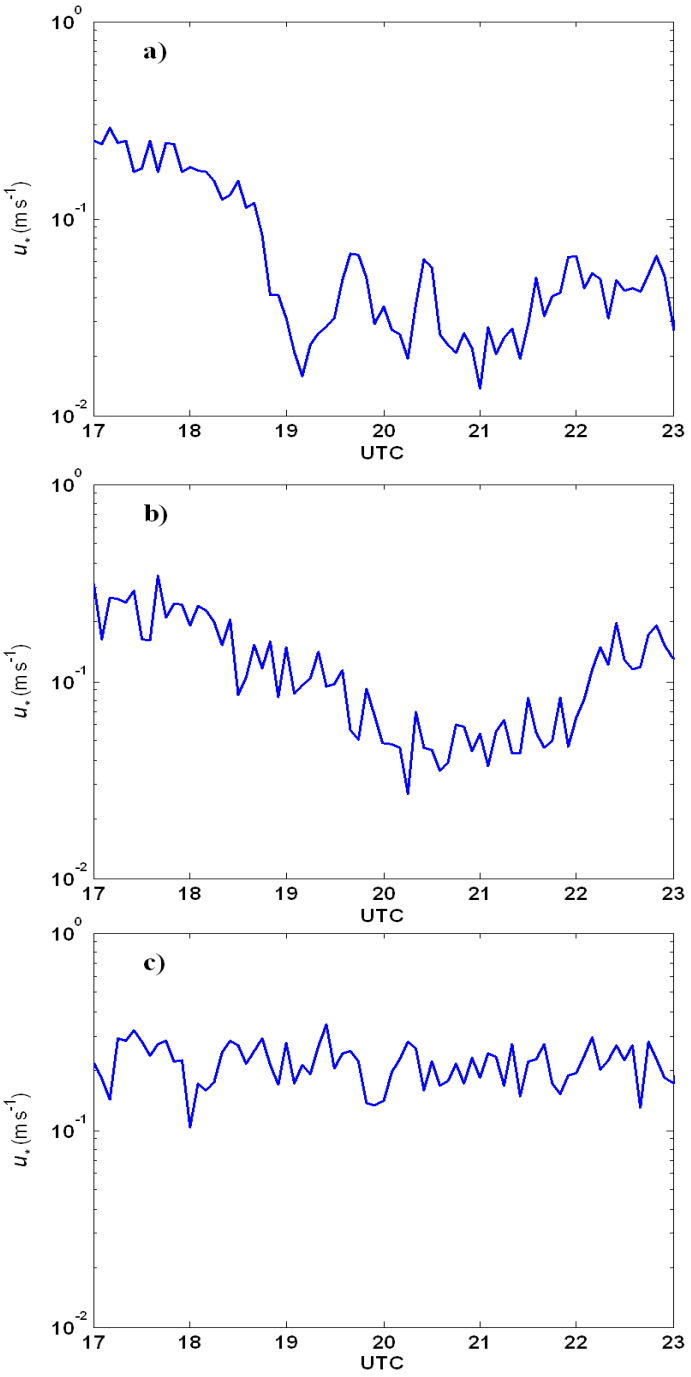

Figure 4.5. Friction velocity (m s^{-1}) calculated with eddy-covariance method for: a) 24 June, b) 25 June, c) 29 June.

Additionally, Taylor's frozen eddies hypothesis (Stull, 1988) can be considered. With this approach, the eddy scale size responsible for turbulence can be estimated by multiplying, at any time, the mean wind speed (Figs. 4.1c, 4.2c, 4.3c) and the temporal scale of the maximum contribution (of turbulence) to the friction velocity. As a whole, it is found neither a common pattern in eddy size, nor a significant tendency to increase or decrease along the transition (not shown): a varying evolution, rather than constant values for the turbulent eddies typical lengthscale. For instance, in Figure 4.4a (24 June) approximately at 17:00 UTC the corresponding eddy size would be 100-300 m. Afterwards, at around 19:30 UTC, the most relevant eddies would reduce their size to 1-5 m. These estimations of eddies length scale values and evolution are in agreement with other studies using different methods (Darbieu et al., 2015).

Analogous MRFD plots are presented for the kinematic heat flux ($\overline{w'T'}$), providing an insight on the contributions of the different scales to upward (positive values) or downward (negative values) fluxes (Figure 4.6). Complementary, the turbulent sensible heat flux obtained with the eddy-covariance method (5-minutes) is shown (Figure 4.7). For 24 and 25 June, a drastic change occurs between 17:00 and 19:00 UTC, due to the decay of the solar radiation: the relative intense positive contributions vanish and the negative values appear at nearly all the scales (Fig 4.6a,b), so the crossover of the sensible heat flux takes place (Fig 4.7a,b). These downward contributions are more intense in the case of 25 June (Fig. 4.6b), compared to 24 June (Fig. 4.6a), probably due to the relative more intense turbulence of the latter. For the larger scales, on 24 June takes place, after sunset, an alternation of positive and negative values. This is an indication of the appearance of counter-gradient fluxes, which are often detected in the nocturnal stable boundary layer, sometimes linked to wave-like activity (Román-Cascón et al., 2015b).

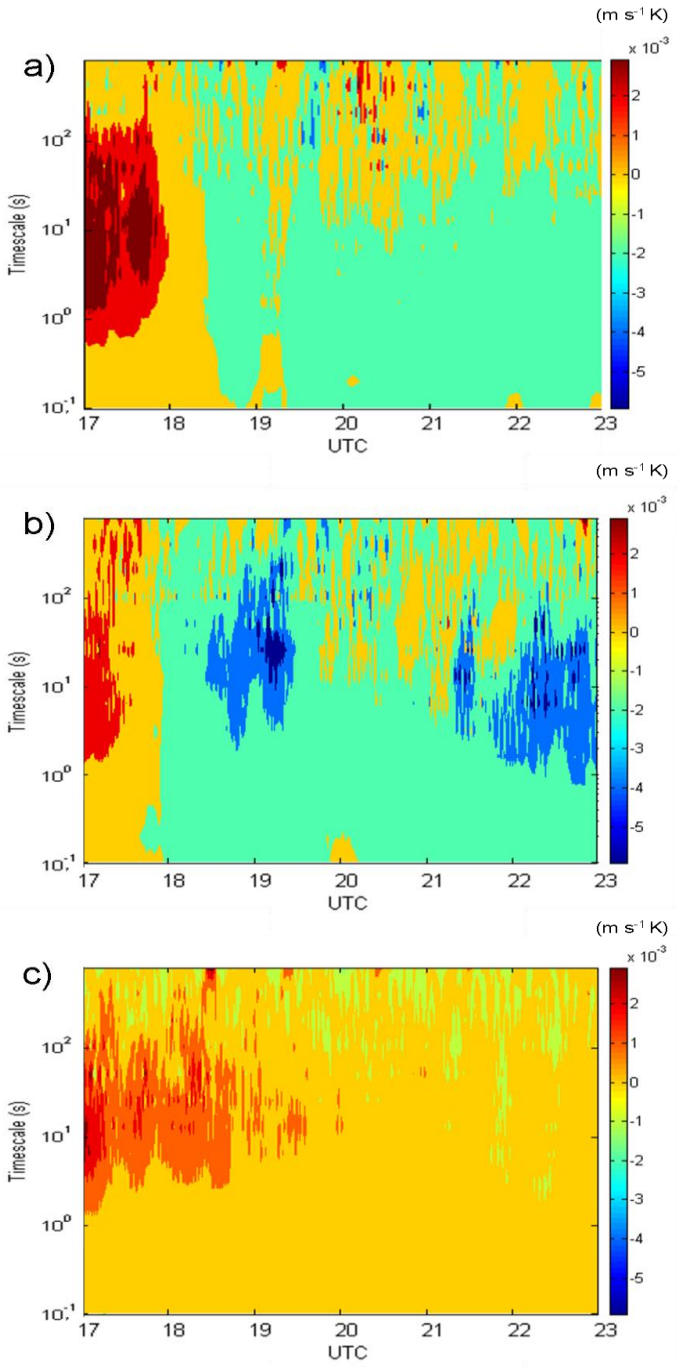

Figure 4.6. Kinematic heat flux MRFD for: a) 24 June; b) 25 June; c) 29 June 2011.

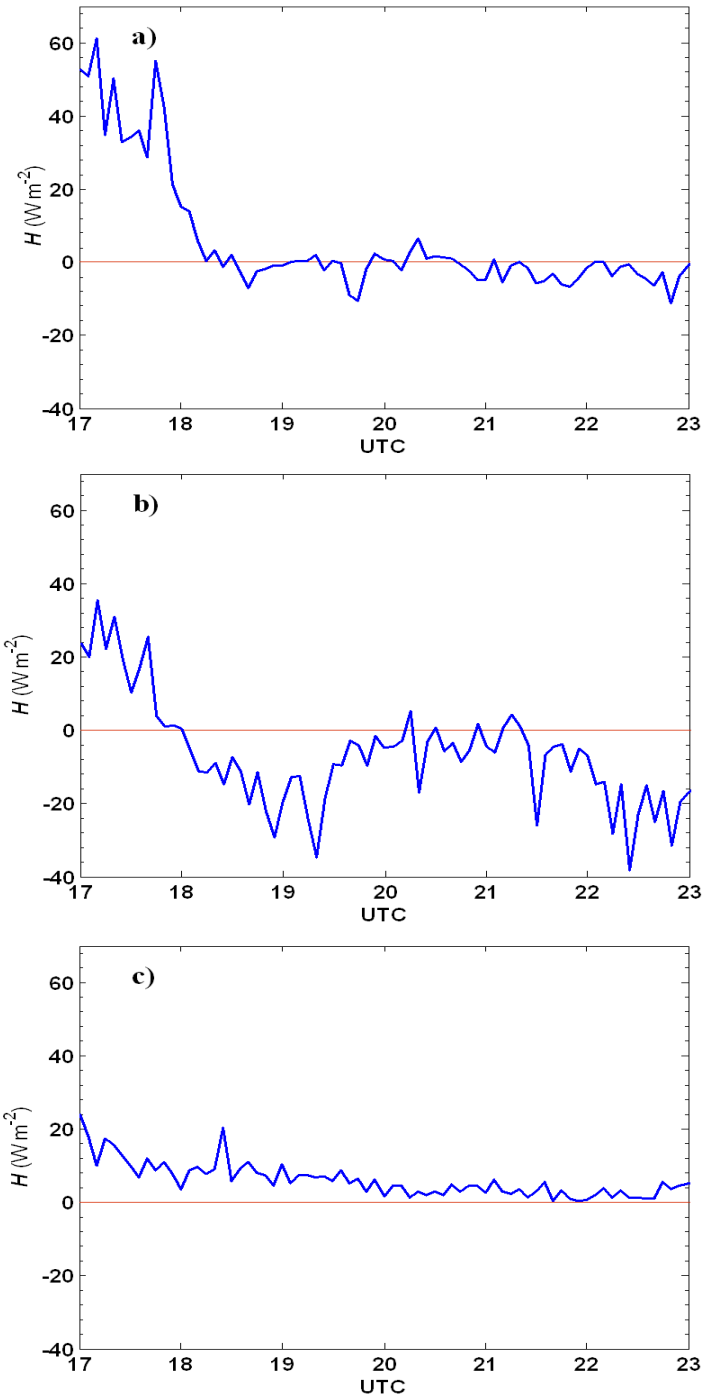

Figure 4.7. Turbulent sensible heat flux calculated with eddy-covariance method for: a) 24 June; b) 25 June; c) 29 June 2011.

For 29 June, the kinematic heat flux evolution is alike (Fig. 4.6c): it is neither as sudden nor as intense as for 24 or 25 June. Additionally, nocturnal negative values are not as substantial as in the other two cases. It is similarly pictured in Fig. 4.7c. As a whole, for 29 June these values are close to zero, which is linked to the temperature homogeneity and a nearly neutrally-stratified ABL (Fig. 4.3a). Together with the fact that the wind speed does not actually decay during this transition, but maintains similar values prior to sunset, this could mean that in this case the mechanical effects clearly prevail over the thermal ones.

Furthermore, it is performed an analysis on the near-surface pressure data from the microbarometers records. In particular, a Butterworth filter is applied to the pressure absolute values, using 45 minutes as the cut-off frequency (Figure 4.8). With this choice, a filtered pressure (δp) time series is obtained, where the larger oscillations (as, for example, corresponding to the diurnal cycle) are removed. Differences between the three days can be found, in particular for the transition period. Firstly, 24 and 25 June show high frequency oscillations during daytime, related to convection and turbulence. When the incoming solar energy is declining, the oscillations reduce their amplitude and frequency, and a nocturnal regime can be obtained. Still, between these two days there are some differences, for example in the amplitude, which is larger for 25 June. The wind speed was slightly higher this day, compared to the previous one (Fig 4.1 and Fig. 4.2).

On the other hand, for 29 June there is not a clear transition from a diurnal to a nocturnal regime, as the oscillations keep the very high frequency signal due to turbulent motions even at around sunset or at night. Only a decrease in the amplitude of the oscillations can be appreciated, but it is still significantly larger than for the other two days.

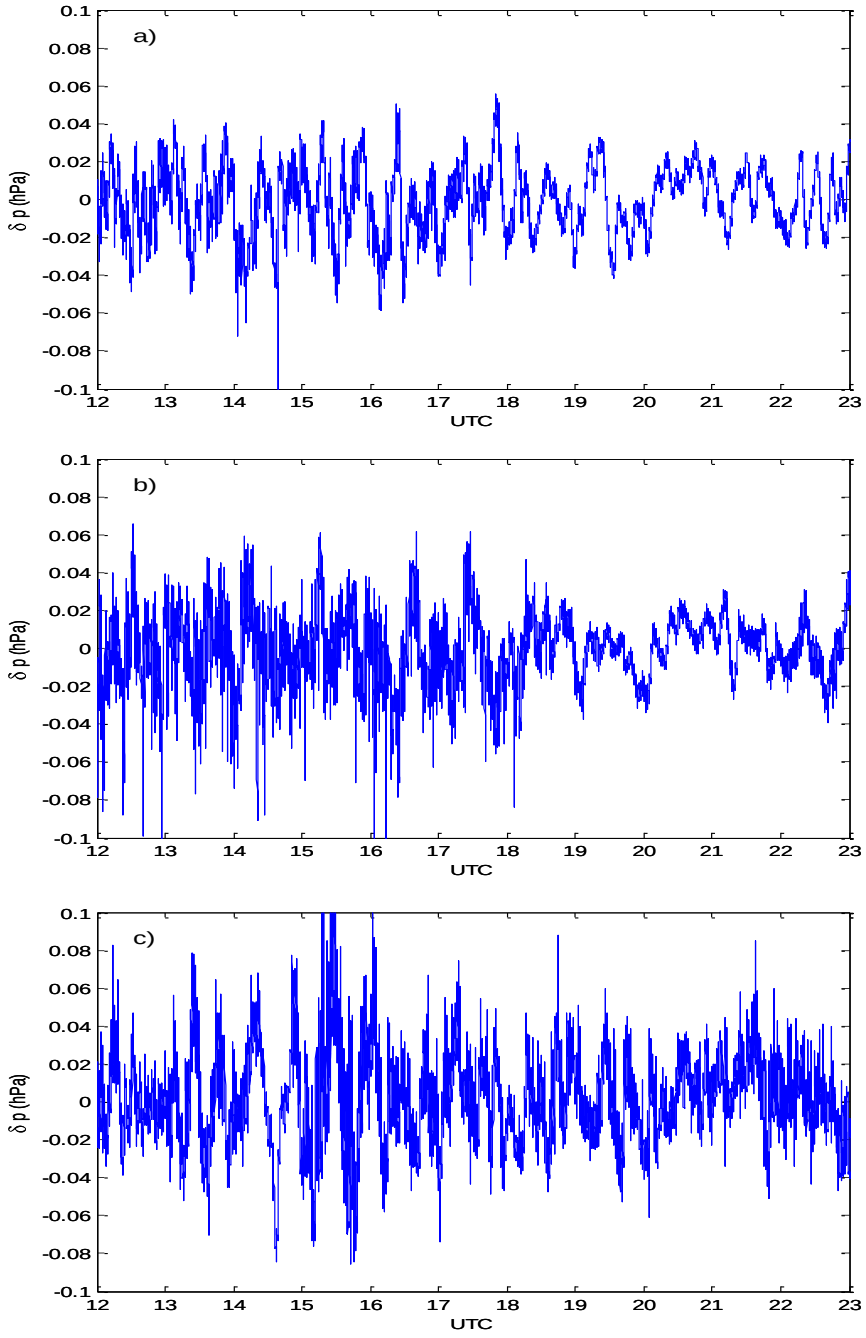

Figure 4.8. Filtered pressure for: a) 24 June; b) 25 June; c) 29 June 2011.

A particular feature can be observed in the night of 24 June: a couple of cycles with a very well defined period, indicating wave-like activity. These wave-like structures can be analysed with the wavelet transform technique. In Figure 4.9, the filtered pressure for 24 June is plotted for a narrower timing, showing the oscillations with some periodicity more clearly. The wavelet analysis reveals two maxima of spectral energy, which are found between 22 and 23 UTC. Different types of waves were detected during the BLLAST field campaign; a couple of these events are studied in detail by Román-Cascón et al. (2015a,b).

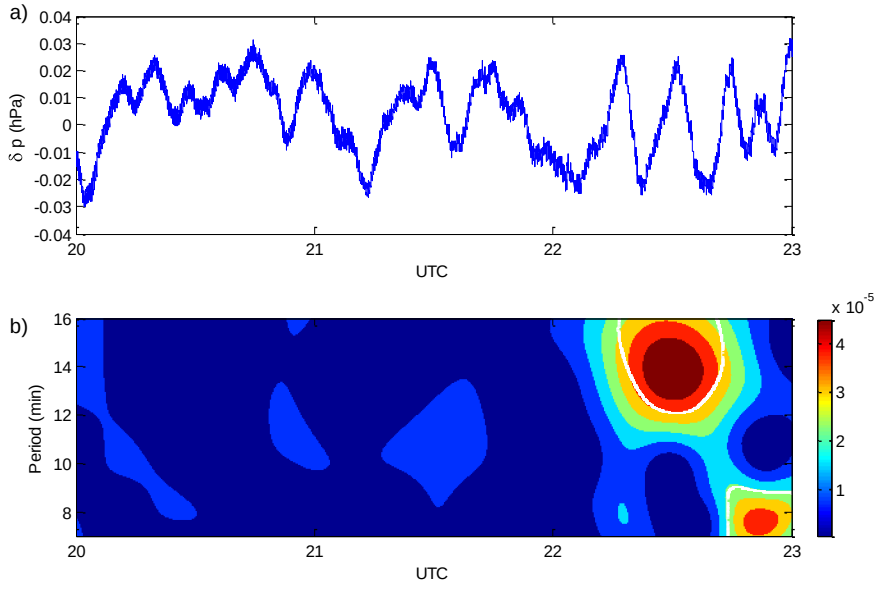

Figure 4.9. a) Filtered pressure and b) wavelet transform energy density per period and time unit ($hPa^2\ s^{-1}$) for the transition of 24 June 2011.

4.2 Statistical values and transition classification

Another observational approach to the transition is performed through statistical analysis.

Data from three months (July, August and September 2009) at CIBA are analysed between 17:00 and 23:00 UTC for each day, focussing on dynamic and thermal variables. A total amount of 85 days is considered for this statistical analysis; the number of cases left up to three months is due to lack of data availability. Figures 4.10, 4.11 and 4.12 show the distribution of the temperature difference between 10 m and 1.5 m and the wind speed (1.5 m) for the total of transitions studied, each one for a sub-period of 2 hours.

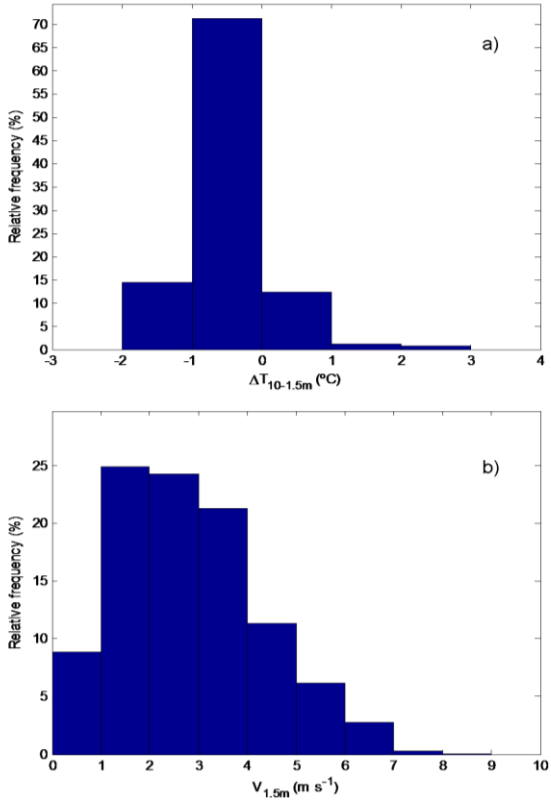

Figure 4.10. Distributions for the time period 17-19 UTC of: temperature difference between 10 and 1.5 m distribution (a) and wind speed at 1.5 m (b).

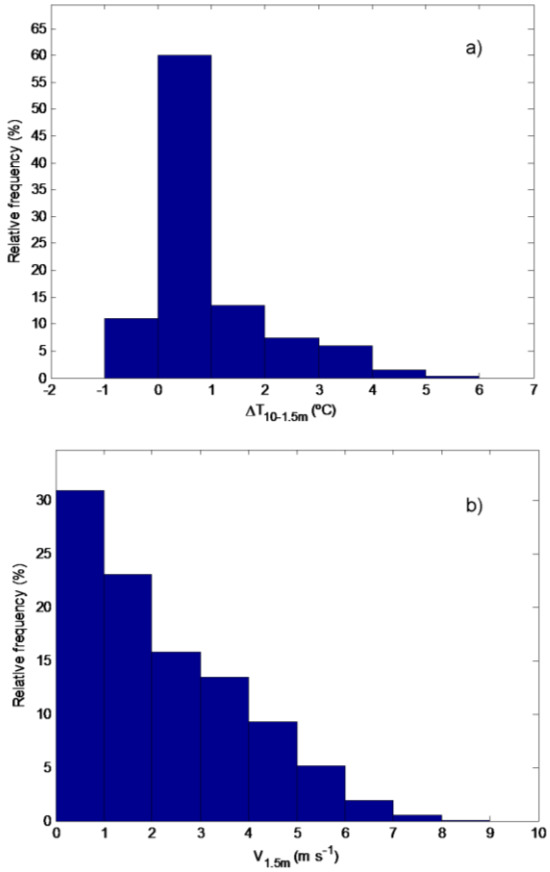

Figure 4.11. Same as Fig. 4.10 for the period 19-21 UTC.

An evolution in these distributions is found: wind presents at 1.5 m values under 1 m s^{-1} for less than 10 % of the data in the 17-19 UTC sub-period (Figure 4.10), while for 19-21 UTC (Figure 4.11) these very low values are obtained for around 30 % of the data. This decay in surface wind produces an increasing stability in 19-21 (a period which includes sunset time for nearly all the days studied) and 21-23 UTC sub-periods: in the first two hours studied (17-19 UTC), less than 20 % of the data present surface-based inversion; then for the next two hours (Figure 4.12) reach 90 %, and finally 96 % in the last one.

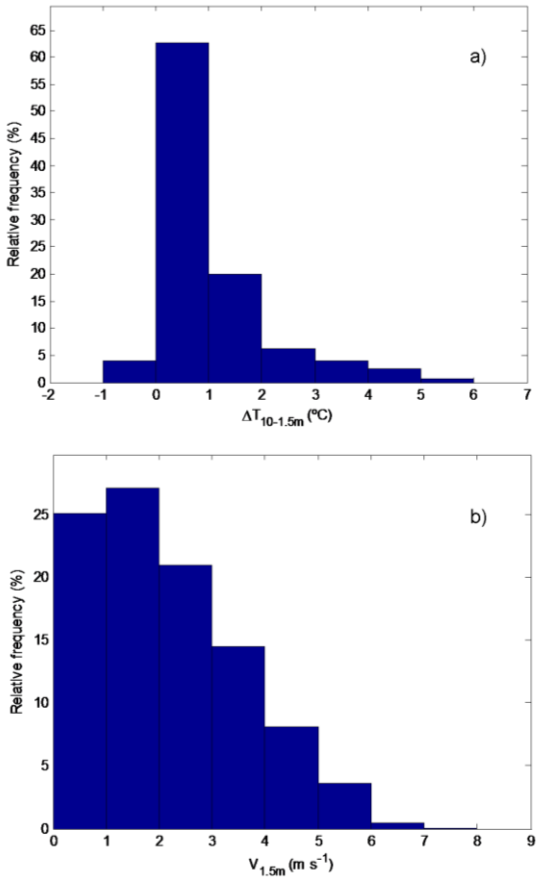

Figure 4.12. Same as Fig. 4.10 for the period 21-23 UTC.

Additionally, three different types of transitions (labelled as "A", "B" and "C") can be identified to develop a classification. In principle, qualitative criteria (like the development of temperature inversions or identifying abrupt changes in wind direction oriented to the terrain slope) were the basis to classify the transitions. Then, some thresholds were found, to finally obtain three groups, whose features are as follows. Firstly, the transitions that are controlled by moderate to high synoptic winds (A). These are quite turbulent evenings, with no surface-based inversion temperature or a very weak one, and where TKE kept reaching values higher than 1.5 m^2 s^{-2}, sometimes not very different from diurnal ones.

Secondly, there are some transitions with very small values of TKE (< 0.5 $m^2\ s^{-2}$) and wind speed before sunset, so that an early and strong surface-based inversion develops (B). This strong stability is very likely to the occurrence of katabatic winds, which can erode the stability and are sometimes are related to the generation of gravity waves (Viana et al., 2010). Finally, a third group of transitions consists of those ones with light to moderate winds before sunset, developing a soft and continuous inversion during the night without important katabatic events (C). TKE values between 0.5 and 1.5 $m^2\ s^{-2}$ are characteristic of the latter group. The three months of data collected for this work show that in this period the most common transitions are type C (39 %), followed by type B (32 %), while type A (18 %) is the least frequent to occur. There are still some cases (11 %) that cannot be easily classified as any of these three types. Examples of the evolution of TKE, temperature difference between 10 and 1.5 meters (ΔT) and wind speed are plotted in Figure 4.13, labelled for each type as A, B or C. For all these days, sunset took place around 19:00 UTC.

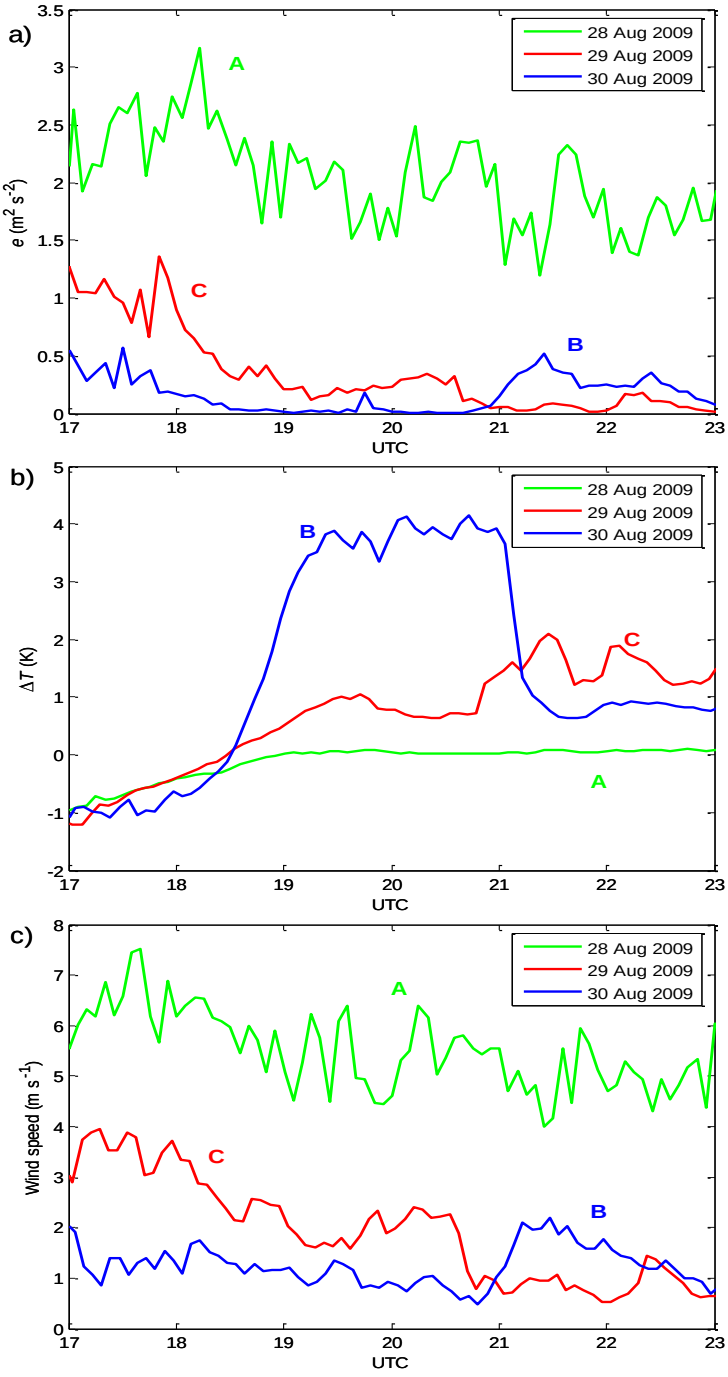

Figure 4.13. Time evolution of TKE (a), temperature difference (b) and wind speed (c) for the three kinds of transitions identified (A, B, C).

4.3 Summary and conclusions

With measurements from two high frequency types of instruments (sonic anemometer and microbarometers), a characterization of the afternoon and evening transition can be performed. Small scale phenomena occur during the transitional period, and they can be identified through MRFD and wavelet techniques. Both tools are very useful to characterize phenomena occurring in the ABL along the afternoon and evening transition. In particular, with MRFD analysis, turbulence and the evolution of different time scales responsible for boundary-layer motions can be studied. Besides, counter-gradient fluxes are identified, as well as periods with no generation of mechanical turbulence around sunset. The microbarometers measurements and wavelet technique allow another characterization of physical processes during the transition.

With another approach to experimental data treatment, based on statistical tools, some criteria are found to classify the transitions from CIBA. Considering a three summer-time months, and according to temperature inversions, abrupt changes in wind direction and TKE thresholds, three types of transitions are found, with a different occurrence frequency. A next step is to find out whether or not this classification could be extended to other locations or seasonal periods different from CIBA and summer, and in case it is appropriate, if the thresholds defined should be significantly varied or not.

Additionally, both observational approaches (case studies characterization with these high frequency devices, and statistical analysis) might be combined if enough data are available. These issues will be explored in the coming chapters.

5. Summer-time comparison of transitions at BLLAST and CIBA

In this chapter, the ABL evening transition at CIBA and BLLAST are compared with measurements from two respective two-month summer periods. After the experimental data analysis, an additional humidity sensitivity experiment with the WRF model is performed in order to evaluate the role of moisture during the transition by increasing the soil humidity at the driest site and reducing it at the other location.

5.1 Dataset and timing reference

Data from a two-month summer period are selected for this site-to-site comparison: June-July 2011 (BLLAST) and July-August 2009 (CIBA). The precipitation records were very different for these periods: 18 mm at the CIBA site (July-August 2009) versus 235 mm at the BLLAST site (June-July 2011). The instruments considered for this study and their heights are shown in Table 5.1. Globally, it is expected that at the mentioned locations and during such a season the prevalent conditions are favourable to study micrometeorological processes, as in most cases large-scale effects are weak. Nevertheless, the transitions corresponding to less stable situations

The main contents of this chapter are published as: Sastre, M., Yagüe, C., Román-Cascón, C. and Maqueda, G.: Atmospheric boundary-layer evening transitions: a comparison between two different experimental sites, Boundary-Layer Meteorol., doi:10.1007/s10546-015-0065-1, 2015.

are not initially disregarded. In this way, we obtain information on the variability at both locations for the whole summertime. Firstly, a dataset of 57 transitions from CIBA and 39 from BLLAST is analysed. The difference in the number of cases is due to data availability. Subsequently, we focus only on the transitions without significant synoptic forcing, based on rain occurrence, surface pressure gradient, geopotential height at 500 hPa, and maximum values of net radiation and sensible heat flux.

Table 5.1. Height a.g.l. of the instrumentation employed at each site.

Instrument	Height (m)	
	CIBA	BLLAST
Sonic anemometer	10	2.4
Thermo-hygrometers	1.5 and 10	2 and 15
Cup anemometers and vanes	10	15

The temporal interval analysed is an 8-h period, considering astronomical sunset as the central and reference time ($t = 0$), so it lasts from 4 h before sunset until 4 h after. Through this approach, comparable timing for both sites is achieved. For some of the calculations, 2-h sub-periods are also defined: between 4 and 2 h before sunset ($t_a = [-4, -2]$ h), the two hours just before sunset ($t_b = [-2, 0]$ h), the next two hours after sunset ($t_c = [0, 2]$ h) and between 2 and 4 h after sunset ($t_d = [2, 4]$ h).

5.2 Average observed values and statistics

Mean time series of all the transition data are shown in Figure 5.1, where an indication of the day-to-day variability is provided by the standard deviation (shadowed region). Compared to the twin plots that only consider the transitions with weak synoptic forcing (Figure 5.2), we observe qualitatively similar average results. The main quantitative differences are found in the increasing standard deviations of the dataset with a smaller number of cases. In Figure 5.2, 39 transitions from CIBA and 21 from BLLAST are used, which correspond to 68 % and 54 % of the total number of transitions shown in Figure 5.1. A focus on the transitions with weak synoptic forcing (Figure 5.2) reveals that CIBA and BLLAST present a common qualitative pattern in the evolution of variables such as $\Delta\theta$ (Figs. 5.2c,d) and wind speed (Figs. 5.2e,f), but differ in the abruptness of changes throughout the transition. The typical turbulence decay in the transition, which starts some hours before sunset, and is initially controlled by the decrease of the input solar energy, reveals a remarkable difference between the two locations: at CIBA the average decay of TKE (Figure 5.2a) is nearly continuous from a mean value of approximately 2 $m^2\ s^{-2}$ (at $t = -4$ h) to nearly 0.35 $m^2\ s^{-2}$ (at $t = 4$ h). At BLLAST (Figure 5.2b) there is a tendency to diminish from a lower mean value of 0.5 $m^2\ s^{-2}$ at $t = -4$ h (reaching a minimum around sunset of $\approx$ 0.06 $m^2\ s^{-2}$) to recover to average values between 0.1 and 0.2 $m^2\ s^{-2}$ from $t = 2$ h to $t = 4$ h. So the range of the mean value evolution is wider at CIBA, but CIBA's transitions are by far more uniform (narrower shadowed region). The more heterogeneous and complex terrain at BLLAST may be responsible for this larger variability.

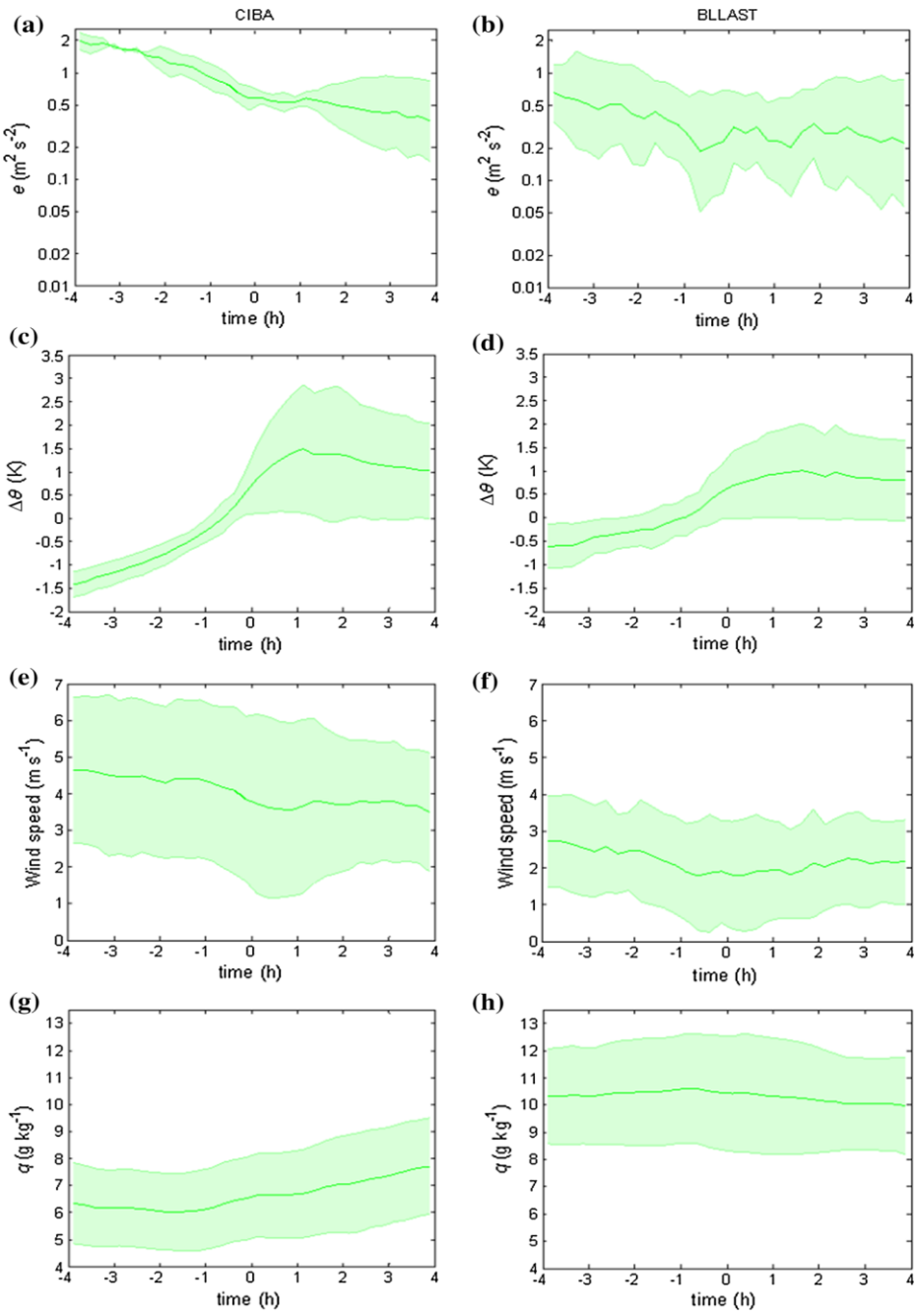

Figure 5.1. Mean temporal evolution of TKE at CIBA (a) and BLLAST (b); potential temperature difference between two levels at CIBA (c) and BLLAST (d); wind speed at CIBA (e) and BLLAST (f); specific humidity at CIBA (g) and BLLAST (h). Shadows indicate standard deviations.

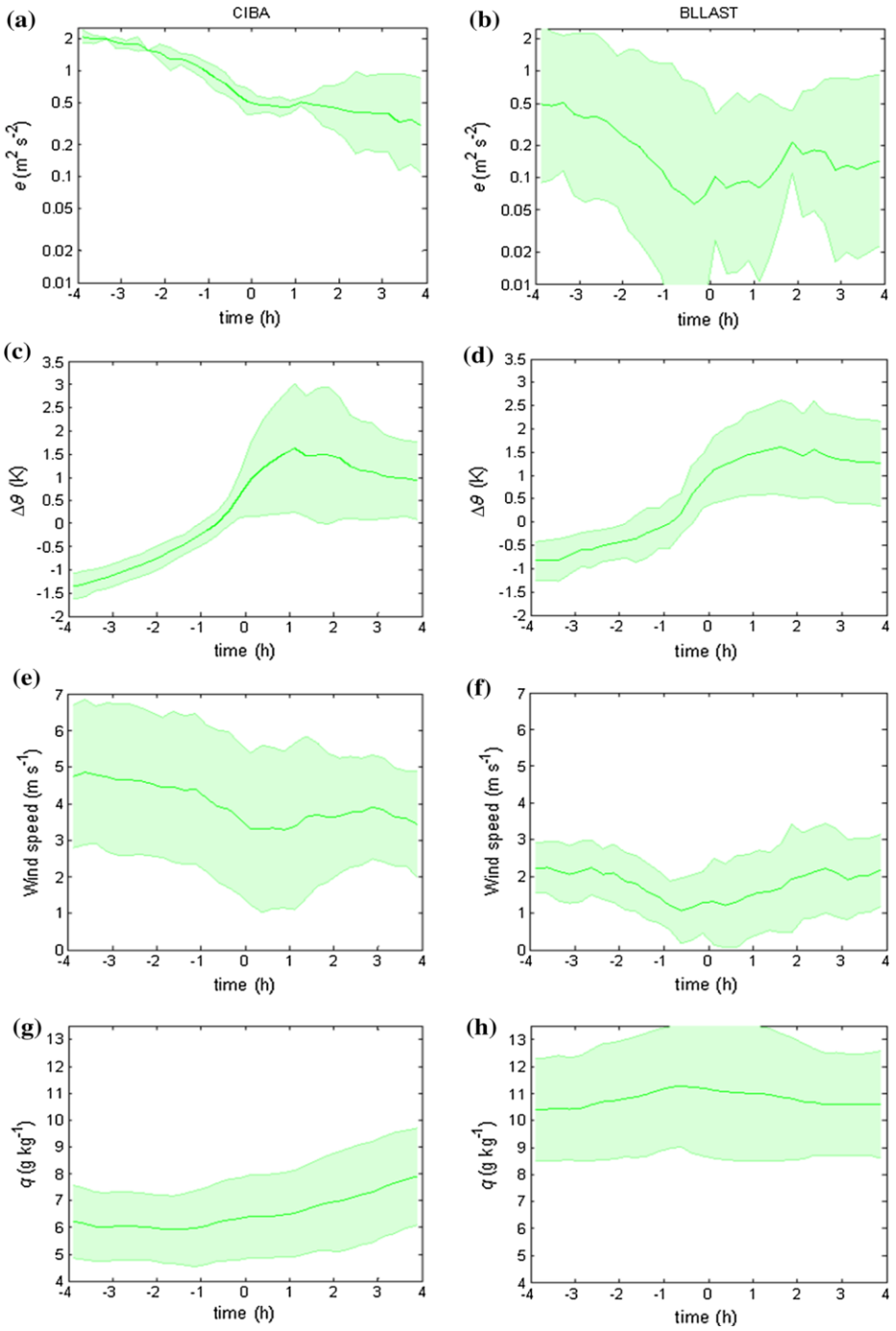

Figure 5.2. Same as Fig. 5.1, considering only transitions with weak synoptic forcing conditions.

Average TKE at CIBA presents an increase of the standard deviation from t = 1 h on, indicating that different nocturnal regimes for a similar synoptic situation can occur (Yagüe et al., 2007). $\Delta\theta$ presents, on average (Figs. 5.2c,d), a considerably larger range at CIBA (from –1.5 to 1.5 K) than at BLLAST (from –0.75 to 1 K). This site-to-site disparity in the heating (day) or cooling (night) is probably linked to soil humidity differences, which are analysed later in this chapter (section 5.4).

Wind speed often experiences, on individual days, a progressive decay during the transition until a minimum value around sunset; afterwards it partially recovers. This effect is captured in the average values (Figs. 5.2e,f). On occasions a drainage flow takes place, and a sudden change in wind direction tends to occur synchronous with the increase in wind speed.

Figure 5.3 (CIBA) and Figure 5.4 (BLLAST) show the wind distribution for the weak synoptic conditions dataset in the four temporal sub-intervals previously defined for the transition (t_a, t_b, t_c, t_d). The predominant direction experiences an evolution due to katabatic winds at both locations, which were characterized as in previous studies in the case of the CIBA site (Yagüe et al., 2007; Cuxart, 2008; Martínez et al., 2010). The flow is actually driven by the respective local slopes (north-east at CIBA and south-south-east at BLLAST). The change of the statistically more frequent direction from t_a to t_d, associated with a drainage or katabatic flow, appears as well when the whole transition dataset is considered (not shown). This is especially remarkable since those statistics would include very different synoptic situations. Consequently, it is shown that katabatic flows are characteristic of the transitional period, but with site-to-site differences. Due to its closeness to mountain ranges, the BLLAST site presents more frequently than CIBA the drainage flow direction after sunset (during t_c and t_d). As a counterpart, the most intense

katabatic events are found at CIBA, probably due to stronger radiative cooling (Stull, 1988).

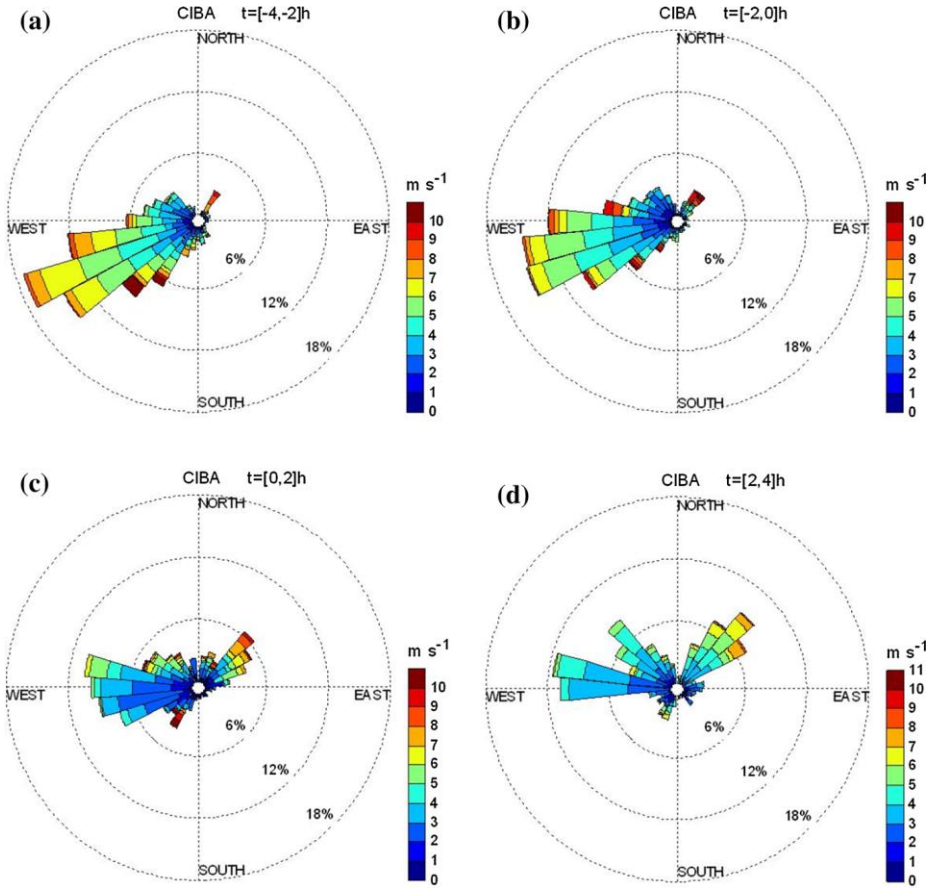

Figure 5.3. Observed wind distribution at the CIBA site for the normalized time interval: a) [–4, –2] h, b) [–2, 0] h, c) [0, 2] h, d) [2, 4] h. The transitions with strong synoptic forcing have not been included.

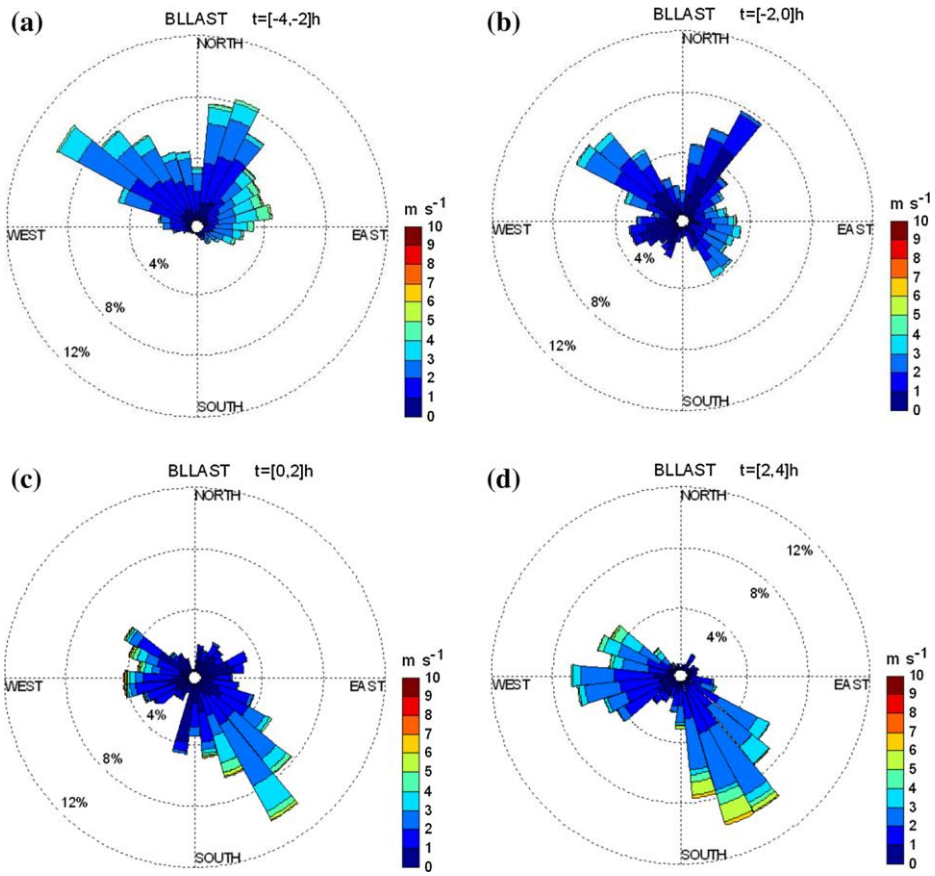

Figure 5.4. Same as Fig. 5.3 for the BLLAST site.

Nevertheless, there is a variable whose time evolution is not similar at both sites, neither on average nor for individual cases, the air specific humidity (Figs. 5.2g,h). At the CIBA site its average pattern is practically constant (6.5 g kg^{-1}) until around t = –1 h, then increasing because of atmospheric boundary-layer depth reduction, associated with nocturnal stability. This happens because water vapour tends to accumulate close to the ground. In accordance with the climatological information (Chapter 2), mean values obtained at BLLAST are somewhat larger than at CIBA during the whole transition. These differences are congruent with soils much more humid at BLLAST than at CIBA. Average temporal evolution at

BLLAST is maintained around its value at $t = -4$ h (10.5 g kg^{-1}) with a small decreasing tendency. This is probably due to nocturnal condensation near the ground (relative humidity at night is frequently over 80 %, not shown). The standard deviation shows a similar range of values at the two sites, except at $t \approx 0$, when the day-to-day variability is larger at the BLLAST site. Moreover, after sunset at the CIBA site a relation between higher values of specific humidity and weaker temperature inversions appears, while the same link is not very clear at BLLAST (not shown). As humidity is the variable with the greater differences between one site and the other, it is worth investigating its connection with the near-surface cooling. We consider three aspects: the soil emissivity, the heat capacity and the radiative absorption in the lower atmosphere. First of all, the emissivity of a surface rises when its moisture increases, so we expect that the higher the soil moisture, the more intense the nocturnal cooling. However, for the typical values of soil moisture the relative variations in emissivity are not large (0.92-0.96, according to Mira et al., 2007), and is even smaller the effect on the near-surface air temperature. On the other hand, considering the greater heat capacity of water, increasing the humidity at the surface would directly trigger lower cooling. Finally, the water vapour close to the surface plays a role in the radiative energy absorption, and consequently having larger values of specific humidity decreases the near-surface cooling. So the net effect of increasing humidity (both at soil and near the surface) would be to reduce near-surface cooling.

Several average parameters for the two sites are summarized in Table 5.2 (CIBA) and Table 5.3 (BLLAST), together with minimum and maximum values, and are classified taking into account the four 2-h sub-periods (t_a, t_b, t_c, t_d). Wind speed mean values and turbulence parameters are larger at the CIBA site, which is linked to a later formation of the surface-based temperature inversion compared to the BLLAST site (Table 5.4). A difference in timing between sites can be found as well in values of the stability indicator ($\Delta\theta/\Delta z$) in Table 5.2 and Table 5.3. For the second

sub-period (t_b) they are very close to zero, but present a different sign (on average). Moreover, both these temperature inversions developing after sunset, as well as the associated stability, are stronger at the CIBA site (see also Figs. 5.2c,d), despite the fact that they start to form later than at the BLLAST site. This is thought to be due to the lower values of soil humidity and surface specific humidity, which, as previously indicated, enable greater cooling.

Table 5.2 CIBA (weak synoptic forcing conditions) average values of wind speed (U), potential temperature difference gradient ($\Delta\theta/\Delta z$), turbulent kinetic energy (e), friction velocity (u_*), and turbulent heat flux (H) for the sub-periods defined. Subscripts indicate height (m) a.g.l. Extreme (maximum and minimum) values for each interval are between brackets.

	t_a = [–4, –2] h	t_b = [–2, 0] h	t_c = [0, 2] h	t_d = [2, 4] h
U_{10} (m s^{-1})	4.7 [0.7, 12.7]	4.1 [0.2, 11.6]	3.4 [0.1, 11.5]	3.7 [0.7, 8.8]
$\Delta\theta/\Delta z_{10\text{-}1.5}$ (K m^{-1})	–0.1 [–0.2, 0]	0 [–0.1, 0.3]	0.2 [0, 0.7]	0.1 [0, 0.6]
e_{10} (m^2 s^{-2})	1.8 [0.1, 8]	0.9 [0.002, 5]	0.5 [0.002, 6]	0.4 [0.003, 3]
u_{*10} (m s^{-1})	0.5 [0.06, 1]	0.3 [0.009, 1]	0.2 [0.003, 1]	0.2 [0.006, 0.8]
H_{10} (W m^{-2})	183 [–37, 607]	20 [–55, 253]	–16 [–91, 57]	–19 [–82, 63]

Table 5.3. Same as Table 5.2 for BLLAST.

	t_a = [–4, –2] h	t_b = [–2, 0] h	t_c = [0, 2] h	t_d = [2, 4] h
U_{15} (m s^{-1})	2.1 [0.2, 4.4]	1.4 [0, 3.8]	1.4 [0, 6.4]	2.1 [0, 5.6]
$\Delta\theta/\Delta z_{15\text{-}2}$ (K m^{-1})	–0.1 [–0.1, 0]	0 [–0.2, 0.1]	0.1 [0, 0.3]	0.1 [0, 0.3]
$e_{2.4}$ (m^2 s^{-2})	0.4 [0.02, 2]	0.1 [0.003, 0.8]	0.1 [0.003, 3]	0.1 [0.004, 1]
$u_{2.4}$ (m s^{-1})	0.2 [0.06, 0.5]	0.1 [0.01, 0.3]	0.09 [0.008, 0.6]	0.1 [0.006, 0.4]
$H_{2.4}$ (W m^{-2})	46 [–28, 185]	0 [–40, 55]	–6 [–65, 21]	–9 [–70, 16]

Table 5.4. Mean time for sensible heat flux (H) and potential temperature difference ($\Delta\theta$) crossover considering weak synoptic forcing transitions, with sunset (t = 0 h) as the time reference.

	H = 0 (W m^{-2})	$\Delta\theta$ = 0 (K)
CIBA	–47 min	–43 min
BLLAST	–1 h 33 min	–1 h 37 min

Focusing on CIBA, two opposite effects of near-surface cooling are observed: on the one hand, moisture, whose lower values favour stronger

inversions, and on the other, more intense turbulence, which inhibits formation of the temperature inversions. At the CIBA site, greater mean stability values ($\Delta\theta/\Delta z$) are obtained, and the role played by humidity is therefore more decisive than the effect of its counterpart mechanical turbulence. Furthermore, condensation occurs close to the surface more frequently at the BLLAST site, causing a slight decrease in specific humidity, releasing latent heat, and undermining the strength of these surface-based inversions. At CIBA, the lower surface humidity supports greater surface heating and convection during daytime, leading to increased TKE, whereas after $t = 0$ h, surface cooling is enhanced as a result of the lower moisture values, thus allowing the possibility of a katabatic event and favouring the development of turbulence. In general terms, greater differences are found between the minimum and the maximum values in every sub-period (Table 5.2 and Table 5.3), as occurs for average evolution (Figure 5.2).

To evaluate the influence of the different sonic anemometer heights (Table 5.1) we focus upon H, friction velocity, and TKE (Tables 5.2 and 5.3 and Figure 5.2), finding higher absolute values at the CIBA site. On the one hand, for diurnal and afternoon conditions, both heights are expected to be included in the surface layer and accordingly, the turbulent fluxes are almost constant. This means that the sonic anemometer measurements are comparable at both sites during the initial part of the transition. On the other hand, if we consider a hypothetical situation of very strong nocturnal stability, then the sonic anemometer at the CIBA site (10 m a.g.l.) might be above the surface layer. This implies that the turbulence measured could not be as intense as if the device had been installed at the same height as its counterpart at the BLLAST site (2.4 m a.g.l.). Nonetheless, as mentioned before, the turbulence values are greater at the CIBA site than at the BLLAST locality. Consequently, if anemometer's heights were the same at both locations, the values of the

turbulent parameters would be even greater at the CIBA site than the ones actually obtained at the BLLAST site during the night.

In the previous chapter of this thesis, three kinds of transitions were described at CIBA (Sastre et al., 2012):

a) windy with practically no temperature inversion

b) early strong inversions with katabatic events

c) intermediate cases with a gentle and continuous inversion during the night.

An attempt to extend this labelling to the BLLAST site dataset proved unsuccessful because transitions which do not fit in any of the three groups represent too high a percentage. This issue suggests that transitional processes exhibit more complexity at the BLLAST site, and the former three-type classification therefore cannot be extended here as it was initially constructed. However, the transitions with katabatic or drainage flow events are also easily identified at BLLAST. A composite of these transitions for both sites (Figure 5.5) reports a similar qualitative evolution as in Fig. 5.2 (weak synoptic forcing transitions). Nevertheless, the katabatic transitions (Fig. 5.5) reveal in the BLLAST site a deeper minimum in the average TKE and stronger nocturnal stability, linked to a decrease in specific humidity. On average, the values in Fig. 5.5h are around 1 g kg^{-1} lower than in Fig. 5.2. For the CIBA site, the main differences are related to the wind field and TKE. Specifically, wind speed evolution exhibits another difference: the katabatic events (Fig. 5.5e) show sustained relative low values, rather than a minimum prior to a change in direction. This is similar to the almost absolute calm around sunset detected at the BLLAST site (Fig. 5.5f). Between $t = -4$ h and $t = -3$ h, relatively weak winds are observed (averaging 3 m s^{-1}, versus nearly 5 m s^{-1} in Fig. 5.2e), and sometimes these lower values extend in time for 1 h longer.

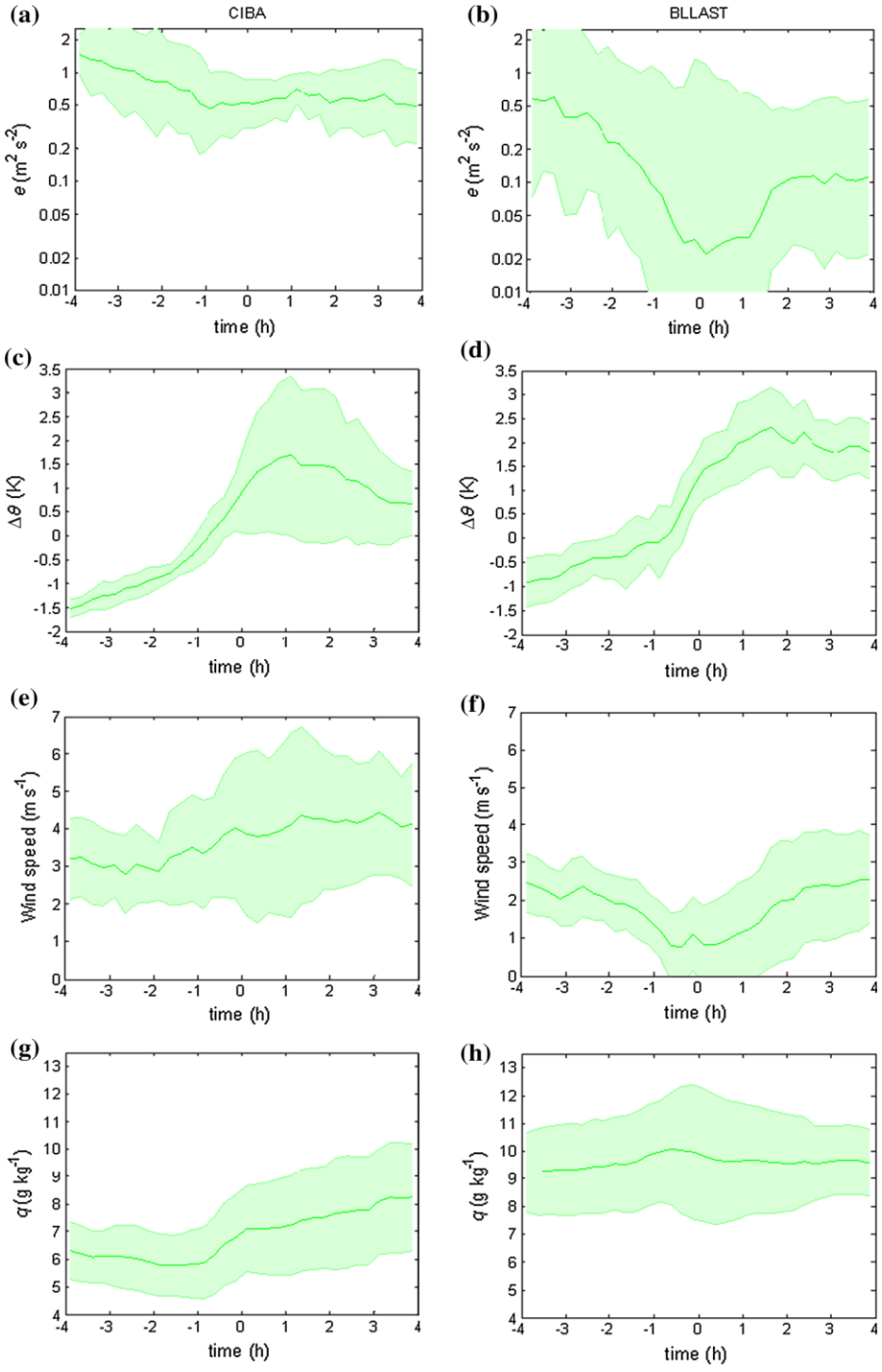

Figure 5.5. Same as Fig. 5.1, considering only transitions with katabatic events.

These conditions favour the katabatic events at the CIBA site, through a decline in the turbulent mixing and more intense radiative cooling. Furthermore, as the katabatic events tend to be more intense at the CIBA site than at the BLLAST site, they are often capable of substantially weakening the temperature inversion already developed. Drainage flows at the BLLAST site can partially erode the inversion, but they are not sufficiently intense to enable erosions as remarkable as those occurring at the CIBA site. This causes an increase in mean $\Delta\theta$ values (initially higher at the CIBA site due to greater surface cooling) at the BLLAST site from $t \approx 1$ h onwards. It is also striking that the absolute values shown in Fig. 5.5 at CIBA may not be totally comparable with their counterpart at the BLLAST site during the nighttime, because of the different heights of the instrumentation (see Table 5.1). Nonetheless, comparison can be made of each site plot in Fig. 5.5 with its analogous plots in Fig. 5.2.

5.3 Case study

For an individual comparison, two days (BLLAST: 2 July 2011; CIBA: 5 August 2009) are selected, as their synoptic situations are similar regarding 500-hPa geopotential height and surface pressure gradient (not shown). Both correspond to quite strong surface-based temperature inversions (reaching $\Delta\theta > 3$ K) subsequently eroded by drainage or katabatic flows (peak values around 3 m s^{-1} and 7 m s^{-1} respectively).

Figure 5.6 shows MRFD plots of the friction velocity. A change in the contributions to the turbulence of the eddy scales takes place during the transition, with qualitative similarities between both days. In the afternoon, convection-related larger scales control the turbulence processes. Subsequently, especially after $t = 1$ h, the most relevant scales are the smaller ones, often associated with mechanical effects.

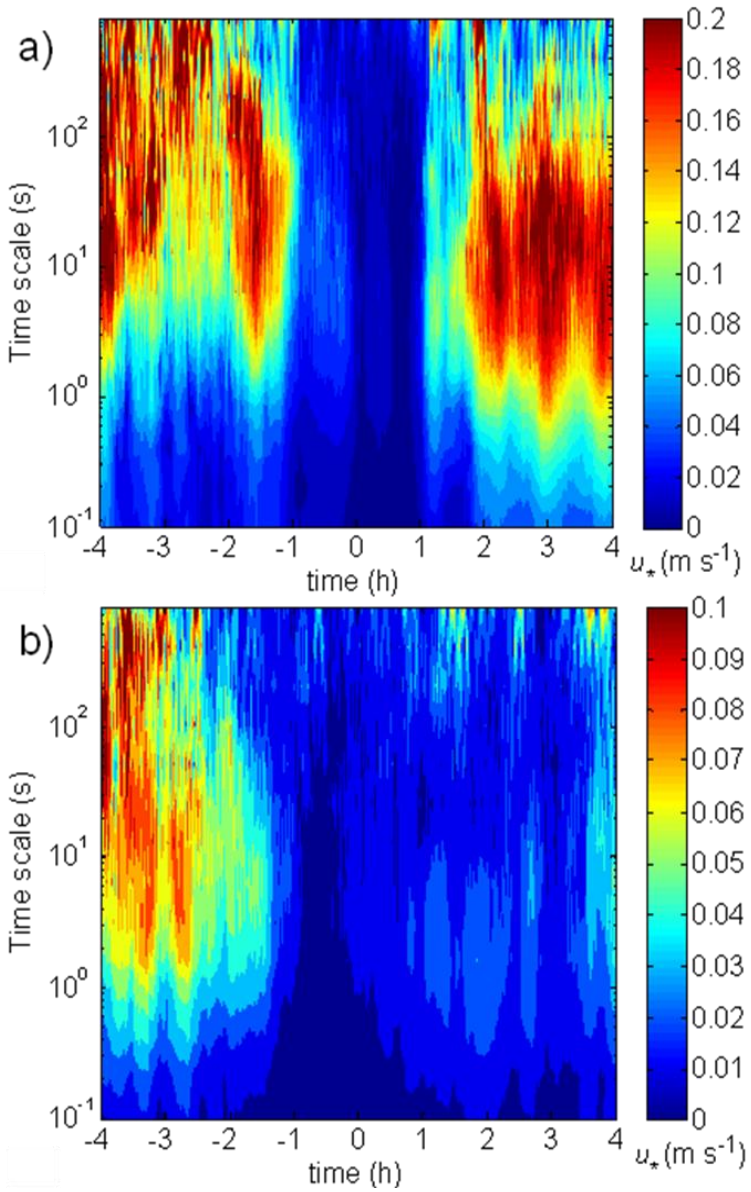

Figure 5.6. MRFD values for friction velocity (m s^{-1}) of the case study: a) 5 August 2009 (CIBA), b) 2 July 2011 (BLLAST). Notice that a different colour bar scale is employed for each plot.

We obtained this result for near-surface data, but a different evolution in time scales is expected to occur at the upper levels. In any case, higher values of friction velocity are reached at the CIBA site, not only in this case study, but for most of the transitions involving fair weather conditions. Turbulence decay begins before t = 0 h, and we find a progressive narrowing of the time scales responsible for this, until a minimum value is obtained at all the time scales represented. These very low values occur earlier in the case of the BLLAST site, likely due to the combination of two factors affecting turbulence production: an earlier decrease in H (diminishing buoyant production) and less wind shear close to the surface (decreases in mechanical production). Following this minimum value, turbulence shows an increase due to a katabatic or drainage flow. The CIBA case exhibits this phenomenon more intensely and abruptly, with contributions comparable to afternoon values, despite the smaller time scales involved. In fact, stronger nocturnal cooling is favoured by lower moisture values, and more intense katabatic wind can therefore be generated (Stull, 1988). This pattern, associated with such flows, is frequently observed at the CIBA site (Viana et al., 2010; 2012).

Figure 5.7a provides the time series of the friction velocity for both transitions. For easier comparison, a normalization is performed in Fig. 5.7, dividing the series according to their corresponding values at the beginning of the period of study (t = –4 h). Greater nocturnal turbulence can be found for the CIBA case, whose values are, as from t = 2 h, as high as the initial ones. This evolution is also linked to $\Delta\theta$ (Fig. 5.7b), as earlier described (section 5.2). The effect of the katabatic flow erodes the inversion formed, and as the wind is more intense for the CIBA case, $\Delta\theta$ is more significantly reduced. Indeed, considering these relative values (Fig. 5.7b), the evolution of $\Delta\theta$ is very similar for both cases until approximately t = –1 h. Then relative cooling occurs abruptly in the BLLAST case study, but erosion of the temperature inversion is nearly complete in the CIBA case study, with $\Delta\theta \approx 0$ K around t = 3-4 h.

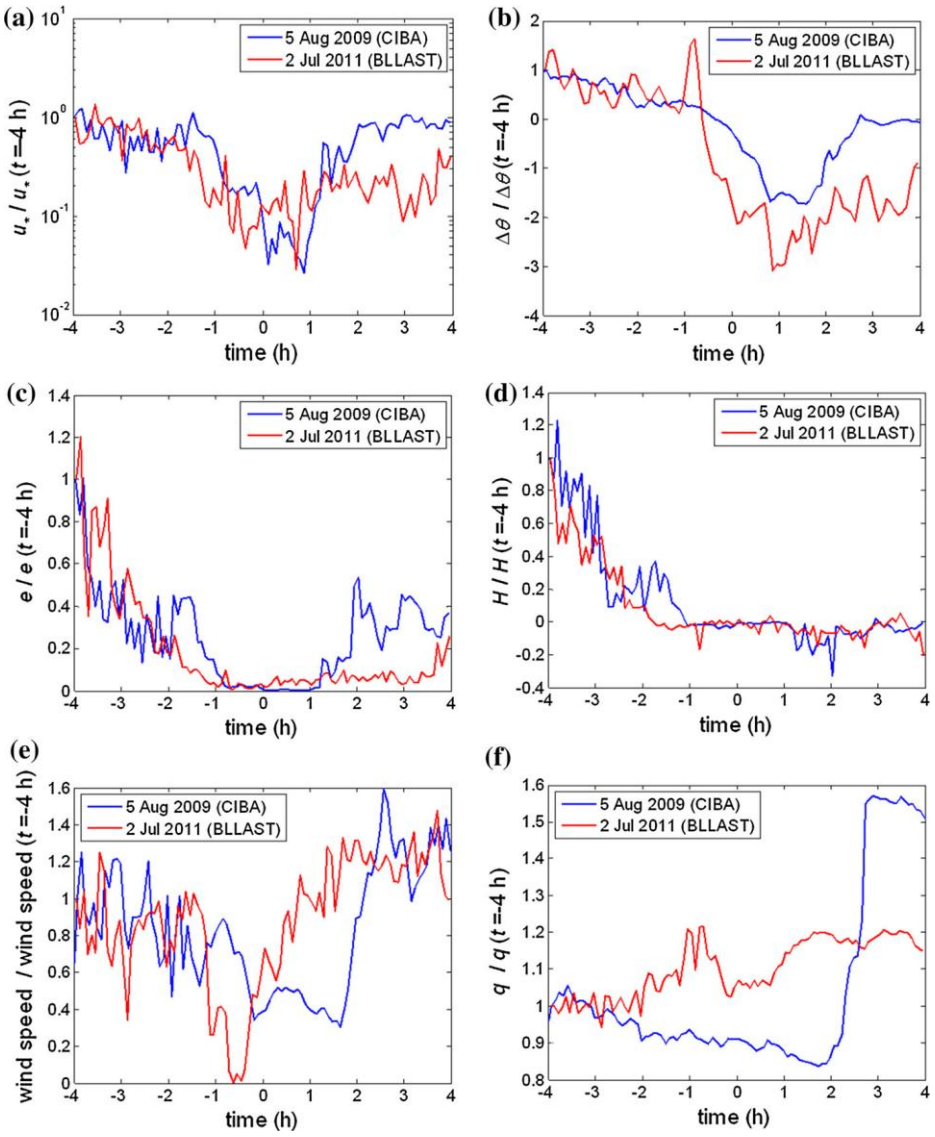

Figure 5.7. Time evolution of the case study chosen for CIBA (blue) and BLLAST (red): a) friction velocity (log scale), b) potential temperature difference between two levels, c) TKE, d) sensible heat flux, e) wind speed, f) specific humidity. A normalization is applied dividing each value by the corresponding value at the beginning of the time period studied ($t = -4$ h).

Despite larger TKE absolute values at CIBA (not shown), in accordance with average calculations (Table 5.2), when normalization is performed, the evolution shows some differences in turbulence behaviour (Fig. 5.7c). In the case of the BLLAST site, after t = –1 h a very homogeneous evolution is obtained, unlike at the CIBA site. The highest relative TKE values alternate between sites: for the initial 2-h period (t_a) BLLAST scores the highest, and during the next 2 h (t_b) the higher values are obtained at CIBA. At the beginning of the third sub-period (t_c), we find very low relative values for CIBA for over 1 h (including wind minimum, see Fig. 5.6a), but afterwards there is an increase in relative TKE. This is linked to the katabatic event, and greater values are maintained at the CIBA site during the last sub-period (t_d). These locally higher relative values of turbulence at BLLAST are apparent, as the absolute values are greater at CIBA, but they highlight the fact that turbulence decay occurs earlier at the BLLAST site. On the other hand, the evolution of normalized H (Fig. 5.7d) is similar for both cases. This means that for H, the biggest differences basically concern the absolute values (typically around 250 W m^{-2} at CIBA versus nearly 70 W m^{-2} at BLLAST when t = –4 h, not shown). Finally, a significant difference is observed between normalised wind speed (Fig. 5.7e) and humidity (Fig. 5.7f). In the case of the CIBA site, the katabatic flow is accompanied by a substantial increase in specific humidity, and these are closely correlated. This is mainly associated with humid advection from the north-east, in agreement with Viana et al. (2010) and Udina et al. (2013). In contrast, the increase in wind speed after its minimum around sunset is not followed by an increase in humidity at the BLLAST site, because in general terms this is relatively high at this site and advection from the Pyrenees does not give rise to significant variation. Moreover, when the wind minimum is reached, a peak humidity value occurs. This might be associated with a local reduction of the PBL volume due to the practical absence of wind. Nevertheless, in our case study the evolution of humidity is not totally representative of the global behaviour

of the BLLAST transitions (Fig. 5.2h). It presents relative humidity values lower than usual, and the typical decrease in specific humidity resulting from condensation does not occur.

5.4 Humidity sensitivity experiment with WRF

With the aim of testing the role played by humidity in transitional processes, two kinds of simulations are performed: 1) considering the standard conditions of each site, and 2) modifying soil moisture. Version 3.5 of the WRF model is here considered, using three nested domains (grids of 9, 3 and 1 km) centred on the coordinates of both BLLAST and CIBA experimental sites. The model works with initial and boundary conditions from NCEP reanalysis (Kalnay et al., 1996); in particular the NCEP FNL (Final) Operational Global Analysis data are on 1x1 degree grids prepared operationally every 6 hours. Regarding the vertical resolution, the modelling tests are performed with 50 eta levels, 28 being located within the first km of the troposphere (eight between the surface and 100 m). The spinup time is 24 hours (Tastula et al., 2015), with a timestep of 3.3 seconds. Considering the model physics, the main options are chosen as follows: the unified Noah land-surface model; YSU as the PBL parametrization; the modified MM5 surface-layer scheme (Jiménez et al., 2012); the rapid radiative transfer model (RRTM) for the longwave radiation (Mlawer et al., 1997); the Dudhia scheme (Dudhia, 1989) for the shortwave radiation; and the WRF single-moment 3-class (WSM3) microphysical scheme (Hong et al., 2004).

The results correspond to a selected transition from BLLAST (Fig. 5.8) and CIBA (Fig. 5.9), which are the same cases as in the previous section.

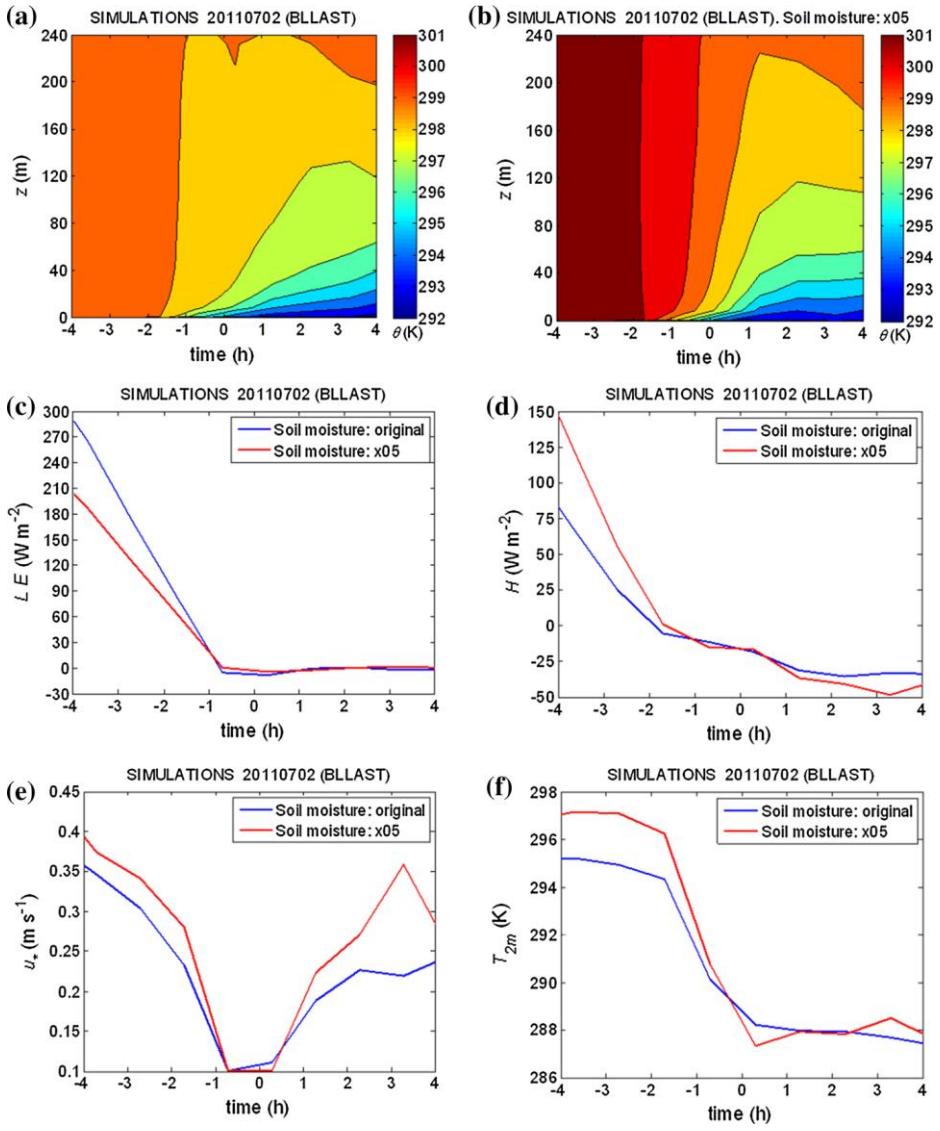

Figure 5.8. WRF model simulations for a BLLAST case with original or modified soil moisture: a) potential temperature at different heights (original soil moisture), b) potential temperature at different heights (reduced soil moisture 50 %), c) latent heat flux, d) sensible heat flux, e) friction velocity, f) 2-m temperature.

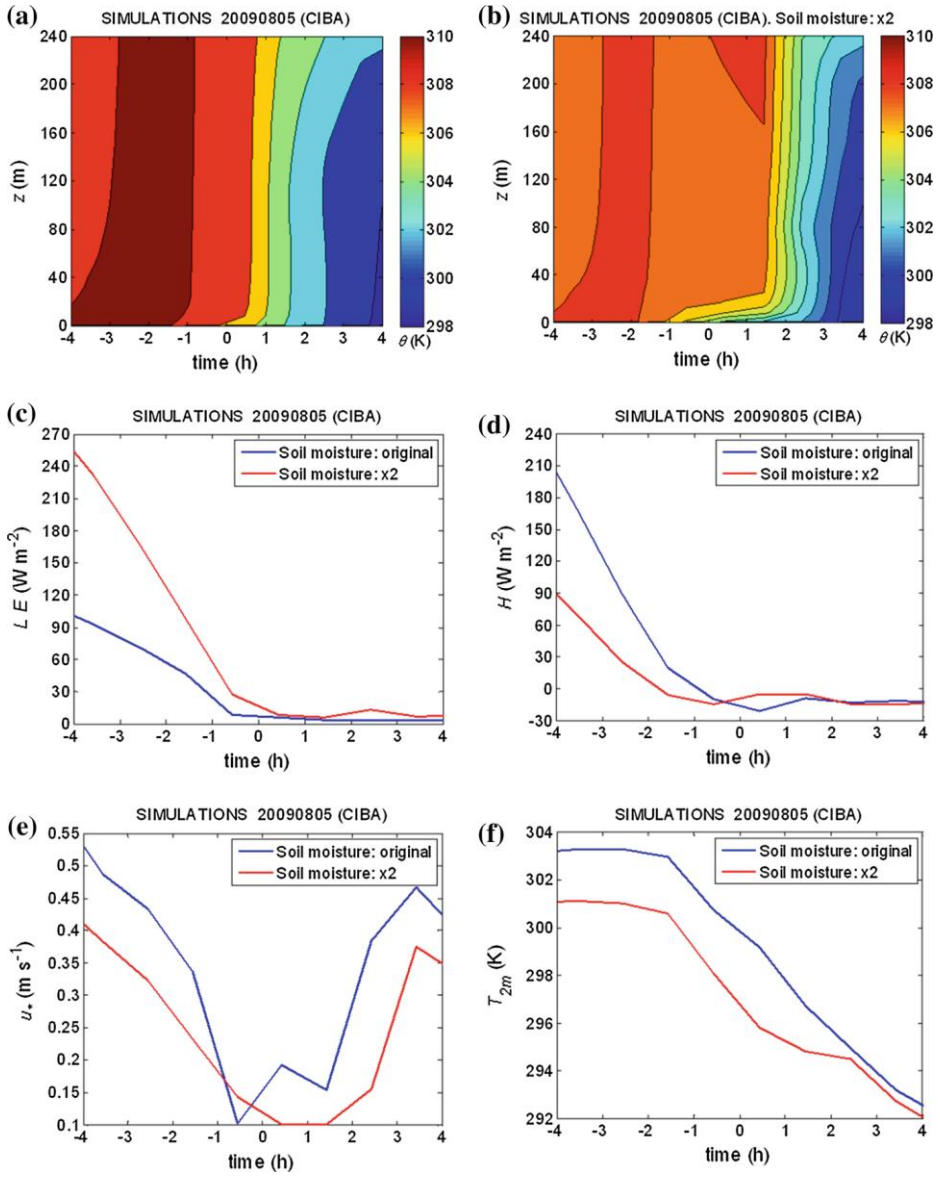

Figure 5.9. WRF model simulations for a CIBA case with original or modified soil moisture: a) potential temperature at different heights (original soil moisture), b) potential temperature at different heights (enhanced soil moisture x2), c) latent heat flux, d) sensible heat flux, e) friction velocity, f) 2-m temperature.

For the CIBA simulations we multiply soil humidity by 2 throughout the inner domain, whereas for the BLLAST simulations, the original soil humidity is divided by 2. In fact, the soil moisture values originally considered by the model at the CIBA site are approximately 50 % of the values initially used for the BLLAST site, in accordance with the average specific humidity values shown in Figs. 5.2g,h. Consequently, in this experiment, simulations with similar soil moisture at both locations are run.

At the BLLAST locality, a decrease in soil moisture has an impact on the temporal evolution of the potential temperature before sunset (Figs. 5.8a,b), giving rise to values of up to 3 K higher than the not-reduced soil moisture simulation. This was somehow to be expected, because of the greater energy availability for sensible heat, as not much is now required for latent heat. One soil variable is modified and consequently the differences are more likely to be bigger close to the surface. Nevertheless, we found that this effect is transmitted to the upper levels too. On the contrary, when surface cooling begins, very similar results for both simulations are rapidly obtained. A parallelism is found for latent heat flux (Fig. 5.8c), sensible heat flux (Fig. 5.8d) and 2-m temperature (Fig. 5.8f), as both types of simulations reach almost the same values after $t = -1$ h. This fact suggests that the role played by humidity is not as relevant after sunset as it is before it. Differences between both simulations in the sensible heat flux (Fig. 5.8d) after $t = 1$ h might be due to a more remarkable increase in nighttime wind (not shown) and turbulence. Indeed, the friction velocity (Fig. 5.8e) shows a very similar qualitative evolution, with a deep minimum around sunset, as in the observations, and with higher afternoon and nocturnal values when soil moisture is reduced (red line). This means that moisture significantly influences turbulence during the transition. Furthermore, considering the simulated 2-m temperature evolution (Fig. 5.8f), the cooling effect is more significant on reducing soil moisture, as afternoon temperature reaches higher values in the reduced humidity

simulation, undergoing a stronger decay between t = –2 h and t = 0 h. Again, this is related to the higher values of turbulence provided by the drier simulation. Nocturnal temperature values do not essentially vary between simulations.

At the CIBA site, the experiment consisted of increasing soil humidity. Most of the results are analogous to the previous experiment for the case of the BLLAST site, but some particular effects were also observed. Firstly, the potential temperature is similarly affected before sunset: if soil moisture is increased, cooler values of θ are reached, even at higher levels (Figs. 5.9a,b). Moreover, surface cooling starts earlier in the case of enhanced humidity. This cooling effect is transmitted to the upper levels, developing a stratified layer very close to the surface (Fig. 5.9b) between t = 0 h and t = 2 h, associated with a long-lasting wind speed minimum (not shown). There is another direct effect of increasing soil moisture: latent heat flux (Fig. 5.9c) doubles its former values at t = –4 h and remains at around this rate throughout practically the whole transition decay; this rate is also observed for the lower nighttime values. For the sensible heat flux (Fig. 5.9d), the simulation with increased moisture (red line) projects the crossover approximately 1 h earlier, which is consistent with observational results (Table 5.4). This means that the values provided, compared with the ones considering standard soil moisture, are reduced before sunset, but from t = 1 h, practically identical results were obtained in both simulations. As for friction velocity (Fig. 5.9e), we observed that the driest simulation enables greater turbulence to occur. This is exactly the same effect as in the BLLAST simulations (Fig. 5.8e), with an equal pattern of afternoon decay, minimum and nocturnal increase. Finally, the 2-m temperature (Fig. 5.9f) modified humidity simulation presents cooler values than the one employing standard humidity (2 K) at t = –4 h. This bias remains almost constant until t = 3 h, when both simulations provide approximately the same value.

To summarise, with higher soil moisture, surface heating is less intense before sunset. This produces a weaker exchange with the upper atmospheric layers and affects wind speed too. In the nighttime, the effect of enhanced soil moisture is directly related to lower near-surface cooling and a to different katabatic flow behaviour pattern. The effect of significant variations in humidity is globally more noteworthy in the CIBA simulations for most of the magnitudes and timing explored, and can also be observed with other variables not presented herein. For example, for t_a sub-period, the boundary-layer height undergoes variations of around 50 % of its original simulated values (not shown). This is seen at both locations and, likewise, these values increase with reduced moisture and vice versa. Subsequently, the two simulations tend to converge since t = –1 h, occurring rapidly at the BLLAST site, but requiring longer at CIBA. Additionally, there is a systematic shift in wind direction between simulations of around 70 º at the CIBA site and less than 40 º at BLLAST from t = –4 h to t = 0 h. Subsequently, for the BLLAST site both simulations provide the same wind direction, whereas for CIBA, the simulations do not converge until t = 3 h. In both cases, this direction corresponds to the respective local terrain slopes. In general terms, at the more heterogeneous BLLAST site, modifying humidity exerts an important effect, but not as much as at the CIBA site, likely due to the fact that at the BLLAST site other effects add complexity, which would appear to act as mechanisms compensating for variations in soil moisture. In any case, although the response of the model to soil moisture changes is essentially similar, we observe certain local differences depending on the site.

5.5 Summary and conclusions

Several similarities from both observational datasets have been found, mainly associated with the qualitative evolution of the meteorological variables controlling the physical processes. Significant

quantitative differences, however, are obtained between CIBA and BLLAST results, especially in the maximum and minimum values of wind speed or sensible heat flux. Additionally, timing differences in katabatic or drainage flows are observed, and are related to the final stage of turbulence decay. Greater surface heating and diurnal convection is found at the CIBA site, showing a direct connection with the lower values for humidity at this location. Constraining the study to transitions with weak synoptic forcing provides insight into the similar variability of both the summertime dataset and that with only fair weather transitions. Moreover, it has helped to better identify the most characteristic events of weak-synoptic-forcing transitions, such as the wind minimum around sunset. Furthermore, the global behaviour of the transition is not very different when considering the complete datasets, or only the group of fair weather transitions.

Using MRFD technique, turbulence and the evolution of different time scales are studied. It is reported that turbulence developing at night, corresponds to smaller time scales, in relation to afternoon turbulence, although the friction velocity at CIBA can reach similar values at night due to a strong katabatic flow. Again, with MRFD periods with no generation of mechanical turbulence around sunset are characterized: they take place at different times depending on the location, despite the fact that both refer to local sunset. A key factor of the differences in radiative surface cooling during the afternoon and evening transition appears to be associated with soil moisture at the specific location, and atmospheric humidity near the surface, also influencing the timing of the typical transitional events. Both the observations and the WRF model experiment confirm that humidity constitutes a very important variable for modulating the effect of turbulence on surface temperature, and once again, differences are found between sites. Soil moisture, apart from influencing the sensible and latent heat fluxes, usually through the relationship with near-surface temperature, plays a role in the friction velocity, which is linked to mechanical turbulence. Globally, the results confirm the fact that drier

conditions favour more intense turbulence. In addition, humidity decisively affects the whole transition, especially before sunset, and not only close to the ground, but also at upper levels. It is significant that the effects of varying soil moisture are more noteworthy at the less humid and more homogeneous site (CIBA), even lasting for several hours after sunset. This indirectly implies that other effects, apart from humidity, are considerable in heterogeneous terrain (BLLAST), for the late afternoon and evening transition processes.

6. Modelling the afternoon and evening transition processes

In the current chapter, the ABL afternoon and evening transition is studied through WRF numerical simulations, using BLLAST field campaign case studies for validation. The aim is to identify and understand model deficiencies and try to provide improvements to the transition modelling. The sensitivity of WRF to PBL and LSM is studied by testing combinations of three PBL parametrizations and three LSM schemes. Other model sensitivity experiments are performed, including tests adding one outer nested domain, or with only a larger one, and simulating with soil temperature and moisture self-spinup.

6.1 Model settings and data used for validation

Several tests are designed, being as follows the basic configuration, used for most of the simulations. Those specific settings which are different for some simulations will be subsequently explained. Three nested model domains with horizontal resolution of 9, 3 and 1 km are centred at 43º7'N, 0º21'E (BLLAST site), with grids consisting of 100×100 cells. There are 50 vertical levels, 28 of them being located within the closest km to the ground, and 8 within the initial 100 m. As spinup time, 12 h are considered

The main results in this chapter are prepared to be submitted to *Atmospheric Chemistry and Physics* as: Sastre, M., Steeneveld, G.-J., Yagüe, C., Román-Cascón, C. and Maqueda G.: WRF tests on atmospheric boundary-layer transitions during the BLLAST campaign.

(Hu et al., 2010) and a timestep of 30 s is computed. We work with three different land-surface model (LSM) options: 5-layers, Noah and Rapid Update Cycle (RUC). For the PBL, three parametrizations are considered: Yonsei University (YSU), Mellor-Yamada-Janjic (MYJ) and Quasi-Normal Scale Elimination (QNSE). Each one of them works with its corresponding surface-layer scheme. Other physical features are: the rapid radiative transfer model (RRTM) for the longwave radiation (Mlawer et al., 1997), the Dudhia scheme (Dudhia, 1989) for the shortwave radiation, and the WRF single-moment 3-class (WSM3) microphysical scheme (Hong et al. 2004).

Data from the BLLAST field campaign (24 June 2011, IOP4 and 25 June 2011, IOP5) are considered to compare with the model output and validate them. Specifically, the following meteorological near-surface observed variables are used: temperature, latent heat flux, sensible heat flux, friction velocity and specific humidity. Besides, vertical profiles of potential temperature, wind speed and specific humidity are studied too.

6.2 WRF experiments

Three groups of experiments are performed:

i) To test three LSM and three PBL schemes. In this experiment one of the PBL model options is fixed, and then we alternate with the three LSM possibilities; then the process is repeated with the other two PBL parametrizations mentioned in the previous section. Afterwards, each one of the LSM is fixed and we vary with the three PBL parametrizations. Altogether, there are nine different simulations, whose smaller domain (1km-resolution) results are used to compare with observations. This allows an analysis on the model sensitivity to LSM and PBL for a certain meteorological magnitude.

ii) To study the influence of varying the number of domains and the domain size. Here are presented simulations with a different number of domains than the ones earlier designed (3 domains), taking as a reference one of the combinations in the previous test (YSU_5lay). On the one hand, an outermost nested domain is added, with a 60×60 cells and a horizontal grid resolution of 27 km (YSU_5lay_4nest). For the validation, again the smaller domain is considered (1km-resolution). On the other hand, a test reducing the number of domains is performed, with just one domain that has 300×300 cells and grid spacing of 2.5 km (YSU_5lay_1dom).

iii) To study the effect of initializing soil variables temperature and moisture using self-spinup (YSU_5lay_SS). Following Angevine et al. (2014) methodology, the soil temperature and moisture for each day's run is taken from the 24-h forecast initialized the previous day. For this purpose, a self cycle for the whole month of June has been previously performed.

The setup for experiments ii) and iii) is summarized in Table 6.1.

As an initial approach, in Figure 6.1 we can find the time evolution (12-24 UTC) of several magnitudes: near-surface air temperature (T), latent (LH) and sensible (SH) heat flux and friction velocity (u_*). An average of seven different BLLAST sites observations is plotted (blue line) with an indication of the standard deviation (shadow). The red lines correspond to each one of the twelve WRF simulations considered in the previous section. From these plots we can observe, as a whole, an overestimation of the turbulence (friction velocity) by the model simulations during daytime, nighttime and the evening transition. This fact is reinforced for the 25 June (right panels) at night. The key for this effect seems to be the higher temperature values of 25 June, as the simulations mostly underestimate the average temperature, whereas on 24 June the simulations were closer to the average value of the observations, nearly all in the shadowed region of

the standard deviation. This suggests that the model setup selected may be appropriate for a not very extreme situation such as on 24 June, but in a warmest case (25 June) a special and different adjustment may be required. Regarding the variability of the BLLAST terrain and land uses, to validate the results we choose, unless it is indicated otherwise, the observations from the sub-site (or its surroundings) with a land use similar to the one considered by the model (in this case, "wheat" observations from edge sub-site). This election is also supported by the fact of presenting, compared with any other set of observations, a balanced agreement in several magnitudes, including the Bowen ratio (sensible / latent heat flux ratio), with simulation YSU_5lay, whose basic settings (including PBL and LSM) are considered for simulations YSU_5lay_4nest, YSU_5lay_1dom and YSU_5lay_SS.

Table 6.1. Setup of the simulations for the sensitivity experiments. In red are indicated the characteristics which are exclusive of a certain simulation.

	YSU_5lay	YSU_5lay _4nest	YSU_5lay_1dom	YSU_5lay_SS
Spinup	12 h	12 h	12 h	Self spinup
Number of domains	3 (nested)	4 (nested)	1	3 (nested)
Horizontal resolution	1 – 3 – 9 km	1 – 3 – 9 – 27 km	2.5 km	1 – 3 – 9 km
Number of grid points per domain	100×100	100×100 60×60 (larger domain)	300×300	100×100

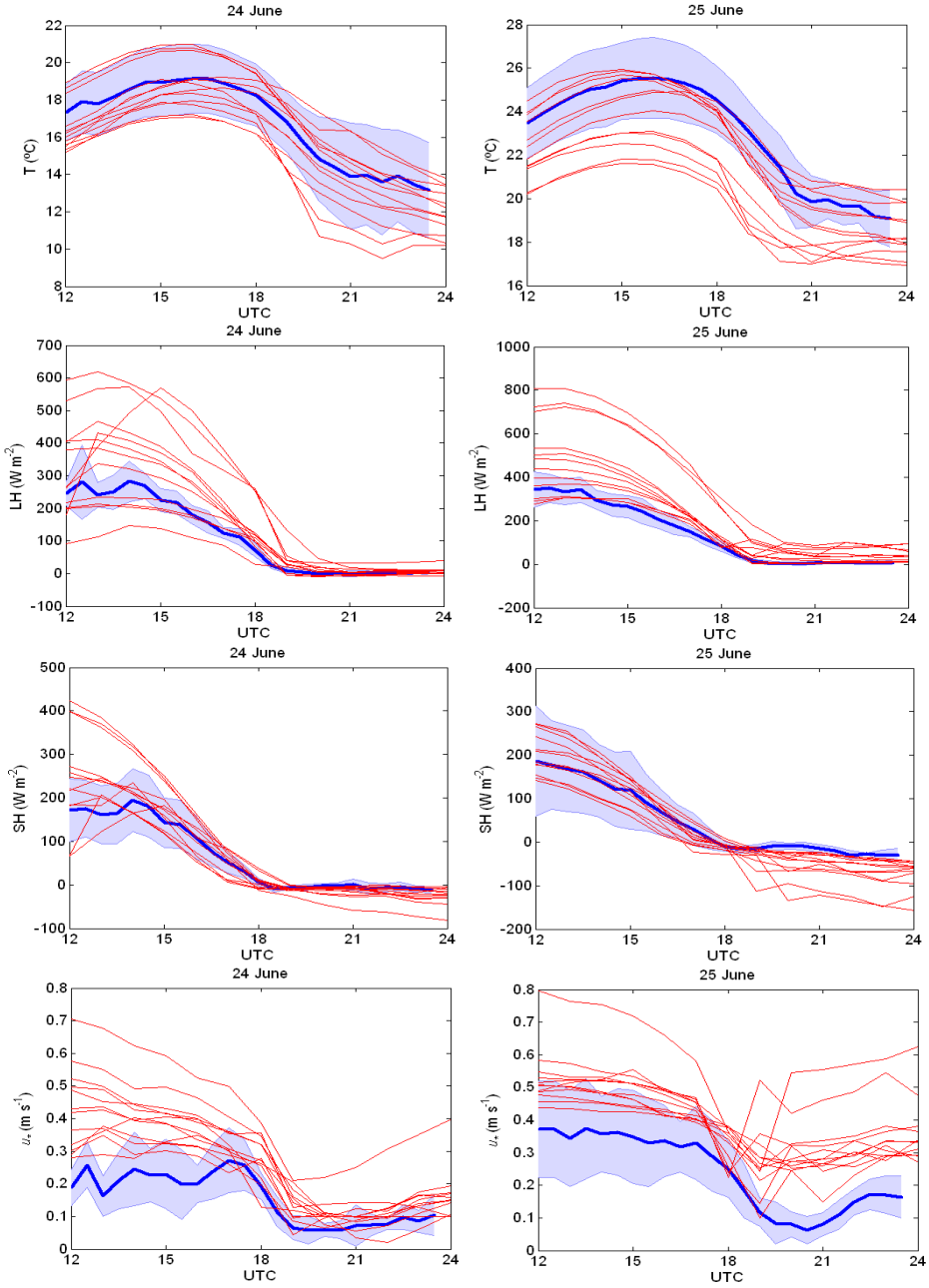

Figure 6.1. Temperature, latent heat flux, sensible heat flux and friction velocity during the evening transition for two days: 24 June 2011 (left) and 25 June (right). Red lines correspond to the twelve different simulations performed. The blue line is the average value of observations from seven BLLAST sub-sites, with the standard deviation (light blue shadow).

6.2.1 Sensitivity on PBL and LSM schemes

We obtain that, regardless of the agreement with observations, the model usually presents more sensitivity to LSM than to the PBL scheme. Figure 6.2 shows the latent heat flux time evolution with a fixed PBL scheme (top panels) or a common LSM (bottom panels), both during 24 (left) and 25 (right) June. There are greater discrepancies between the former simulations (fixed PBL) than between the latter (fixed LSM).

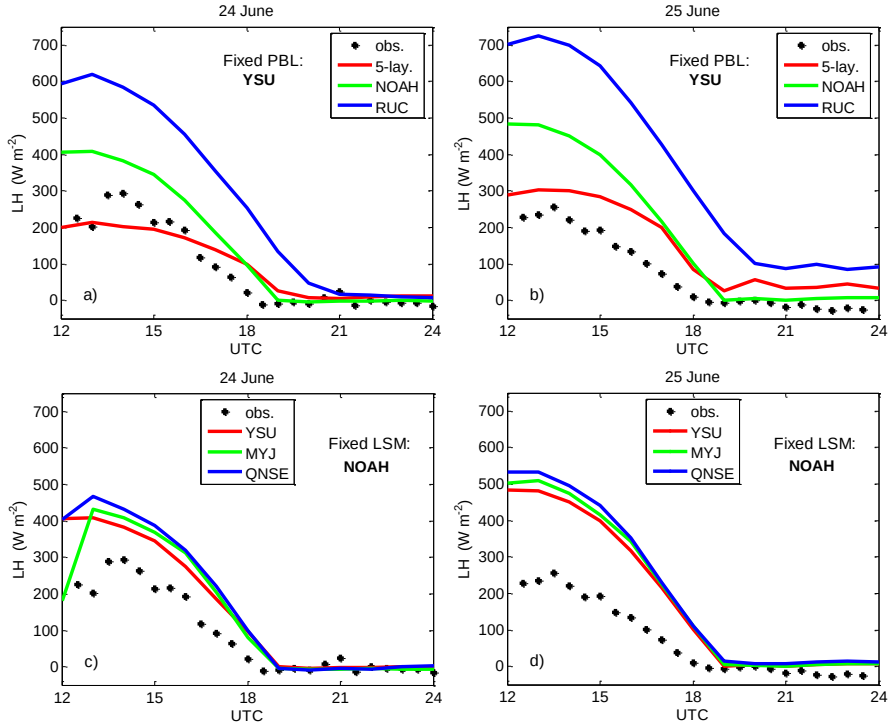

Figure 6.2. Time evolution of the latent heat flux observed (black line) and simulated (colour lines): a) fixed PBL (YSU) for 24 June, b) fixed PBL (YSU) for 25 June, c) fixed LSM (NOAH) for 24 June, d) fixed LSM (NOAH) for 25 June.

For other variables or common model schemes, the results are similar (not shown). This means that for these case studies the influence of the soil in the simulations is crucial, perhaps even more than the PBL processes. Consequently, choosing the most appropriate LSM in each case is more

relevant than selecting an excellent PBL scheme, because for the evening transitions the model has more sensitivity to LSM.

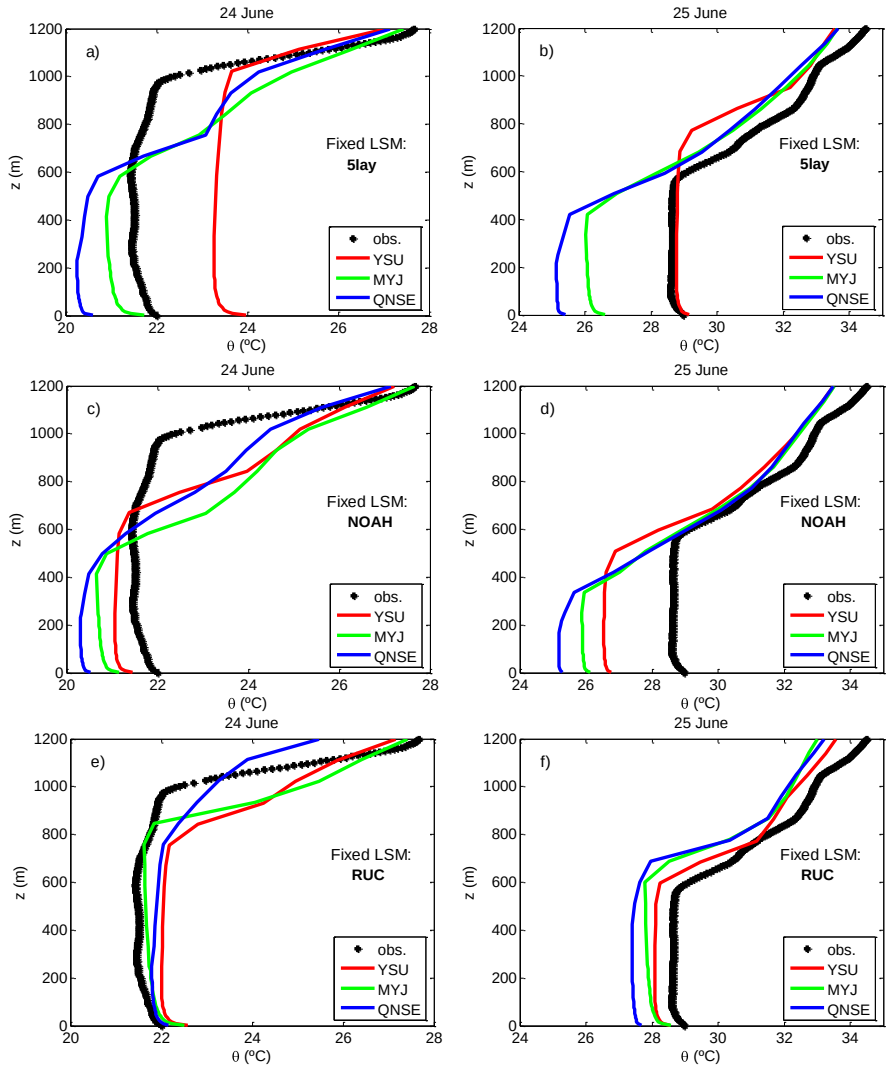

Figure 6.3. Observed (black dots) and simulated (colour lines) potential temperature profiles at 17:00 UTC for day 24 (left panels) and 25 (right panels) June for a different fixed LSM: 5-lay (up), NOAH (middle) and RUC (bottom).

To study how is the model able to represent the vertical structure of the atmospheric boundary layer we plot potential the temperature profiles at

17:00 UTC (Figure 6.3) for IOP4 (left) and IOP5 (right). Two main aspects of the simulations results are here considered: the accuracy (regarding the observations) of the near-surface value and a correct representation of the boundary-layer height. We find that for the three LSM studied the simulations with YSU (red line) as PBL is, for near-surface values, always warmest than MYJ (green) and QNSE (blue), being the latter actually the coolest one. Regarding the boundary-layer height, for 24 June all the simulations significantly underestimate it, except the combination 5lay_YSU (red line in the upper-left panel), whose value is very similar to the one from observations, in spite of overestimating the potential temperature near surface nearly 2 ºC. For 25 June, this LSM-PBL combination provides a very accurate value for the near-surface potential temperature, but overestimates the boundary-layer height. Results with NOAH (panels in the middle) provide poor agreement with the observed boundary-layer height on both 24 and 25 June. Simulations using RUC (bottom panels) tend to overestimate the potential temperature during 24 June, but underestimate it for the warmest day (25 June). The boundary-layer height is underestimated on 24 June, whereas on 25 June the simulations reach a good agreement with observations. Nevertheless, this good result might be circumstantial, and more related to an unexpected great reduction of the observed PBL height, as far as these RUC sets of simulations do not differ a lot from 24 to 25 June, whilst observations actually do. Globally, a different agreement with observations at surface or at higher levels is found from these tests.

As a whole, good results have been obtained with the combination YSU_5lay. In the following subsections, this is the one considered as the basic configuration from which modifications are made.

6.2.2 Number of domains influence

To find out whether modifying the domains configuration of the simulations can provide a more accurate agreement with the observations two other simulations are evaluated: with four nested domains (YSU_5lay_4nest) and with only one large domain (YSU_5lay_1dom).

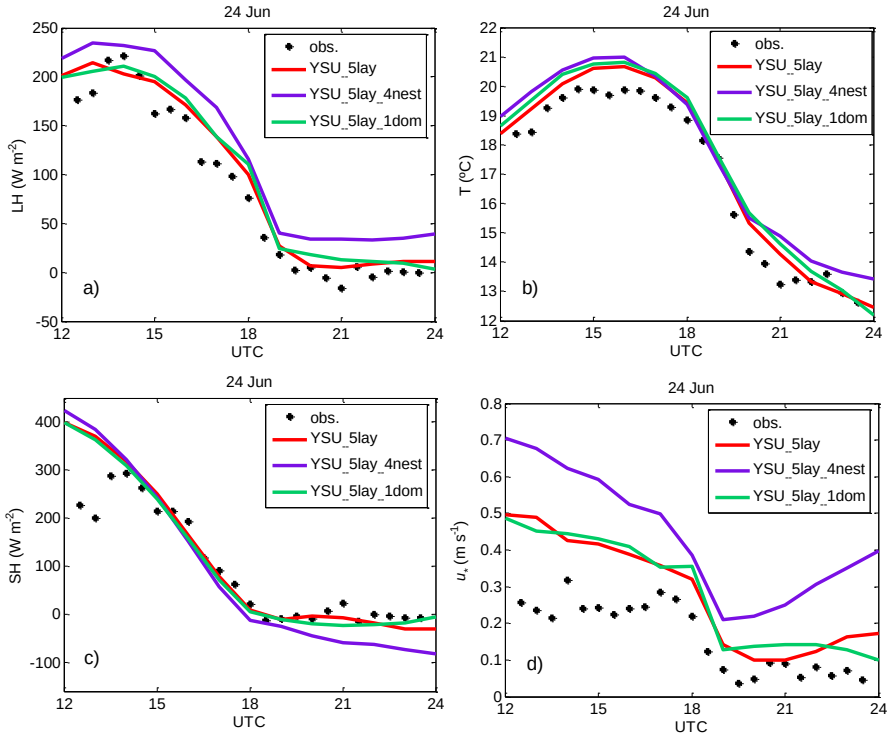

Figure 6.4. Comparison of simulated (colour lines) and observed (black dots) time evolution of: a) latent heat flux, b), near-surface temperature, c) sensible heat flux and d) friction velocity for 24 June, to test the influence of the number of the domains and its size.

The time evolution of several atmospheric variables near surface (Figure 6.4) is similarly represented by the three simulations considered (YSU_5lay, YSU_5lay_4nest and YSU_5lay_1dom). Vertical profiles (Figure 6.5) of specific humidity, potential temperature and horizontal wind speed for 24 June at two different times of the evening transition

(17:00 UTC and 23:00 UTC) show very slight differences from the initial configuration too.

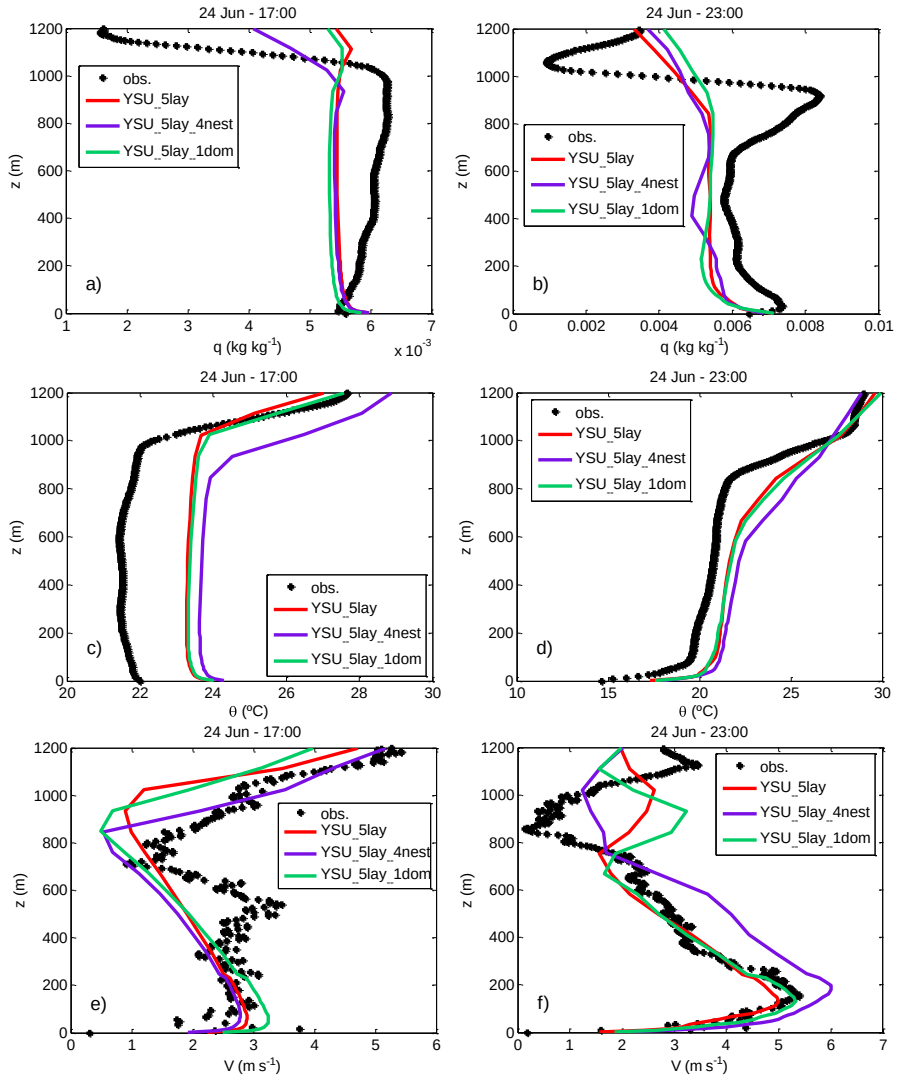

Figure 6.5. Observed (black dots) and simulated (colour lines) vertical profiles to test the influence of the number of the domains considered. Plots correspond to 24 June at 17:00 UTC (left panels) and 23:00 UTC (right panels) specific humidity (up), potential temperature (middle) and wind speed (bottom).

This result is relevant in terms of computational costs: as far as the results do not essentially vary, it seems not to be necessary working with complex domain configurations, but a simple one (YSU_5lay_1dom) can provide basically the same results when evaluating the vertical structure of the boundary layer or the time evolution during the transition of a day with not very extreme characteristics like 24 June is. Actually, the most remarkable variations provided by the simulation with four nested domains in Fig. 6.4 and Fig. 6.5 (YSU_5lay_4nest) do not seem to improve the initial configuration but get away from the observed values. This fact might be due to erroneous results in the larger of the four domains, whose failure is transmitted to the nested domains, eventually giving a result which disagrees with observations.

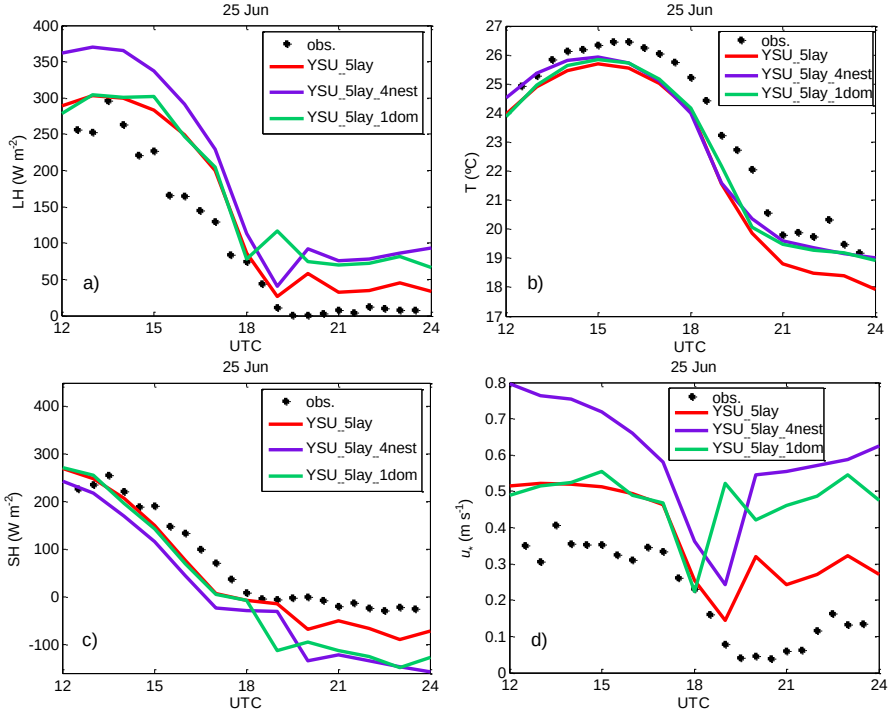

Figure 6.6. Same as Fig. 6.4 for 25 June.

For 25 June time evolution (Figure 6.6) only the near-surface temperature is simulated more accurately with the configurations of one or four domains. Turbulence at night is overestimated generally, being still YSU_5lay the closest to the observations.

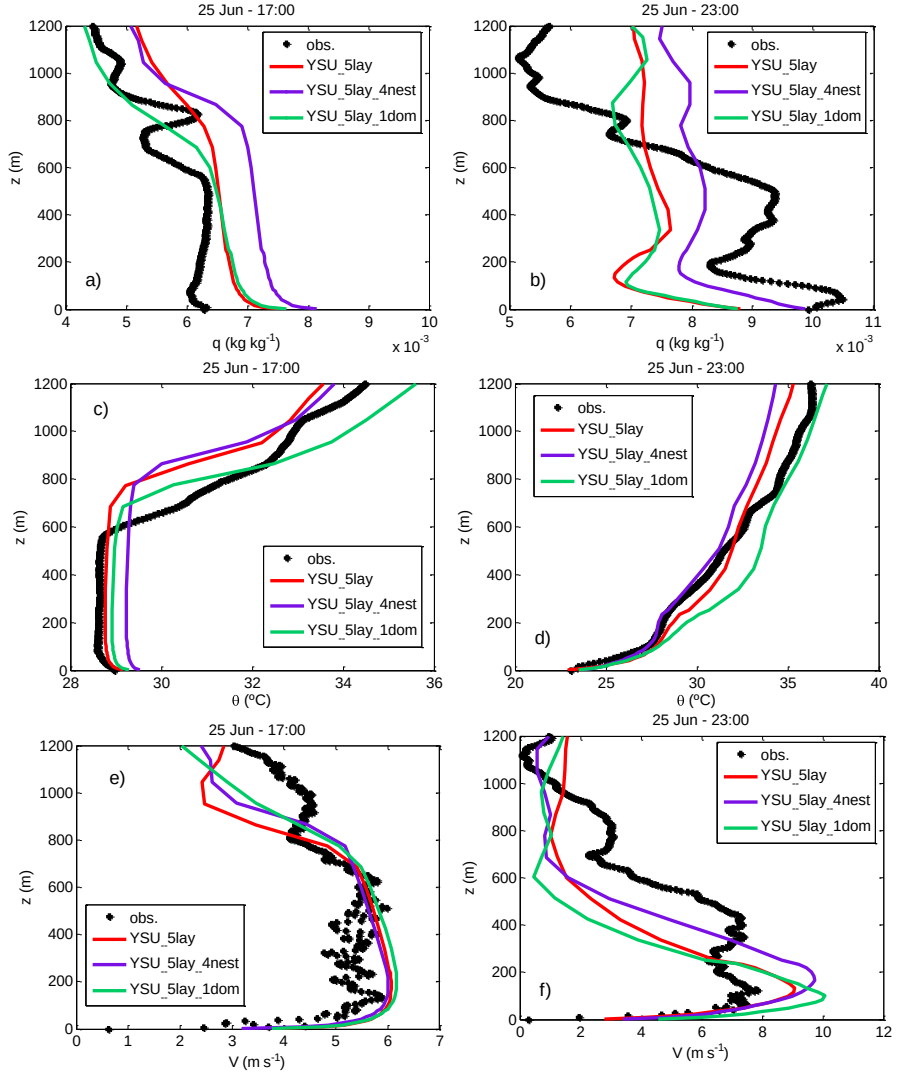

Figure 6.7. Same as Fig. 6.5 for 25 June.

For the vertical profiles (Figure 6.7) the differences among simulations tend to increase with height, being the most relevant result how simulation

YSU_5lay_4nest is able to properly reproduce the vertical structure of the low atmosphere defined by the potential temperature. This includes the warm-air intrusion from above. As a whole, for a warmer day like 25 June the different model configurations, based on the number of domains considered, provide results which significantly differ from each other. However, increasing the number of nested domains only has clearly improved the agreement with observations for the potential temperature profile.

6.2.3 Comparison with soil self-spinup simulations

The effect of using self-spinup is much more noticeable for 24 June (Figure 6.8) than for 25 June (Figure 6.9). On the one hand, on 24 June, the self-spinup simulation (YSU_5lay_SS) makes both SH and LH smaller and in closer agreement with the observations. Nevertheless, this reduction of the values does not occur proportionally, as far as the Bowen ratio is also modified. Lower temperatures are obtained both during day and night time, and this cooling effect from the surface is propagated to the upper levels in the simulation (potential temperature in Figure 6.8). On the other hand, very slight differences between simulations YSU_5lay and YSU_5lay_SS are found for 25 June (Figure 6.9). This fact might mean that the warmest situations perhaps do not require soil variables self-spinup as much as days with cooler temperatures.

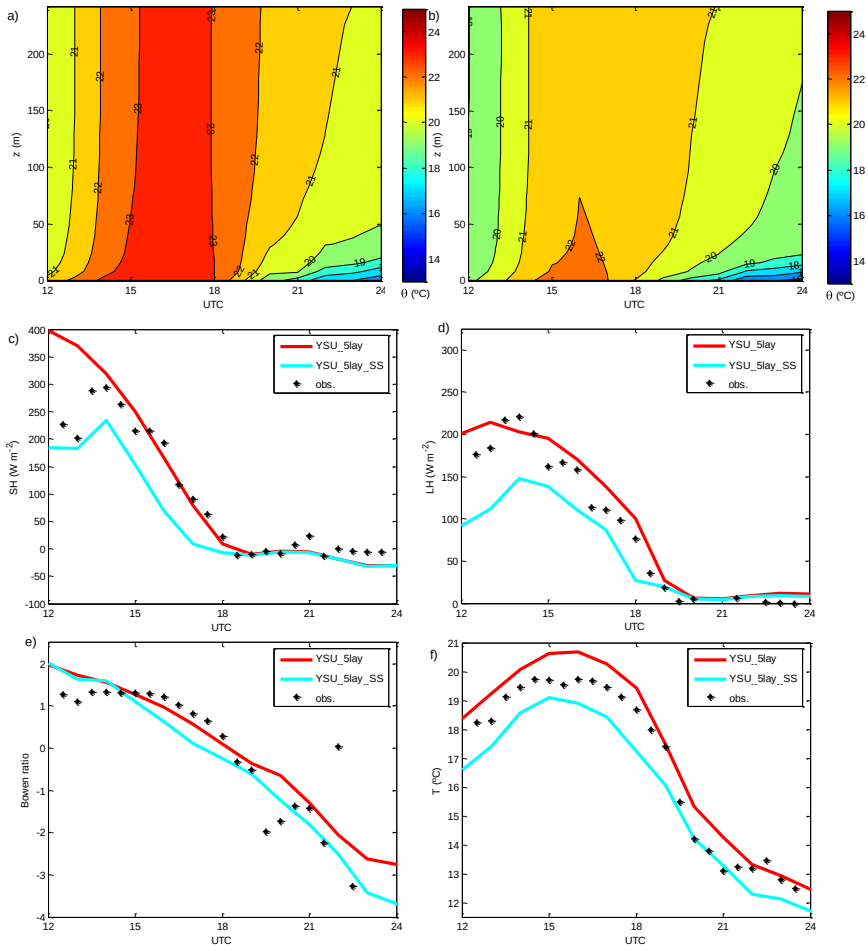

Figure 6.8. Time-evolution comparison between simulations YSU_5lay and YSU_5lay_SS for 24 June. Upper panels: potential temperature (left panel: YSU_5lay; right panel: YSU_5lay_SS). Middle: sensible and latent heat flux. Down: Bowen ratio and air temperature.

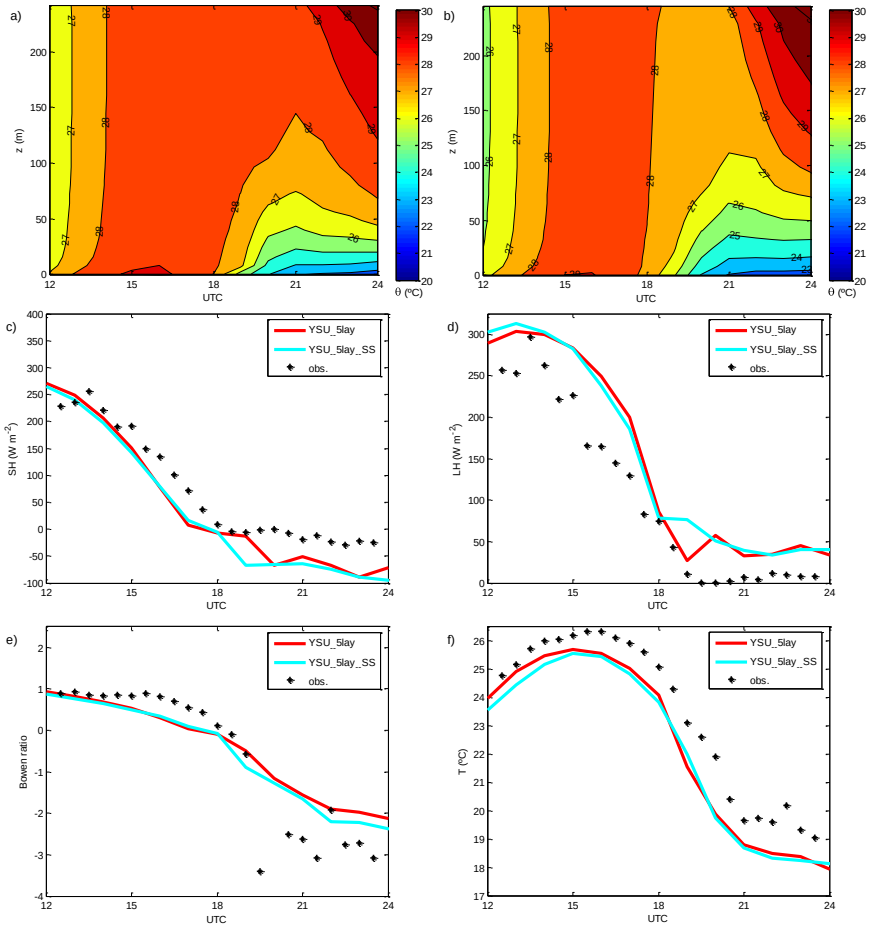

Figure 6.9. Same as Fig. 6.8 for 25 June. Scales are comparable.

6.3 Summary and conclusions

The ABL evening transitions have been studied through numerical simulations, considering as well the issue of non-homogeneous land uses for the validation with experimental measurements. These results indicate that WRF results are more sensitive to the selected LSM than to the selected PBL schemes during the evening transition. This fact suggests that a convenient LSM election will favour obtaining better results in the simulations, whereas the PBL prescribed will be useful to a finest

agreement with observations, but globally not very abrupt changes would be expected due only to a variation in the PBL parametrization. Furthermore, in this case the combination of a relatively simple PBL (YSU) and a LSM (5lay) schemes globally provide good results, and quite often closer to observations than other more sophisticated schemes. This might be somehow due to the complexity of the more advanced schemes: in certain situations, using the latter may mean adding potential sources of errors.

The vertical structure of the low atmosphere and the near-surface temporal evolution give contrasting agreement between simulations and measurements, provided that the same combination of PBL and LSM is considered. Very often, the best combination to characterise the vertical structure does not obtain such good results for the near-surface micrometeorological variables or temporal evolution.

Different results have been obtained in the agreement simulations-observations depending on the day evaluated and the kind of test performed. Greater differences among simulations are usually obtained for the warmest day, which might mean that this one has more difficult processes to be reproduced by the model. However, for the self-spinup tests it occurs oppositely: the warmest day is not very intensively affected when the self-spinup method is applied.

An increase in the number of domains of the simulations has not provided significantly better results, except in one very specific situation. Additionally, a configuration with only one domain performed quite successfully, considering its reduced computational costs. This result is in agreement with previous studies where using one-domain simulations better results were obtained than with nested-domains simulations (Warner et al., 1997; Leduc and Laprise, 2009; Leduc et al., 2011; Steeneveld et al., 2015).

Plotting together the one-site (wheat) observations and the twelve simulations considered (Figure 6.10) we find that the simulations globally tend to underestimate near-surface temperature, probably due to a latent heat flux overestimation. As a consequence, sensible heat flux is underestimated during daytime (but overestimated at night). Humidity evolution is not well represented by any of these configurations considered, whereas turbulence (friction velocity) is generally overestimated.

A possible way to improve modelling results during the evening transition might be linked to modifying the vegetation considered by the model, so that physical processes are better represented. This could be done by adapting methods like the one presented by Refslund et al. (2014).

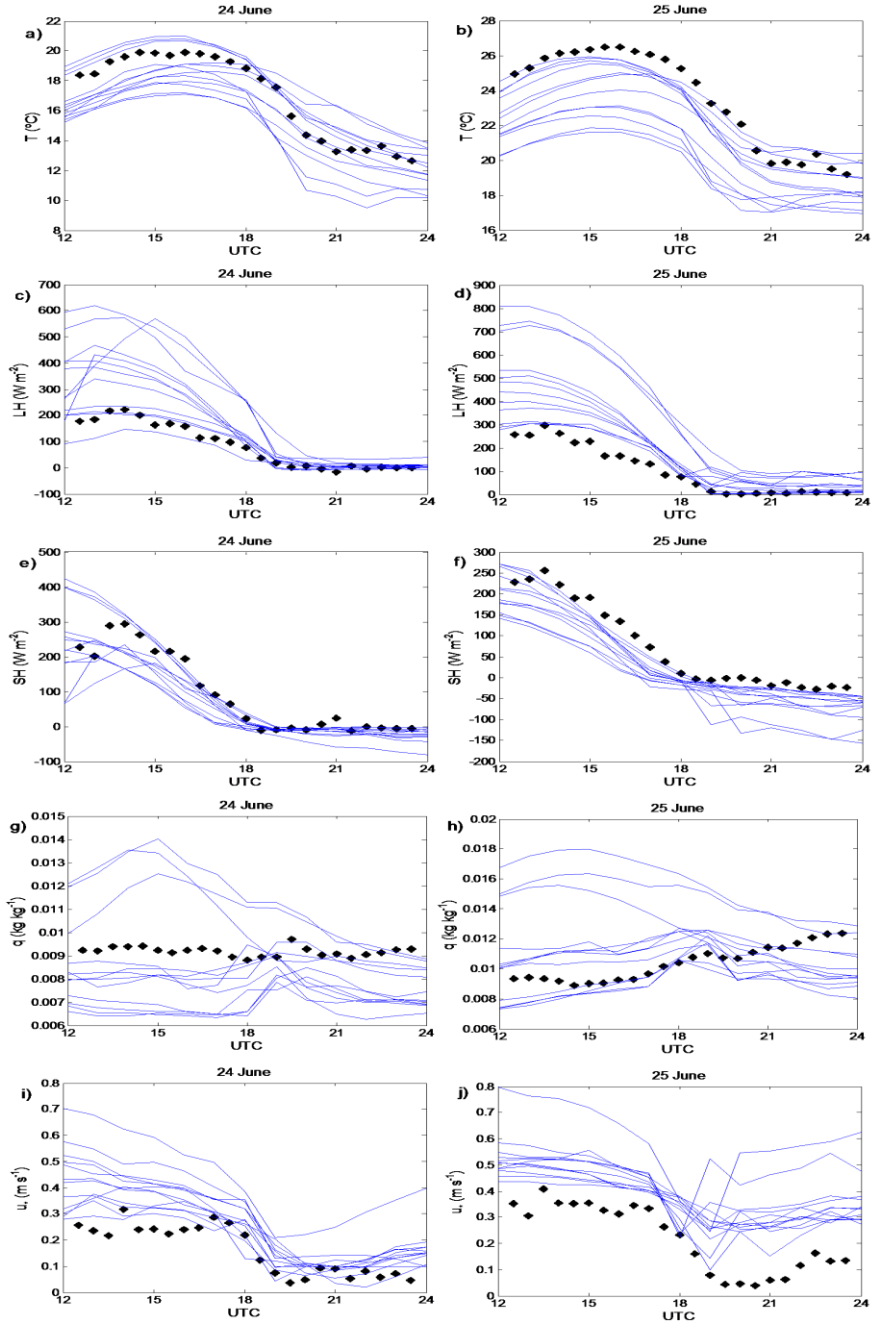

Figure 6.10. Near-surface evolution (24 and 25 June) during the evening transition of: a) and b) air-temperature; c) and d) latent heat flux; e) and f) sensible heat flux; g) and h) specific humidity; i) and j) friction velocity. Black dots correspond to measurements (wheat sub-site); blue lines are the twelve simulations performed.

7. Seasonal analysis of the atmospheric evening transitions

So far in this thesis the evening transitions have been studied considering observations or simulations during the summer time. Nevertheless, in different seasons, the behavior of the ABL during this transition might not be likewise. In this chapter, a seasonal analysis is presented from CIBA data along several years. The influence on different atmospheric variables as well as on particulate matter (PM) concentrations is addressed.

7.1 Specific methodology and dataset

Data from the permanent instrumentation at CIBA are analysed in this chapter, considering years from 2008 to 2013. The months assigned for each season are the following: June, July, August (JJA) are summer; September, October, November (SON) correspond to autumn; December, January, February (DJF) are winter; March, April, May (MAM) are spring. This is analogous to the grouping made by Wingo and Knupp (2015), who studied ABL afternoon-to-evening transitions in Alabama, USA (34º43' N, 86º38' W) regarding autumn, summer and spring differences. For the study in the current chapter, winter is additionally included. Significant climatic differences can be definitely found between JJA and DJF, being SON and

This chapter is in preparation for submission to a peer-review journal as: Sastre, M., Yagüe, C., Román-Cascón, C. and Maqueda, G.: Observational seasonal study of the atmospheric boundary layer evening transitions.

MAM intermediate seasons, which share some common characteristics. For this reason, it is reasonable that some aspects of the evening transition to a nocturnal boundary layer occur in different ways depending on the season considered.

The temporal interval of study includes eight hours, as in Chapter 5: from 4 h before to 4 h after sunset, being the latter the time reference (t = 0). This is a longer time-period than the one considered by Wingo and Knupp (2015): from 3 hours prior to 2 hours after sunset. As large-scale forcing is intended to have relatively low influence, transitions with a cloud cover larger than two oktas have been disregarded, in accordance with Wingo and Knupp (2015) criterion of 20-30% of cumulus cloud cover. With these restrictions, and admitting that instrumentation and good quality data are not permanently available during the whole 2008-2013 period, the remaining number of transitions is: 235 (JJA), 159 (SON), 96 (DJF) and 140 (MAM).

7.2 Atmospheric variables: average evolution and variability

Mean time evolution of several atmospheric variables, with 20-minutes averages, reveals some seasonal similarities and differences. Furthermore, to have a global picture of every season, for each sub-period defined for the transition (see Chapter 5), the averages of several variables have been calculated, as well as the corresponding standard deviations for winter, spring, summer and autumn (Table 7.1, Table 7.2, Table 7.3 and Table 7.4, respectively).

Figure 7.1 displays the wind speed, friction velocity and TKE, which have an analogous global evolution during the four seasons and the same absolute values pattern: greater at JJA and lower at DJF, with intermediate values for MAM and SON. These means are season-to-season compared using statistical hypothesis testing, obtaining that they are

different for each season (significance level: 5 %), except the pair spring-autumn.

Table 7.1. Winter (DJF) mean values (standard deviation between brackets) of wind speed (U), potential temperature difference gradient ($\Delta\theta/\Delta z$), turbulent kinetic energy (e), turbulent heat flux (H), specific humidity (q) and particulate matter up to 10, 2.5 or 1 μm (*PM10*, *PM2.5* and *PM1*, respectively) for the four sub-periods used. Subscripts indicate height (m) a.g.l.

	t_a = [–4, –2] h	t_b = [–2, 0] h	t_c = [0, 2] h	t_d = [2, 4] h
U_{10} (m s^{-1})	3.0 (1.9)	2.7 (1.7)	2.2 (1.4)	2.3 (1.5)
$\Delta\theta/\Delta z_{10\text{-}1.5}$ (K m^{-1})	–0.13 (0.06)	–0.07 (0.06)	0.14 (0.15)	0.20 (0.20)
e_{10} (m^2 s^{-2})	0.8 (0.6)	0.4 (0.5)	0.2 (0.3)	0.2 (0.3)
H_{10} (W m^{-2})	130 (62)	26 (38)	–10 (15)	–11 (15)
$q_{1.5}$ (g kg^{-1})	4.4 (1.0)	4.5 (1.1)	4.1 (1.0)	3.9 (0.9)
$PM10_1$ (μg m^{-3})	12.6 (8.3)	13.8 (8.9)	15.8 (10.5)	15.3 (9.5)
$PM2.5_1$ (μg m^{-3})	10.7 (7.3)	11.2 (7.6)	13.2 (8.9)	13.2 (8.4)
$PM1_1$ (μg m^{-3})	9.8 (7.1)	10.1 (7.4)	11.7 (8.5)	12.1 (8.1)

Table 7.2. Same as Table 7.1 for spring (MAM).

	t_a = [–4, –2] h	t_b = [–2, 0] h	t_c = [0, 2] h	t_d = [2, 4] h
U_{10} (m s^{-1})	3.8 (2.4)	3.6 (2.3)	3.0 (2.0)	3.2 (1.9)
$\Delta\theta/\Delta z_{10\text{-}1.5}$ (K m^{-1})	–0.11 (0.06)	–0.02 (0.08)	0.16 (0.15)	0.16 (0.16)
e_{10} (m^2 s^{-2})	1.2 (0.7)	0.6 (0.6)	0.3 (0.4)	0.3 (0.5)
H_{10} (W m^{-2})	145 (79)	16 (40)	–19 (19)	–21 (19)
$q_{1.5}$ (g kg^{-1})	5.3 (1.7)	5.6 (1.9)	5.6 (1.7)	5.7 (1.7)
$PM10_1$ (μg m^{-3})	13.0 (7.4)	14.8 (8.2)	17.3 (8.9)	17.7 (8.8)
$PM2.5_1$ (μg m^{-3})	8.3 (5.7)	9.1 (5.9)	11.2 (6.6)	12.9 (7.3)
$PM1_1$ (μg m^{-3})	5.8 (4.5)	6.4 (5.0)	8.2 (5.7)	10.3 (6.7)

Table 7.3. Same as Table 7.1 for summer (JJA).

	t_a = [–4, –2] h	t_b = [–2, 0] h	t_c = [0, 2] h	t_d = [2, 4] h
U_{10} (m s^{-1})	4.3 (1.9)	4.1 (2.0)	3.5 (1.8)	3.5 (1.6)
$\Delta\theta/\Delta z_{10\text{-}1.5}$ (K m^{-1})	–0.17 (0.05)	–0.07 (0.06)	0.11 (0.13)	0.10 (0.14)
e_{10} (m^2 s^{-2})	1.5 (0.8)	0.9 (0.7)	0.5 (0.6)	0.4 (0.5)
H_{10} (W m^{-2})	180 (90)	28 (47)	–20 (18)	–20 (15)
$q_{1.5}$ (g kg^{-1})	6.3 (1.6)	6.3 (1.6)	6.9 (1.8)	7.6 (1.8)
$PM10_1$ (µg m^{-3})	10.0 (6.0)	12.4 (7.3)	16.1 (7.9)	15.2 (7.9)
$PM2.5_1$ (µg m^{-3})	4.3 (3.1)	5.2 (4.4)	7.4 (4.7)	8.6 (4.7)
$PM1_1$ (µg m^{-3})	2.8 (2.1)	3.2 (2.2)	5.0 (3.2)	6.4 (4.0)

Table 7.4. Same as Table 7.1 for autumn (SON).

	t_a = [–4, –2] h	t_b = [–2, 0] h	t_c = [0, 2] h	t_d = [2, 4] h
U_{10} (m s^{-1})	3.6 (1.8)	3.3 (1.9)	2.6 (1.8)	2.7 (1.7)
$\Delta\theta/\Delta z_{10\text{-}1.5}$ (K m^{-1})	–0.17 (0.05)	–0.08 (0.06)	0.17 (0.17)	0.22 (0.23)
e_{10} (m^2 s^{-2})	1.2 (0.7)	0.7 (0.6)	0.3 (0.5)	0.3 (0.4)
H_{10} (W m^{-2})	173 (79)	34 (48)	–14 (20)	–16 (19)
$q_{1.5}$ (g kg^{-1})	6.0 (1.8)	5.9 (1.8)	5.9 (1.8)	6.0 (1.7)
$PM10_1$ (μg m^{-3})	12.5 (7.7)	13.7 (7.8)	16.8 (8.8)	14.9 (8.2)
$PM2.5_1$ (μg m^{-3})	5.9 (4.2)	6.6 (4.8)	9.3 (6.1)	10.1 (6.8)
$PM1_1$ (μg m^{-3})	4.3 (3.6)	4.8 (4.1)	6.8 (5.4)	7.7 (5.7)

This implies that, on average, the wind speed for all the four seasons at CIBA provides the main contributions to these two turbulence-related magnitudes, which is in line with the results shown in Chapter 5. Some differences appear in the timing of the largest rate of decay beginning, on average, later in winter, but in any case at least one hour

before sunset. This decay lasts until reaching a minimum value between sunset and $t = 1$ h.

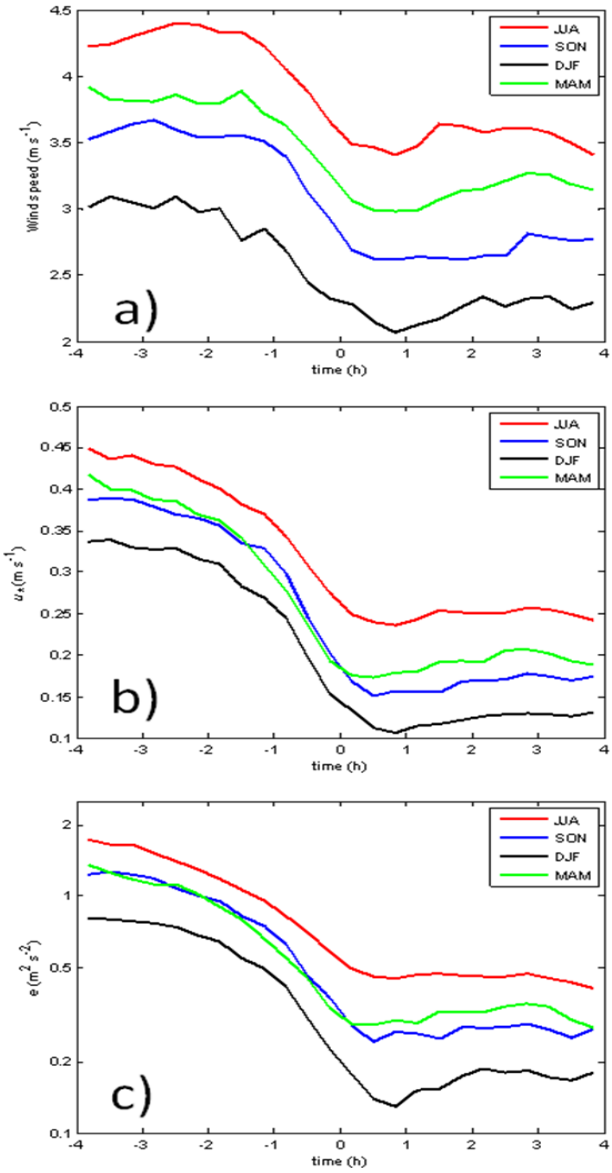

Figure 7.1. Time evolution of wind speed (a), friction velocity (b) and TKE (c) during the different seasons.

On the other hand, a very seasonal-dependent evolution is shown by the specific humidity (Fig. 7.2). Summer (JJA) absolute values tend to slightly diminish until nearly one hour prior to sunset and then a great increase occurs.

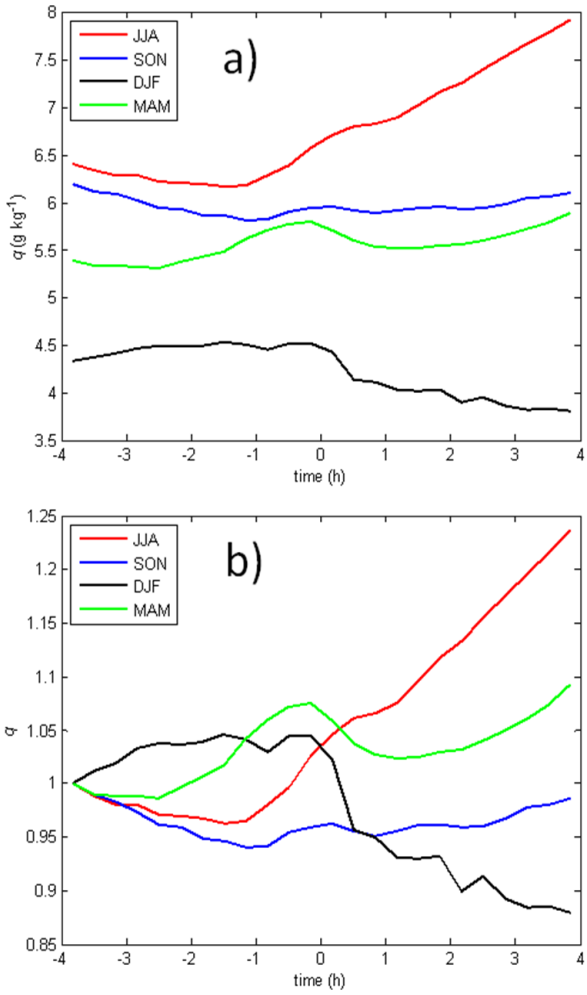

Figure 7.2. Specific humidity evolution during the transition: (a) absolute values, and (b) the same, normalized by the respective values at $t = -4$ h.

This result is in accordance with previous studies for summer transitions at various locations (Sastre et al., 2015; Wingo and Knupp, 2015).

Nevertheless, the records for the other three seasons behave in another way. In winter (DJF), the absolute values are clearly smaller than at the other seasons; besides they even get reduced at around sunset. The typical winter conditions favour that the humidity values usually are closer to saturation than in summer, so that condensation is more likely to occur, and therefore q is reduced. For autumn (SON) the evolution is quite plain during the whole period, whereas in spring (MAM) the mean absolute values are below the ones corresponding to autumn (SON), with a relatively strong increase (as in summer) starting at around $t = -1.5$ h, but a decrease is found just before sunset for nearly one hour. Then, in the nighttime, a steady increase occurs again. Consequently for q, a marked difference in the two intermediate seasons (SON and MAM) is obtained, revealing that in terms of specific humidity, MAM is more similar to JJA than SON is.

In this seasonal analysis, the absolute values of q are not totally linked to the soil humidity, assuming the latter depends basically on rainfall. The leading contributors to the total annual precipiation are autumn and spring, but larger values of q are obtained in summer even a few hours before sunset. This suggests that the soil evaporates differently depending on the season. Globally, and except for summer (JJA), the evolution of the humidity is different than in the location studied by Wingo and Knupp (2015), so it can be addressed as a seasonal difference which is actually site dependent.

To study seasonal differences in the atmospheric stability, the difference in potential temperature ($\Delta\theta$) between two levels (10 and 1.5 m) is plotted (Figure 7.3). Summer and autumn have greater diurnal values than winter and spring, whereas the nocturnal inversions develop more strongly in autumn and winter; besides, the average evolution shows in the four seasons the change of sign in $\Delta\theta$ between 45 and a few minutes before sunset. Despite these results are compatible with earlier findings (Busse and

Knupp, 2012; Wingo and Knupp, 2015), here a distinctive aspect is found: the surface-based thermal inversion starts to develop considerably earlier in spring than in the other seasons. This aspect was not observed at other observational sites, so it might be due to local processes, either meteorological or soil related. For example, the surface experiences changes from one to another season, particularly affecting the vegetation cover, which could play a role in the emisivity, therefore influencing the surface cooling.

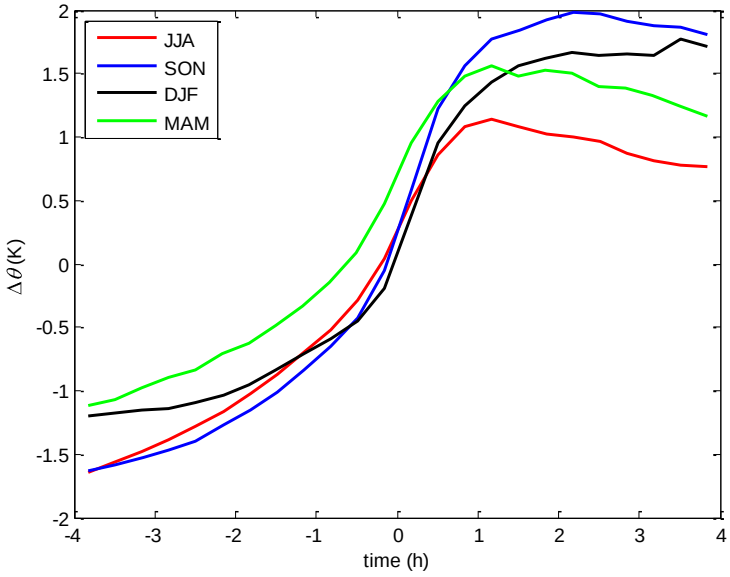

Figure 7.3. Average evolution of the potential temperature difference between two vertical levels (10 and 1.5 m) during the transition.

Regarding the variability of the transitions in a particular season, the winter cases for q are more homogeneous than for the other periods of the year (Figure 7.4), all the time along the 8 hours here studied. However for most of the other variables studied, there are not very significant differences in the standard deviation from one to another season. Focusing on the evolution of this statistical parameter along the transition (Table 7.1, Table 7.2, Table 7.3 and Table 7.4), in the stability indicator ($\Delta\theta/\Delta z$) we

find a tendency to increase with time, being these standard deviation values remarkably larger after sunset for every season. This implies that the difference of temperatures in two vertical levels for the nighttime period is not as homogeneous as in the daytime, regardless of the season.

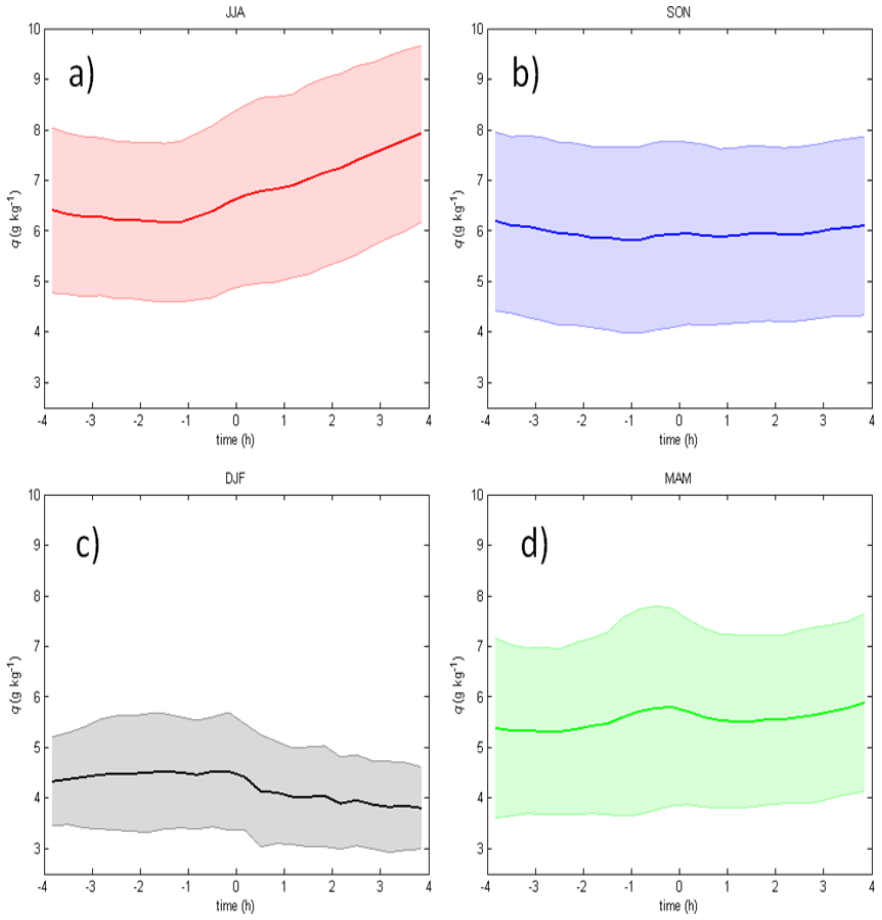

Figure 7.4. Mean temporal evolution (thick line) of the air specific humidity for each season: a) summer; b) autumn, c) winter; d) spring (d). Shadows indicate the standard deviation.

7.3 Wind distributions

An analysis on the wind speed and direction in the four temporal sub-intervals has been performed separately for the four seasons. The results for summer (not shown) are, as expected, highly similar to the ones presented in Chapter 5, where a smaller dataset (2 months) was employed, which would mean that the period studied in Chapter 5 is representative of the summer at CIBA. As a reminder, for this season there are two preferred directions at CIBA: mainly west before sunset, and north-east gaining importance as time goes on. The pattern for the other seasons resembles to that one, except for winter (Figure 7.5), where north-east is predominant for the whole 8 hours studied.

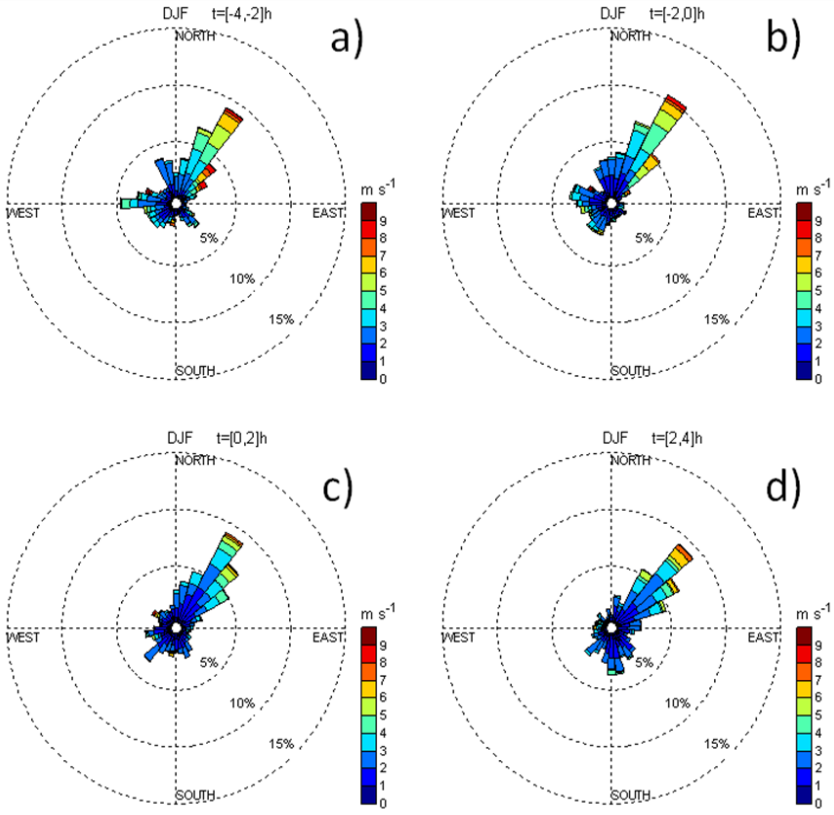

Figure 7.5. Observed wind distribution in winter (DJF) for the normalized time intervals: a) [−4, −2] h; b) [−2, 0] h; c) [0, 2] h; d) [2, 4] h.

Additionally, the second most frequent direction turns from west to south. These differences are probably related to synoptic-scale processes, rather than micro-scale effects.

7.4 Particulate matter concentration

Long-term monitoring of particulate matter (PM) is relevant due to the impact on human health (Delfino et al., 2005; Pope and Dockery, 2006). The spatial and temporal characterization of these concentrations is an area of research whose interest remains high, especially considering a seasonal characterization (Wang et al., 2015b). Now the evolution of PM concentration at CIBA along the transition is studied from the database earlier in this chapter described, regarding the time of the year and particle size (Figure 7.6). A fact, for all the seasons, is that particles of intermediate size (between 1 and 2.5 μm; green bars in Figure 7.6) have a minor presence compared to the finer (up to 1 μm; blue bars) or the coarser (between 2.5 and 10 μm; red bars) ones. The relative importance of each PM group varies depending on the time of the year: a huge predominance of the smaller particles is found in winter, whereas in summer and autumn the bigger ones have similar or slightly larger concentrations than the former. These findings are compatible with the global results obtained by Wang et al. (2015b), not focused on the transition period though. Besides, these seasonal differences are strongly influenced by the relative importance of the primary and secondary mechanisms of atmospheric aerosol formation (affecting PM growth), which differ along the seasons. Those processes were studied, among others, by Gómez-Moreno et al. (2007) or Zhang et al. (2012).

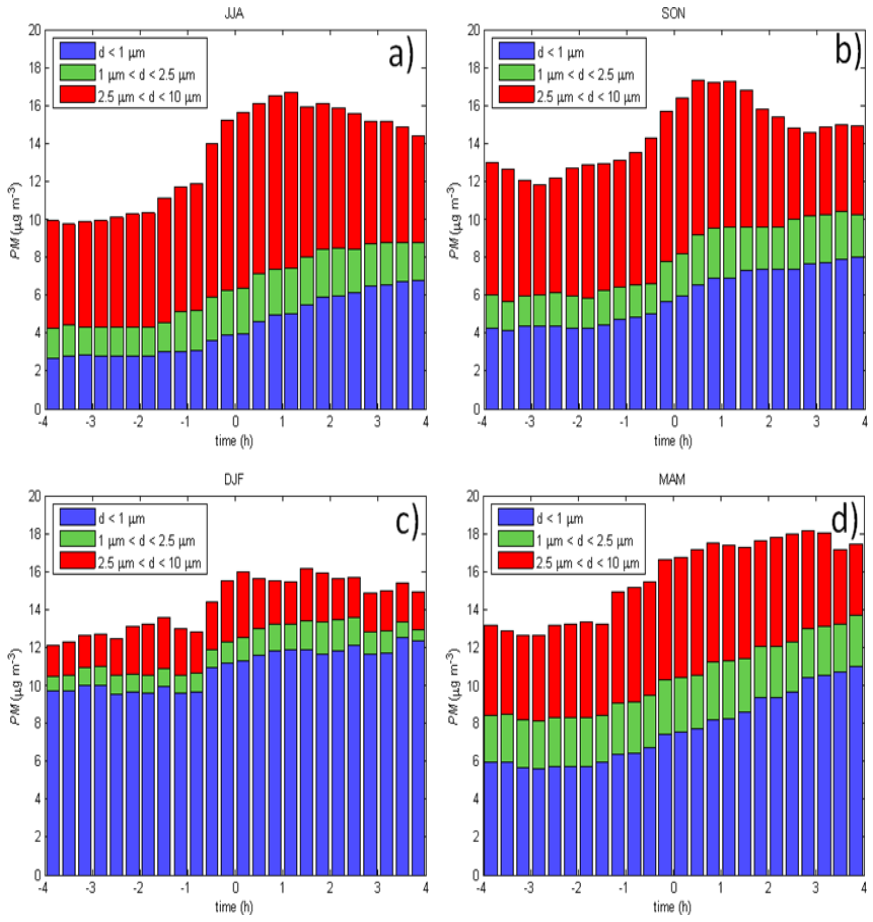

Figure 7.6. Averages of PM concentration for: a) summer; b) autumn; c) winter; and d) spring. Particle diameter is considered in three groups: up to 1 μm (blue bars, *PM1*), between 1 and 2.5 μm (green) and between 2.5 and 10 μm (red). The sum of the three bars for a certain time provides *PM10.*

A particular feature occurring during the transitional period is the increase of PM concentration, as can be seen in Figure 7.7, where the values at $t = -4$ h have been taken as a reference by subtracting the corresponding values for the whole plot. This increase is linked to the reduction of the ABL volume due to the decay in the solar energy input, but affects differently depending on the group of particles and the season.

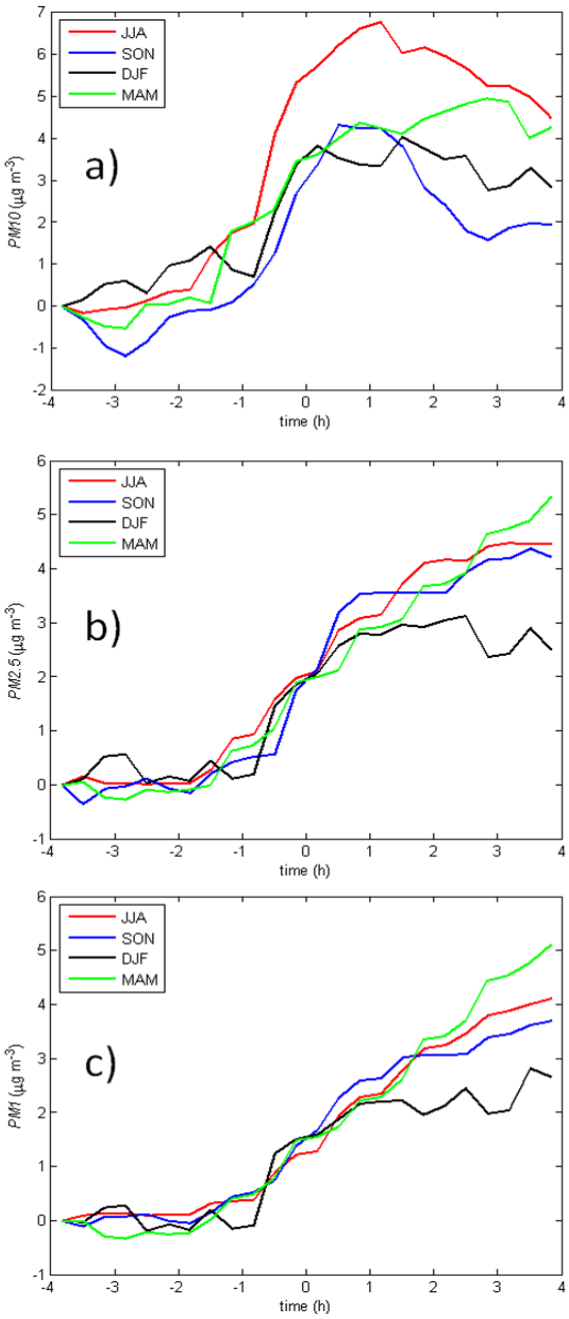

Figure 7.7. Variation experienced in the PM concentrations during the transition, related to their respective values at $t = -4$ h: a) *PM10*; b) *PM2.5*; c) *PM1*.

PM2.5 and *PM1* begin their great rise between 2 and 1 hour prior to sunset, except for winter; in that case it starts closer to sunset. Actually, in winter this increase in the values of *PM2.5* and *PM1* takes shorter than in the other seasons, as at $t = 1$ h a steady state is reached, whilst in the other seasons the concentrations have not reached the maximum value. *PM10* rises the most in summer (Figure 7.7a), mainly due to the relative contribution of the coarse particles (Figure 7.8). The maxima of the latter PM are directly linked to the decrease in turbulence and the wind minimum around sunset (Figure 7.1). Afterwards, the bigger particles concentration is reduced probably due to nocturnal drainage flows, which are relatively frequent at CIBA and other locations (Román-Cascón et al., 2015b; Sastre et al., 2015). Their relative importance is higher at night. Similarly, the absolute values of *PM10* (Figure 7.6) reach a maximum around sunset, except for spring, where it keeps rising for longer. This differing behavior of spring might be linked to other processes, particularly soil-atmosphere interactions (Moene and van Dam, 2014).

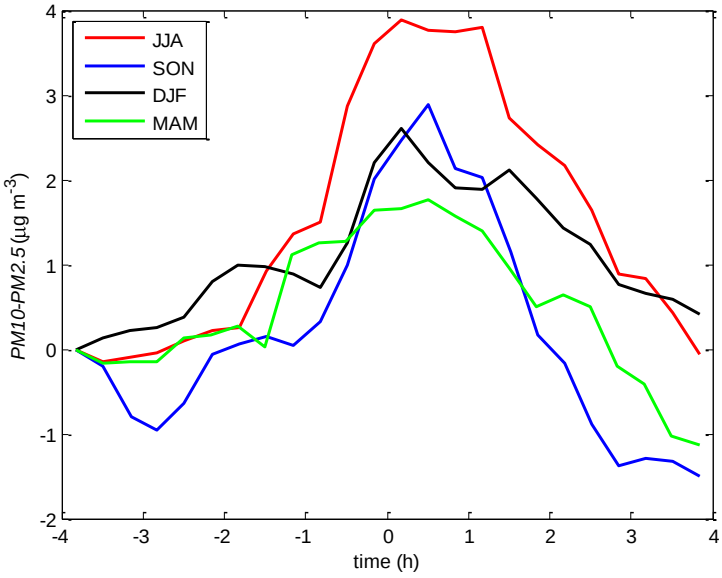

Figure 7.8. Variation of the coarser PM (*PM10* – *PM2.5*) related to their respective values at $t = -4$ h for each season.

An estimation of the spread of PM values from one to another individual case can be obtained from the standard deviation shown in Table 7.1, Table 7.2, Table 7.3 and Table 7.4. This statistical parameter increases with time, at least until the third sub-period (t_c). A season-to-season difference is that PM concentration appears with a larger spread in winter, being the summer cases the ones presenting less spread, especially for *PM1* (Figure 7.9). This result is linked to the larger absolute values of concentration in winter, but also indicates that in summer the conditions directly affecting this concentration do not vary a lot.

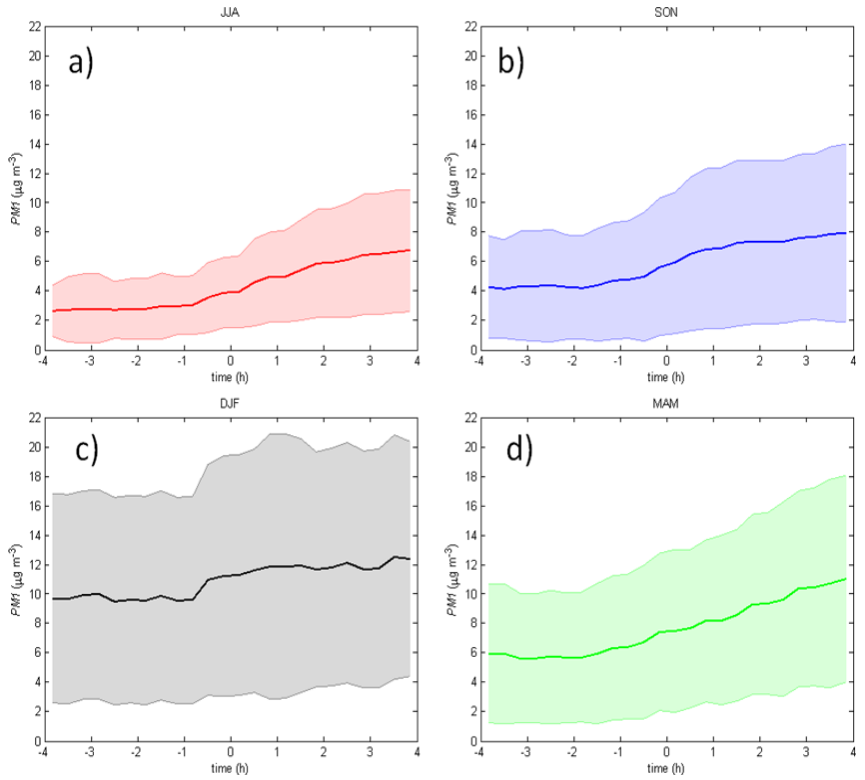

Figure 7.9. Mean temporal evolution (thick line) and standard deviation (shadows) of *PM1* in: a) summer; b) autumn; c) winter; d) spring.

7.5 Summary and conclusions

The ABL afternoon and evening transition has been studied regarding the seasonal differences and similarities from CIBA experimental measurements, supporting most of the findings from previous studies at another location (Busse and Knupp, 2012; Wingo and Knupp, 2015). Certain variables (like wind speed, friction velocity, TKE) display a twin pattern in their time evolution for all the seasons, differing basically in their absolute values. On the contrary, the air specific humidity behaves differently for each season, which is distinct to the results of Wingo and Knupp (2015) at another location. Consequently, the humidity evolution is more site-dependent than other variables (Sastre et al., 2015), both in the average evolution and variability.

An approach to the different processes linked to the PM concentrations during the transition has been presented, finding a common pattern of increasing values near sunset. Several influences play a role in the PM concentrations, including stability, turbulence and ABL thickness. The relative importance of the bigger PM (between 2.5 and 10 μm) is addressed and linked to the wind minimum around sunset, especially for summer. The competing thermal and mechanical effects result in PM concentration reduction, either settling on the ground or being advected, or increase, depending on each case for a specific season and particle group. Additionally, other effects, like differences in soil cover, or biological processes, which include vegetation, are thought to play a role in these transitional concentrations. Therefore, a multi-disciplinary study is recommended to improve knowledge in these processes.

8. Concluding remarks

The physical processes characteristic of the ABL afternoon and evening transition are studied in this thesis through both observational and numerical approaches. This is done to potentially provide improvements in the modelling of these processes, so that many human activities can benefit from these advances. The studies here presented include analysing the different temporal and spatial scales involved, statistical calculations for the principal ABL variables, a comparison between BLLAST and CIBA sites observations, and a study on the impact of the transitional processes along different seasonal periods. Additionally, numerous experiments with the WRF mesoscale model have been performed.

The first approach through observations (Chapter 4) revealed that high-frequency instruments, like microbarometers and sonic anemometers, are very useful to characterize this ABL transition. Furthermore, a 3-type classification was developed for CIBA (Sastre et al., 2012), but the aim to extend it to the BLLAST site measurements was not successful, probably due to the heterogeneity of the latter. It is also in Chapter 4 where the differences between case studies point up the need to study the transitions with weak and strong synoptic forcing separately, doing so for Chapter 5 results. There, sunset is taken systematically as the timing reference, which is found especially useful to compare observations from the two contrasting sites of BLLAST and CIBA. Results from Chapter 5 suggest that, for the establishment of the nocturnal stable boundary layer, moisture is particularly relevant. For this reason, an extra experiment with the WRF

model was performed (Sastre et al., 2015), evaluating the role of soil moisture during the transition by increasing the soil humidity at the driest site (CIBA) and reducing it at the other location (BLLAST). These simulations revealed that humidity can delay or modify the vertical thermal stratification, and turbulence intensity is as well affected through different rates of evaporation. Varying soil humidity produces very marked effects at both sites until 1 h before sunset. Afterwards, this artificial change plays a major role at the less humid and more homogeneous site (CIBA), with intense and long-lasting effects after sunset. This indirectly means that there are other effects apart from humidity, probably linked to heterogeneity, which are very considerable for BLLAST. These might be able to cancel, or at least reduce, the influence of moisture variations.

Next to these promising results with WRF, a full Chapter 6 shows experiments with this model, comparing with two case study observations. In particular, combinations of three PBL parametrizations and three LSM schemes are tested to study the sensitivity of WRF to the mentioned characteristics. It is found that the vertical structure of the lower atmosphere and the time evolution of surface variables have different agreement between the simulations and observations for a particular choice of PBL and LSM. Furthermore, tests on the model setup are performed, particularly on the number and size of the domains and the soil self-spinup. These appear as useful ways to better understand the role of such aspects on the matching of simulations with observations along the transition. These results are in agreement with Leduc et al. (2011) and Steeneveld et al. (2015), as far as good performance is obtained for 1-domain simulations.

As all the previous chapters in this thesis were related to summer-time, a seasonal analysis was developed, to deep into the similarities and differences in the transition regarding the time of the year. With a large dataset of CIBA measurements, most of the results from previous studies at

another location (Busse and Knupp, 2012; Wingo and Knupp, 2015) are supported, including timing of different events like turbulence decay or the decrease in temperature. Nonetheless, specific humidity behaves differently for each season at CIBA site, unlike Wingo and Knupp (2015) results. This links again with the results in the previous chapters, where moisture had a particular importance for the establishment of a stable nocturnal boundary layer. Additionally, the varying importance of some processes related to the PM concentrations (stability, turbulence and ABL depth) during the transition are presented, finding a common pattern of increasing PM values near sunset, directly linked to the minimum in wind speed at the same time. The absolute values are usually larger in winter, and the size of the PM varies from the predominant finer particles in winter to the importance of coarser particles in summer. These differences can be attributed to the larger values of wind speed in summer, avoiding that these particles settle. Actually, the wind plays a double role: it can keep the particles in the ABL instead of on the soil, but it can advect them away too.

8.1 Main conclusions

The principal conclusions of this thesis, connected to the objectives presented in Chapter 1, are now summarized:

- During the transition, there is an average qualitative evolution of the ABL variables regardless of the observational site.

- The main differences from one to another site involve extreme (absolute) values, time lags and katabatic wind occurrence.

- Soil and air humidity affect decisively the whole transition, showing an interaction with turbulence. This influence is particularly noticeable before sunset, and not only close to the ground, but also at upper levels.

- MRFD is a useful multiscale technique in the study of turbulence and the evolution of different time scales responsible for boundary-layer processes along the afternoon and evening transition, showing that, in general, turbulence developing at night corresponds to smaller time scales than afternoon turbulence.

- WRF simulations have shown more sensitivity to changes in the LSM scheme for a fixed PBL than opposite during the transition, making a convenient LSM election crucial to obtain appropriate simulation results.

- Simulations with the combination of relatively simple PBL (YSU) and LSM (5lay) schemes in WRF globally provide good results, often closer to observations than other more sophisticated (and computationally expensive) setups.

- Using one-domain simulations provides good results rather than increasing the number of nested domains for the afternoon and evening transition numerical tests.

- On a seasonal basis, the specific humidity evolution is significantly more site-dependent than other variables, considering both the average evolution and its variability.

8.2 Prospects and future research

The study presented in this thesis could be applied to other conditions and experimental sites, or extended in different aspects, opening new paths of research or providing new approaches to current meteorology issues. Here are exposed some of these possibilities as prospects and potential future work:

- To provide a systematic characterization of the wave events occurring along the afternoon and evening ABL transition. Additionally, a numerical study on different WRF configurations could be performed to properly capture these events. Wave-turbulence interactions can be especially challenging and worth analyzing.

- To extend the study of this thesis to an urban environment, paying special attention to the pollutants concentrations and their evolution during the transition.

- To deep into the modelling of the afternoon and evening transition, modifying the vegetation considered by WRF, so that physical processes are better represented. Additionally, an intercomparison between results from different models, looking for strategies to provide better results for the transition forecasting. Actually, this is already work in progress in the context of the BLLAST project (Jiménez et al., 2014).

- The methods employed in this thesis could be applied in order to characterise the morning transition of the ABL. This include an

analysis on the different scales involved, a statistical study of the main atmospheric variables, a comparison between two observational sites, and to focus on the season-to-season differences, as well as designing analogous numerical simulation experiments. Afterwards, a fruitful exercise would be comparing which are the key aspects in both morning and late afternoon and evening transitions.

References

Acevedo, O. C. and Fitzjarrald, D. R.: The early evening surface-layer transition: temporal and spatial variability, J. Atmos. Sci., 58(17), 2650–2667, doi:10.1175/1520-0469(2001)058<2650:TEESLT>2.0.CO;2, 2001.

Agencia Estatal de Meteorología (Spain) and Instituto de Meteorologia (Portugal): Iberian Climate Atlas, ISBN: 978-84-7837-079-5, 2011.

André, J. C. and Mahrt, L.: The nocturnal surface inversion and influence of clear-air radiative cooling, J. Atmos. Sci., 39(4), 864–878, doi:10.1175/1520-0469(1982)039<0864:TNSIAI>2.0.CO;2, 1982.

Angevine, W. M.: Transitional, entraining, cloudy, and coastal boundary layers, Acta Geophys., 56(1), 2–20, doi:10.2478/s11600-007-0035-1, 2008.

Angevine, W. M., Baltink, H. K. and Bosveld, F. C.: Observations of the morning transition of the convective boundary layer, Boundary-Layer Meteorol., 101(2), 209–227, doi:10.1023/A:1019264716195, 2001.

Angevine, W. M., Bazile, E., Legain, D. and Pino, D.: Land surface spinup for episodic modeling, Atmos. Chem. Phys., 14(15), 8165–8172, doi:10.5194/acp-14-8165-2014, 2014.

Arya, S. P.: Introduction to micrometeorology, Academic Press, San Diego, 420 pp., 2001.

Aubinet, M., Vesala, T. and Papale, D.: Eddy covariance: a practical guide to measurement and data analysis, Springer, Berlin, 460 pp., 2012.

Baklanov, A. A., Grisogono, B., Bornstein, R., Mahrt, L., Zilitinkevich, S. S., Taylor, P., Larsen, S. E., Rotach, M. W. and Fernando, H. J. S.: The nature, theory, and modelling of atmospheric planetary boundary layers, Bull. Am. Meteorol. Soc., 92(2), 123–128, doi:10.1175/2010BAMS2797.1, 2011.

Beare, R. J., Edwards, J. M. and Lapworth, A. J.: Simulation of the observed evening transition and nocturnal boundary layers: Large-eddy simulation, Q. J. R. Meteorol. Soc., 132(614), 81–99, doi:10.1256/qj.05.64, 2006.

Benjamin, S. G., Grell, G. A., Brown, J. M., Smirnova, T. G. and Bleck, R.: Mesoscale weather prediction with the RUC hybrid isentropic–terrain-following coordinate model, Mon. Weather Rev., 132(2), 473–494, doi:10.1175/1520-0493(2004)132<0473:MWPWTR>2.0.CO;2, 2004.

Beyrich, F. and Mengelkamp, H.-T.: Evaporation over a heterogeneous land surface: EVA_GRIPS and the LITFASS-2003 experiment—an overview, Boundary-Layer Meteorol., 121(1), 5–32, doi:10.1007/s10546-006-9079-z, 2006.

Blay-Carreras, E.: Transitional periods of the Atmospheric Boundary Layer, PhD thesis, Universitat Politècnica de Catalunya, Spain, 2014.

Blay-Carreras, E., Pardyjak, E. R., Pino, D., Alexander, D. C., Lohou, F. and Lothon, M.: Countergradient heat flux observations during the evening transition period, Atmos. Chem. Phys., 14(17), 9077–9085, doi:10.5194/acp-14-9077-2014, 2014a.

Blay-Carreras, E., Pino, D., Vilà-Guerau de Arellano, J., van de Boer, A., De Coster, O., Darbieu, C., Hartogensis, O., Lohou, F., Lothon, M. and Pietersen, H.: Role of the residual layer and large-scale subsidence on the development and evolution of the convective boundary layer, Atmos. Chem. Phys., 14(9), 4515–4530, doi:10.5194/acp-14-4515-2014, 2014b.

Bonin, T., Chilson, P., Zielke, B. and Fedorovich, E.: Observations of the early evening boundary-layer transition using a small unmanned aerial system, Boundary-Layer Meteorol., 146(1), 119–132, doi:10.1007/s10546-012-9760-3, 2013.

Borge, R., Alexandrov, V., del Vas, J. J., Lumbreras, J. and Rodríguez, E.: A comprehensive sensitivity analysis of the WRF model for air quality applications over the Iberian Peninsula, Atmos. Environ., 42(37), 8560–8574, doi:10.1016/j.atmosenv.2008.08.032, 2008.

Brazel, A. J., Fernando, H. J. S., Hunt, J. C. R., Selover, N., Hedquist, B. C. and Pardyjak, E.: Evening transition observations in Phoenix, Arizona, J. Appl. Meteorol., 44(1), 99–112, doi:10.1175/JAM-2180.1, 2005.

Busse, J. and Knupp, K.: Observed characteristics of the afternoon–evening boundary layer transition based on sodar and surface data, J. Appl. Meteorol. Climatol., 51(3), 571–582, doi:10.1175/2011JAMC2607.1, 2012.

Canut G., Legain, D., Piguet, B., Moulin, E. and Tzanos D.: The eddy-covariance method applied in a tethered- balloon, 21st Symposium on Boundary Layers and Turbulence (AMS), 9-13 June 2014, Leeds, UK, 2014.

Carrillo, J., Guerra, J. C., Cuevas, E. and Barrancos, J.: Characterization of the marine boundary layer and the trade-wind inversion over the sub-tropical North Atlantic, Boundary-Layer Meteorol., doi:10.1007/s10546-015-0081-1, 2015.

Casso-Torralba, P., Vilà-Guerau de Arellano, J., Bosveld, F., Soler, M. R., Vermeulen, A., Werner, C. and Moors, E.: Diurnal and vertical variability of the sensible heat and carbon dioxide budgets in the atmospheric surface layer, J. Geophys. Res., 113(D12), D12119, doi:10.1029/2007JD009583, 2008.

Caughey, S. J., Wyngaard, J. C. and Kaimal, J.: Turbulence in the evolving stable boundary layer, J. Atmos. Sci., 36(6), 1041–1052, doi:10.1175/1520-0469(1979)036<1041:TITESB>2.0.CO;2, 1979.

Chen, F. and Dudhia, J.: Coupling an advanced land surface–hydrology model with the Penn State–NCAR MM5 modeling system. Part I: Model implementation and sensitivity, Mon. Weather Rev., 129(4), 569–585, doi:10.1175/1520-0493(2001)129<0569:CAALSH>2.0.CO;2, 2001.

Clarke, R. H.: Observational studies in the atmospheric boundary layer, Q. J. R. Meteorol. Soc., 96, 91–114, doi: 10.1002/qj.49709640709, 1970.

Collaud Coen, M., Praz, C., Haefele, A., Ruffieux, D., Kaufmann, P. and Calpini, B.: Determination and climatology of the planetary boundary layer height above the Swiss plateau by in situ and remote sensing measurements as well as by the COSMO-2 model, Atmos. Chem. Phys., 14(23), 13205–13221, doi:10.5194/acp-14-13205-2014, 2014.

Cuxart, J., Yague, C., Morales, G., Terradellas, E., Orbe, J., Calvo, J., Fernandez, A., Soler, M. R., Infante, C., Buenestado, P., Espinalt, A., Joergensen, H. E., Rees, J. M., Vila, J., Redondo, J. M., Cantalapiedra, I. R. and Conangla, L.: Stable atmospheric boundary-layer experiment in Spain (SABLES 98): a report, Boundary-Layer Meteorol., 96(3), 337–370, doi:10.1023/A:1002609509707, 2000.

Cuxart, J.: Nocturnal basin low-level jets: an integrated study, Acta Geophys., 56(1), 100–113, doi:10.2478/s11600-007-0042-2, 2008.

Darbieu, C., Lohou, F., Lothon, M., Vilà-Guerau de Arellano, J., Couvreux, F., Durand, P., Pino, D., Patton, E. G., Nilsson, E., Blay-Carreras, E. and Gioli, B.: Turbulence vertical structure of the boundary layer during the afternoon transition, Atmos. Chem. Phys., 15(17), 10071–10086, doi:10.5194/acp-15-10071-2015, 2015.

Daubechies, I.: The wavelet transform, time-frequency localization and signal analysis, IEEE Trans. Inf. Theory, 36(5), doi:10.1109/18.57199, 1990.

Daubechies, I.: Ten lectures on wavelets, CBMS Lecture Notes Series, Society for Industrial and Applied Mathematics, Philadelphia, PA, USA, 357 pp., 1992.

Delfino, R. J., Sioutas, C. and Malik, S.: Potential role of ultrafine particles in associations between airborne particle mass and cardiovascular health, Environ. Health Perspect., 113(8), 934–946, doi:10.1289/ehp.7938, 2005.

Doran, J. C., Fast, J. D. and Horel, J.: The VTMX 2000 campaign, Bull. Am. Meteorol. Soc., 83(4), 537–551, doi:10.1175/1520-0477(2002)083<0537:TVC>2.3.CO;2, 2002.

Dudhia, J.: Numerical study of convection observed during the winter monsoon experiment using a mesoscale two-dimensional model, J. Atmos. Sci., 46(20), 3077–3107, doi:10.1175/1520-0469(1989)046<3077:NSOCOD>2.0.CO;2, 1989.

Dudhia, J.: A multi-layer soil temperature model for MM5, Proceedings of the Sixth PSU/NCAR Mesoscale Model Users Workshop, Boulder, CO, 49-50, 1996.

Edwards, J. M., Basu, S., Bosveld, F. C. and Holtslag, A. A. M.: The impact of radiation on the GABLS3 large-eddy simulation through the night and during the morning transition, Boundary-Layer Meteorol., 152(2), 189–211, doi:10.1007/s10546-013-9895-x, 2014.

Ek, M. B., Mitchell, K.E., Lin, Y., Rogers, E., Grunmann, P., Koren, V., Gayno, G, and Tarpley J. D.: Implementation of Noah land surface model advances in the National Centers for Environmental Prediction operational mesoscale Eta model, J. Geophys. Res., 108(D22), 8851, doi:10.1029/2002JD003296, 2003.

Eymard, L. and Weill, A.: A study of gravity waves in the planetary boundary layer by acoustic sounding, Boundary-Layer Meteorol., 17(2), 231–245, doi:10.1007/BF00117982, 1979.

Farge, M.: Wavelet transforms and their applications to turbulence, Annu. Rev. Fluid Mech., 24(1), 395–457, doi:10.1146/annurev.fluid.24.1.395, 1992.

Fernández-Gálvez, J., Guerrero-Rascado, J. L., Molero, F., Lyamani, H., Revuelta, M. A., Navas-Guzmán, F., Sastre, M., Bravo-Aranda, J. A., Fernández, A. J., Granados-Muñoz, M. J., Gómez-Moreno, F. J., Olmo, F. J., Pujadas, M. and Alados-Arboledas, L.: Aerosol size distribution from inversion of solar radiances and measured at ground-level during SPALI10 campaign, Atmos. Res., 127, 130–140, doi:10.1016/j.atmosres.2012.03.015, 2013.

Fernando, H. J. S., Princevac, M., Pardyjak, E. and Dato, A.: The decay of convective turbulence during evening transition period. In: Proceedings of the 11th Conference on Mountain Meteorology and MAP Meeting, Bartlett (NH), USA, paper 10.3, https://ams.confex.com/ams/pdfpapers/76878.pdf, 2004.

Fernando, H. J. S., Verhoef, B., Di Sabatino, S., Leo, L. S. and Park, S.: The Phoenix Evening Transition Flow Experiment (TRANSFLEX), Boundary-Layer Meteorol., 147(3), 443–468, doi:10.1007/s10546-012-9795-5, 2013.

Fitzjarrald, D. R. and Lala, G. G.: Hudson valley fog environments, J. Appl. Meteorol., 28, 1303–1328, doi:10.1175/1520-0450(1989)028%3C1303:HVFE%3E2.0.CO;2, 1989.

Foken, T.: Micrometeorology, Springer, Berlin, 308 pp., 2008.

Foufoula-Georgiou, E., and Kumar, P. (Eds.): Wavelets in Geophysics. Academic Press, London, 373 pp., 1995.

Garratt, J. R.: The atmospheric boundary layer, Cambridge University Press, New York, 316 pp., 1992.

Gioli, B., Miglietta, F., Vaccari, F. P., Zaldei, A. and De Martino, B.: The Sky Arrow ERA, an innovative airborne platform to monitor mass, momentum and energy exchange of ecosystems, Ann. Geophys., 49(1), 109–116, 2006.

Gómez-Moreno, F. J., Núñez, L., Plaza, J., Alonso, D., Pujadas, M. and Artíñano, B.: Annual evolution and generation mechanisms of particulate nitrate in Madrid, Atmos. Environ., 41(2), 394–406, doi:10.1016/j.atmosenv.2006.07.040, 2007.

Grant, A. L. M.: An observational study of the evening transition boundary-layer, Q. J. R. Meteorol. Soc., 123(539), 657–677, doi:10.1002/qj.49712353907, 1997.

Grimsdell, A. W. and Angevine, W. M.: Observations of the afternoon transition of the convective boundary layer, J. Appl. Meteorol., 41, 3–11, doi:10.1175/1520-0450(2002)041<0003:OOTATO>2.0.CO;2, 2002.

Haar, A.: Zur Theorie der orthogonalen Funktionensysteme, Math. Ann., 69(3), 331–371, doi:10.1007/BF01456326, 1910.

Holtslag, B.: GEWEX Atmospheric Boundary-Layer Study (GABLS) on stable boundary layers, Boundary-Layer Meteorol., 118(2), 243–246, doi:10.1007/s10546-005-9008-6, 2006.

Holtslag, A. A. M. and Boville, B. A.: Local versus nonlocal boundary-layer diffusion in a global climate model, J. Clim., 6(10), 1825–1842, doi:10.1175/1520-0442(1993)006<1825:LVNBLD>2.0.CO;2, 1993.

Holtslag, A. A. M., Svensson, G., Baas, P., Basu, S., Beare, B., Beljaars, A. C. M., Bosveld, F. C., Cuxart, J., Lindvall, J., Steeneveld, G. J., Tjernström, M. and Van De Wiel, B. J. H.: Stable atmospheric boundary layers and diurnal cycles: challenges for weather and climate models, Bull. Am. Meteorol. Soc., 94(11), 1691–1706, doi:10.1175/BAMS-D-11-00187.1, 2013.

Hong, S.-Y., Dudhia, J. and Chen, S.-H.: A revised approach to ice microphysical processes for the bulk parameterization of clouds and precipitation, Mon. Weather Rev., 132(1), 103–120, doi:10.1175/1520-0493(2004)132<0103:ARATIM>2.0.CO;2, 2004.

Hong, S.-Y., Noh, Y. and Dudhia, J.: A new vertical diffusion package with an explicit treatment of entrainment processes, Mon. Weather Rev., 134(9), 2318–2341, doi:10.1175/MWR3199.1, 2006.

Howell, J. F. and Mahrt, L.: Multiresolution flux decomposition, Boundary-Layer Meteorol., 83(1), 117–137, doi:10.1023/A:1000210427798, 1997.

Hu, X.-M., Nielsen-Gammon, J. W. and Zhang, F.: Evaluation of three planetary boundary layer schemes in the WRF model, J. Appl. Meteorol. Climatol., 49(9), 1831–1844, doi:10.1175/2010JAMC2432.1, 2010.

Huang, M., Huang, B. and Huang, A. H.: Implementation of 5-layer thermal diffusion scheme in weather research and forecasting model with Intel Many Integrated Cores, SPIE Remote Sens., 9247, 924709, doi:10.1117/12.2069426, 2014.

Janjić, Z. I.: The step-mountain eta coordinate model: Further developments of the convection, viscous sublayer, and turbulence closure schemes, Mon. Weather Rev., 122(5), 927–945, doi:10.1175/1520-0493(1994)122<0927:TSMECM>2.0.CO;2, 1994.

Janjic, Z.I.: The surface layer in the NCEP Eta Model. In: Proceedings of the 11th Conference on numerical weather prediction, Norfolk (VA), USA, pp. 354–355, 1996.

Jensen, D. D., Nadeau, D. F., Hoch, S. W. and Pardyjak, E. R.: Observations of near-surface heat-flux and temperature profiles through the early evening

transition over contrasting surfaces, Boundary-Layer Meteorol., doi:10.1007/s10546-015-0067-z, 2015.

Jiménez, P. A., Dudhia, J., González-Rouco, J. F., Navarro, J., Montávez, J. P. and García-Bustamante, E.: A revised scheme for the WRF surface layer formulation, Mon. Weather Rev., 140(3), 898–918, doi:10.1175/MWR-D-11-00056.1, 2012.

Jiménez, M.A., Angevine, W.M., Bazile, E., Couvreux, F., Cuxart, J., Pino, D. and Sastre, M.: An intercomparison of mesoscale simulations during the Boundary Layer Late Afternoon and Sunset Turbulence (BLLAST) experimental field campaign, EGU General Assembly 2014, Vienna, Austria, 2014.

Kaimal, J. C. and Finnigan, J. J.: Atmospheric Boundary Layer Flows: their structure and measurements, Oxford University Press, New York, 289 pp., 1994.

Kalnay, E., Kanamitsu, M., Kistler, R., Collins, W., Deaven, D., Gandin, L., Iredell, M., Saha, S., White, G., Woollen, J., Zhu, Y., Leetmaa, A., Reynolds, R., Chelliah, M., Ebisuzaki, W., Higgins, W., Janowiak, J., Mo, K. C., Ropelewski, C., Wang, J., Jenne, R. and Joseph, D.: The NCEP/NCAR 40-Year Reanalysis Project, Bull. Am. Meteorol. Soc., 77(3), 437–471, doi:10.1175/1520-0477(1996)077<0437:TNYRP>2.0.CO;2, 1996.

Kelvin, J.: Evaporation in fen wetlands, PhD thesis, Cranfield University, United Kingdom, 2011.

Kleczek, M. A., Steeneveld, G.-J. and Holtslag, A. A. M.: Evaluation of the Weather Research and Forecasting mesoscale model for GABLS3: Impact of boundary-layer schemes, boundary conditions and spin-up, Boundary-Layer Meteorol., 152(2), 213–243, doi:10.1007/s10546-014-9925-3, 2014.

Klein, P. M., Hu, X.-M. and Xue, M.: Impacts of mixing processes in nocturnal atmospheric boundary layer on urban ozone concentrations, Boundary-Layer Meteorol., 150(1), 107–130, doi:10.1007/s10546-013-9864-4, 2014.

Kolmogorov, A. N.: The local structure of turbulence in incompressible viscous fluid for very large Reynolds numbers, Dokl. Akad. Nauk. SSSR, 30, 299–303, 1941a.

Kolmogorov, A.N.: Dissipation of energy in isotropic turbulence, Dokl. Akad. Nauk. SSSR, 32, 19–21, 1941b.

Lapworth, A.: Factors determining the decrease in surface wind speed following the evening transition, Q. J. R. Meteorol. Soc., 129(591), 1945–1968, doi:10.1256/qj.02.163, 2003.

Lapworth, A.: The morning transition of the nocturnal boundary layer, Boundary-Layer Meteorol., 119(3), 501–526, doi:10.1007/s10546-005-9046-0, 2006.

Lapworth, A.: Observations of the site dependency of the morning wind and the role of gravity waves in the transitions, Q. J. R. Meteorol. Soc., 141(686), 27–36, doi:10.1002/qj.2340, 2015.

Lapworth, A. J. and Claxton, B. M.: The effect of terrain on the evening wind, Q. J. R. Meteorol. Soc., 136(652), 1763–1772, doi:10.1002/qj.675, 2010.

Leduc, M. and Laprise, R.: Regional climate model sensitivity to domain size, Clim. Dyn., 32(6), 833–854, doi:10.1007/s00382-008-0400-z, 2009.

Leduc, M., Laprise, R., Moretti-Poisson, M. and Morin, J.-P.: Sensitivity to domain size of mid-latitude summer simulations with a regional climate model, Clim. Dyn., 37(1-2), 343–356, doi:10.1007/s00382-011-1008-2, 2011.

Lee, S.-M., Fernando, H. J. S. and Grossman-Clarke, S.: MM5-SMOKE-CMAQ as a modeling tool for 8-h ozone regulatory enforcement: application to the state

of Arizona, Environ. Model. Assess., 12(1), 63–74, doi:10.1007/s10666-006-9053-7, 2007.

Legain, D., Bousquet, O., Douffet, T., Tzanos, D., Moulin, E., Barrie, J. and Renard, J.-B.: High-frequency boundary layer profiling with reusable radiosondes, Atmos. Meas. Tech., 6(8), 2195–2205, doi:10.5194/amt-6-2195-2013, 2013.

LeMone, M., Grossman, R., Coulter, R., Wesley, M., Klazura, G., Poulos, G., Blumen, W., Lundquist, J. K., Cuenca, R., Kelly, S., Brandes, E., Oncley, S., McMillen, R. and Hicks, B.: Land-atmosphere interaction research, early results, and opportunities in the Walnut River Watershed in southeast Kansas: CASES and ABLE, Bull. Am. Meteorol. Soc., 81, 757–779, doi:10.1175/1520-0477(2000)081<0757:LIRERA>2.3.CO;2, 2000.

Lenschow, D. H., Stankov, B. B. and Mahrt, L.: The rapid morning boundary-layer transition, J. Atmos. Sci., 36(11), 2108–2124, doi:10.1175/1520-0469(1979)036<2108:TRMBLT>2.0.CO;2, 1979.

Liu, G., Liu, Y. and Endo, S.: Evaluation of surface flux parameterizations with long-term ARM observations, Mon. Weather Rev., 141(2), 773–797, doi:10.1175/MWR-D-12-00095.1, 2013.

Lohou, F., Saïd, F., Lothon, M., Durand, P. and Serça, D.: Impact of boundary-layer processes on near-surface turbulence within the West African monsoon, Boundary-Layer Meteorol., 136(1), 1–23, doi:10.1007/s10546-010-9493-0, 2010.

Lohou, F., Kergoat, L., Guichard, F., Boone, A., Cappelaere, B., Cohard, J.-M., Demarty, J., Galle, S., Grippa, M., Peugeot, C., Ramier, D., Taylor, C. M. and Timouk, F.: Surface response to rain events throughout the West African monsoon, Atmos. Chem. Phys., 14(8), 3883–3898, doi:10.5194/acp-14-3883-2014, 2014.

Lothon, M., Saïd, F., Lohou, F. and Campistron, B.: Observation of the diurnal cycle in the low troposphere of West Africa, Mon. Weather Rev., 136(9), 3477–3500, doi:10.1175/2008MWR2427.1, 2008.

Lothon, M. and Lenschow, D. H.: Studying the afternoon transition of the planetary boundary layer, Eos, Trans. Am. Geophys. Union, 91(29), 253–254, doi:10.1029/2010EO290001, 2010.

Lothon, M., Lohou, F., Pino, D., Couvreux, F., Pardyjak, E. R., Reuder, J., Vilà-Guerau de Arellano, J., Durand, P., Hartogensis, O., Legain, D., Augustin, P., Gioli, B., Lenschow, D. H., Faloona, I., Yagüe, C., Alexander, D. C., Angevine, W. M., Bargain, E., Barrié, J., Bazile, E., Bezombes, Y., Blay-Carreras, E., van de Boer, A., Boichard, J. L., Bourdon, A., Butet, A., Campistron, B., de Coster, O., Cuxart, J., Dabas, A., Darbieu, C., Deboudt, K., Delbarre, H., Derrien, S., Flament, P., Fourmentin, M., Garai, A., Gibert, F., Graf, A., Groebner, J., Guichard, F., Jiménez, M. A., Jonassen, M., van den Kroonenberg, A., Magliulo, V., Martin, S., Martinez, D., Mastrorillo, L., Moene, A. F., Molinos, F., Moulin, E., Pietersen, H. P., Piguet, B., Pique, E., Román-Cascón, C., Rufin-Soler, C., Saïd, F., Sastre-Marugán, M., Seity, Y., Steeneveld, G. J., Toscano, P., Traullé, O., Tzanos, D., Wacker, S., Wildmann, N. and Zaldei, A.: The BLLAST field experiment: Boundary-Layer Late Afternoon and Sunset Turbulence, Atmos. Chem. Phys., 14(20), 10931–10960, doi:10.5194/acp-14-10931-2014, 2014.

Mahrt, L.: The early evening boundary layer transition, Q. J. R. Meteorol. Soc., 107, 329–343, doi:10.1002/qj.49710745205, 1981.

Mahrt, L.: Stably Stratified Atmospheric Boundary Layers, Annu. Rev. Fluid Mech., 46(1), 23–45, doi:10.1146/annurev-fluid-010313-141354, 2014.

Martin, S., Bange, J. and Beyrich, F.: Meteorological profiling of the lower troposphere using the research UAV "M²AV Carolo," Atmos. Meas. Tech., 4(4), 705–716, doi:10.5194/amt-4-705-2011, 2011.

Martínez, G., Valero, F. and Vázquez, L.: Characterization of the Martian convective boundary layer, J. Atmos. Sci., 66(7), 2044–2058, doi:10.1175/2009JAS3007.1, 2009.

Martínez, D., Jiménez, M. A., Cuxart, J. and Mahrt, L.: Heterogeneous nocturnal cooling in a large basin under very stable conditions, Boundary-Layer Meteorol., 137(1), 97–113, doi:10.1007/s10546-010-9522-z, 2010.

Martínez, G., Valero, F. and Vázquez, L.: The TKE budget in the convective Martian planetary boundary layer, Q. J. R. Meteorol. Soc., 137(661), 2194–2208, 2011.

Martínez, G. M., Valero, F., Vázquez, L. and Elliott, H. M.: The Martian planetary boundary layer: Turbulent kinetic energy and fundamental similarity scales, Sol. Syst. Res., 47(6), 446–453, doi:10.1134/S003809461306004X, 2013.

Martínez, G. M., Rennó, N., Fischer, E., Borlina, C. S., Hallet, B., de la Torre Juárez, M., Vasavada, a R., Ramos, M., Hamilton, V., Gomez-Elvira, J. and Haberle, R. M.: Surface energy budget and thermal inertia at Gale Crater: Calculations from ground-based measurements, J. Geophys. Res. Planets, 119, doi:10.1002/2014JE004618, 2014.

Mellor, G. L. and Yamada, T.: Development of a turbulence closure model for geophysical fluid problems, Rev. Geophys., 20(4), 851–875, doi:10.1029/RG020i004p00851, 1982.

Meyers, S. D., Nelly, B. G. and O'Brien, J. J.: An introduction to wavelet analysis in oceanography and meteorology: with application to the dispersion of Yanai waves., Mon. Wea. Rev., 121, 2858-2866, 1993.

Mira, M., Valor, E., Boluda, R., Caselles, V. and Coll, C.: Influence of soil water content on the thermal infrared emissivity of bare soils: Implication for land surface temperature determination, J. Geophys. Res., 112(F4), F04003, doi:10.1029/2007JF000749, 2007.

Mlawer, E. J., Taubman, S. J., Brown, P. D., Iacono, M. J. and Clough, S. A.: Radiative transfer for inhomogeneous atmospheres: RRTM, a validated correlated-k model for the longwave, J. Geophys. Res., 102(D14), 16663, doi:10.1029/97JD00237, 1997.

Moene, A. F. and van Dam, J. C.: Transport in the Atmosphere-Vegetation-Soil continuum, Cambridge University Press, New York, 446 pp., 2014.

Morlet, J.: Sampling theory and wave propagation, Proc. 51st Annu. Meet. Soc. Explor. Geophys., Los Angeles, 1981.

Nadeau, D. F., Pardyjak, E. R., Higgins, C. W., Fernando, H. J. S. and Parlange, M. B.: A simple model for the afternoon and early evening decay of convective turbulence over different land surfaces, Boundary-Layer Meteorol., 141(2), 301–324, doi:10.1007/s10546-011-9645-x, 2011.

Nieuwstadt, F. T. M. and Brost, R. A.: The decay of convective turbulence, J. Atmos. Sci., 43(6), 532–546, doi:10.1175/1520-0469(1986)043<0532:TDOCT>2.0.CO;2, 1986.

Nieuwstadt, F. T. M. and Duynkerke, P. G. G.: Turbulence in the atmospheric boundary layer, Atmos. Res., 40, 111–142, doi:10.1016/0169-8095(95)00034-8, 1996.

Nilsson, E. O., Sahlée, E. and Rutgersson, A.: Turbulent momentum flux characterization using extended multiresolution analysis, Q. J. R. Meteorol. Soc., 140(682), 1715–1728, doi:10.1002/qj.2252, 2014.

Oldroyd, H. J., Pardyjak, E. R., Huwald, H. and Parlange, M. B.: Adapting tilt corrections and the governing flow equations for steep, fully three-dimensional, mountainous terrain, Boundary-Layer Meteorol., doi:10.1007/s10546-015-0066-0, 2015.

Ouwersloot, H. G., Vilà-Guerau de Arellano, J., Nölscher, A. C., Krol, M. C., Ganzeveld, L. N., Breitenberger, C., Mammarella, I., Williams, J. and Lelieveld, J.: Characterization of a boreal convective boundary layer and its impact on atmospheric chemistry during HUMPPA-COPEC-2010, Atmos. Chem. Phys., 12(19), 9335–9353, doi:10.5194/acp-12-9335-2012, 2012.

Papadopoulos, K. H. and Helmis, C. G.: Evening and morning transition of katabatic flows, Boundary-Layer Meteorol., 92(2), 195–227, doi:10.1023/A:1002070526425, 1999.

Pardyjak, E. R., Fernando, H. J. S., Hunt, J. C. R., Grachev, A. A. and Anderson, J.: A case study of the development of nocturnal slope flows in a wide open valley and associated air quality implications, Meteorol. Zeitschrift, 18(1), 85–100, doi:10.1127/0941-2948/2009/362, 2009.

Peña, A., Floors, R., Sathe, A., Gryning, S.-E., Wagner, R., Courtney, M. S., Larsén, X. G., Hahmann, A. N. and Hasager, C. B.: Ten years of boundary-layer and wind-power meteorology at Høvsøre, Denmark, Boundary-Layer Meteorol., doi:10.1007/s10546-015-0079-8, 2015.

Petrosyan, A., Galperin, B., Larsen, S. E., Lewis, S. R., Määttänen, A., Read, P. L., Renno, N., Rogberg, L. P. H. T., Savijärvi, H., Siili, T., Spiga, A., Toigo, A. and Vázquez, L.: The Martian atmospheric boundary layer, Rev. Geophys., 49(3), RG3005, doi:10.1029/2010RG000351, 2011.

Pietersen, H. P., Vilà-Guerau de Arellano, J., Augustin, P., van de Boer, A., de Coster, O., Delbarre, H., Durand, P., Fourmentin, M., Gioli, B., Hartogensis, O., Lohou, F., Lothon, M., Ouwersloot, H. G., Pino, D. and Reuder, J.: Study of

a prototypical convective boundary layer observed during BLLAST: contributions by large-scale forcings, Atmos. Chem. Phys., 15(8), 4241–4257, doi:10.5194/acp-15-4241-2015, 2015.

Pope, C. A. and Dockery, D. W.: Health effects of fine particulate air pollution: lines that connect, J. Air Waste Manage. Assoc., 56(6), 709–742, doi:10.1080/10473289.2006.10464485, 2006.

Poulos, G. S., Blumen, W., Fritts, D. C., Lundquist, J. K., Sun, J., Burns, S. P., Nappo, C., Banta, R., Newsom, R., Cuxart, J., Terradellas, E., Balsley, B. and Jensen, M.: CASES-99: A comprehensive investigation of the stable nocturnal boundary layer, Bull. Am. Meteorol. Soc., 83(4), 555–581, doi:10.1175/1520-0477(2002)083<0555:CACIOT>2.3.CO;2, 2002.

Prandtl, L.: Über Flüssigkeitsbewegung bei sehr kleiner Reibung, Proceedings of the Third International Math. Congress, Heidelberg, pp. 484–491, 1904.

Refslund, J., Dellwik, E., Hahmann, A. N., Barlage, M. J. and Boegh, E.: Development of satellite green vegetation fraction time series for use in mesoscale modeling: application to the European heat wave 2006, Theor. Appl. Climatol., 117(3-4), 377–392, doi:10.1007/s00704-013-1004-z, 2014.

Reuder, J., Jonassen, M. O. and Ólafsson, H.: The Small Unmanned Meteorological Observer SUMO: Recent developments and applications of a micro-UAS for atmospheric boundary layer research, Acta Geophys., 60(5), 1454–1473, doi:10.2478/s11600-012-0042-8, 2012.

Revuelta, M. A., Sastre, M., Fernández, A. J., Martín, L., García, R., Gómez-Moreno, F. J., Artíñano, B., Pujadas, M. and Molero, F.: Characterization of the Eyjafjallajökull volcanic plume over the Iberian Peninsula by lidar remote sensing and ground-level data collection, Atmos. Environ., 48, 46–55, doi:10.1016/j.atmosenv.2011.05.033, 2012.

Reynolds, O.: On the dynamical theory of incompressible viscous fluids and the determination of the criterion, Philos. Trans. R. Soc. London, Ser. A, 186, 123–164, 1895.

Román-Cascón, C., Yagüe, C., Sastre, M., Maqueda, G., Salamanca, F. and Viana, S.: Observations and WRF simulations of fog events at the Spanish Northern Plateau, Adv. Sci. Res., 8, 11–18, doi:10.5194/asr-8-11-2012, 2012.

Román-Cascón, C., Yagüe, C., Viana, S., Sastre, M., Maqueda, G., Lothon, M. and Gómara, I.: Near-monochromatic ducted gravity waves associated with a convective system close to the Pyrenees, Q. J. R. Meteorol. Soc., 141(689), 1320–1332, doi:10.1002/qj.2441, 2015a.

Román-Cascón, C., Yagüe, C., Mahrt, L., Sastre, M., Steeneveld, G.-J., Pardyjak, E., van de Boer, A. and Hartogensis, O.: Interactions among drainage flows, gravity waves and turbulence: a BLLAST case study, Atmos. Chem. Phys., 15(15), 9031–9047, doi:10.5194/acp-15-9031-2015, 2015b.

Román-Cascón, C., Steeneveld, G.-J., Yagüe, C., Sastre, M., Arrillaga, J. A. and Maqueda, G.: Forecasting radiation fog at climatologically contrasting sites: evaluation of statistical methods and WRF, Q. J. R. Meteorol. Soc., submitted, 2015c.

Saïd, F., Corsmeier, U., Kalthoff, N., Kottmeier, C., Lothon, M., Wieser, A., Hofherr, T. and Perros, P.: ESCOMPTE experiment: intercomparison of four aircraft dynamical, thermodynamical, radiation and chemical measurements, Atmos. Res., 74(1-4), 217–252, doi:10.1016/j.atmosres.2004.06.012, 2005.

San José, R., Casanova, J. L., Viloria, R. E. and Casanova, J.: Evaluation of the turbulent parameters of the unstable surface boundary layer outside Businger's range, Atmos. Environ., 19(10), 1555–1561, doi:10.1016/0004-6981(85)90206-9, 1985.

Sandeep, A., Rao, T. N. and Rao, S. V. B.: A comprehensive investigation on afternoon transition of the atmospheric boundary layer over a tropical rural site, Atmos. Chem. Phys., 15(13), 7605–7617, doi:10.5194/acp-15-7605-2015, 2015.

Salamanca, F., Martilli, A. and Yagüe, C.: A numerical study of the Urban Heat Island over Madrid during the DESIREX (2008) campaign with WRF and an evaluation of simple mitigation strategies, Int. J. Climatol., 32(15), 2372–2386, doi:10.1002/joc.3398, 2012.

Sastre, M., Yagüe, C., Román-Cascón, C., Maqueda, G., Salamanca, F. and Viana, S.: Evening transitions of the atmospheric boundary layer: characterization, case studies and WRF simulations, Adv. Sci. Res., 8, 39–44, doi:10.5194/asr-8-39-2012, 2012.

Sastre, M., Steeneveld, G.-J., Yagüe, C., Román-Cascón, C., Maqueda, G. and van de Boer, A.: Sensitivity of LSM and PBL schemes in WRF simulations of the Atmospheric Boundary Layer during the BLLAST campaign, BLLAST Workshop 2013, Bergen, Norway, http://bllast.sedoo.fr/workshops/august2013/slides/presentations/Sastre_WRF-PBL-LSM.pdf, 2013.

Sastre, M., Yagüe, C., Román-Cascón, C. and Maqueda, G.: Atmospheric boundary-layer evening transitions: a comparison between two different experimental sites, Boundary-Layer Meteorol., doi:10.1007/s10546-015-0065-1, 2015.

Skamarock, W. C. and Klemp, J. B.: A time-split nonhydrostatic atmospheric model for weather research and forecasting applications, J. Comput. Phys., 227(7), 3465–3485, doi:10.1016/j.jcp.2007.01.037, 2008.

Skamarock, W. C., Klemp, J. B., Dudhia, J., Gill, D. O., Barker, D. M., Duda, M. G., Huang, X.-Y., Wang, W. and Powers, J. G.: A description of the Advanced Research WRF version 3, NCAR Technical note TN-475, 113 pp., 2008.

Smirnova, T. G., Brown, J. M. and Benjamin, S. G.: Performance of different soil model configurations in simulating ground surface temperature and surface fluxes, Mon. Weather Rev., 125, 1870–1884, 1997.

Smirnova, T. G., Brown, J. M., Benjamin, S. G. and Kim, D.: Parameterization of cold-season processes in the MAPS land-surface scheme, J. Geophys. Res., 105(D3), 4077, doi:10.1029/1999JD901047, 2000.

Seibert, P., Beyrich, F., Gryning, S. E., Joffre, S., Rasmussen, A. and Tercier, P.: Review and intercomparison of operational methods for the determination of the mixing height, Atmos. Environ., 34(7), 1001–1027, doi:10.1016/S1352-2310(99)00349-0, 2000.

Soler, M. R., Udina, M. and Ferreres, E.: Observational and numerical simulation study of a sequence of eight atmospheric density currents in Northern Spain, Boundary-Layer Meteorol., 153(2), 195–216, doi:10.1007/s10546-014-9942-2, 2014.

Sorbjan, Z.: Structure of the atmospheric boundary layer, Prentice Hall, New Jersey, 317 pp., 1989.

Sorbjan, Z.: Decay of convective turbulence revisited, Boundary-Layer Meteorol., 82(3), 503–517, doi:10.1023/A:1000231524314, 1997.

Sorbjan, Z.: A numerical study of daily transitions in the convective boundary layer, Boundary-Layer Meteorol., 123(3), 365–383, doi:10.1007/s10546-006-9147-4, 2007.

Steele, C. J., Dorling, S. R., von Glasow, R. and Bacon, J.: Idealized WRF model sensitivity simulations of sea breeze types and their effects on offshore windfields, Atmos. Chem. Phys., 13(1), 443–461, doi:10.5194/acp-13-443-2013, 2013.

Steeneveld, G. J., Ronda, R. J. and Holtslag, A. A. M.: The challenge of forecasting the onset and development of radiation fog using mesoscale atmospheric models, Boundary-Layer Meteorol., 154(2), 265–289, doi:10.1007/s10546-014-9973-8, 2015.

Sterk, H. A. M., Steeneveld, G. J. and Holtslag, A. A. M.: The role of snow-surface coupling, radiation, and turbulent mixing in modeling a stable boundary layer over Arctic sea ice, J. Geophys. Res. Atmos., 118(3), 1199–1217, doi:10.1002/jgrd.50158, 2013.

Stull, R. B.: An introduction to boundary layer meteorology, Kluwer Academic Publishers, Dordrecht, 666 pp., 1988.

Sun, J., Mahrt, L., Nappo, C. and Lenschow, D. H.: Wind and temperature oscillations generated by wave–turbulence interactions in the stably stratified boundary layer, J. Atmos. Sci., 72(4), 1484–1503, doi:10.1175/JAS-D-14-0129.1, 2015a.

Sun, J., Nappo, C. J., Mahrt, L., Belušić, D., Grisogono, B., Stauffer, D. R., Pulido, M., Staquet, C., Jiang, Q., Pouquet, A., Yagüe, C., Galperin, B., Smith, R. B., Finnigan, J. J., Mayor, S. D., Svensson, G., Grachev, A. A. and Neff, W. D.: Review of wave-turbulence interactions in the stable atmospheric boundary layer, Rev. Geophys., doi:10.1002/2015RG000487, 2015b.

Sukoriansky, S., Galperin, B. and Perov, V.: A quasi-normal scale elimination model of turbulence and its application to stably stratified flows, Nonlinear Process. Geophys., 13(1), 9–22, doi:10.5194/npg-13-9-2006, 2006.

Sukoriansky, S.: Implementation of the Quasi-Normal Scale Elimination (QNSE) Model of stably stratified Turbulence in WRF. Technical report, Report on WRF-DTC Visit, Developmental Testbed Center, 109 pp., 2008.

Svensson, G., Holtslag, A. A. M., Kumar, V., Mauritsen, T., Steeneveld, G. J., Angevine, W. M., Bazile, E., Beljaars, A., Bruijn, E. I. F., Cheng, A., Conangla, L., Cuxart, J., Ek, M., Falk, M. J., Freedman, F., Kitagawa, H., Larson, V. E., Lock, A., Mailhot, J., Masson, V., Park, S., Pleim, J., Söderberg, S., Weng, W. and Zampieri, M.: Evaluation of the diurnal cycle in the atmospheric boundary layer over land as represented by a variety of single-column models: the second GABLS experiment, Boundary-Layer Meteorol., 140(2), 177–206, doi:10.1007/s10546-011-9611-7, 2011.

Tastula, E.-M., Galperin, B., Dudhia, J., LeMone, M. A., Sukoriansky, S. and Vihma, T.: Methodical assessment of the differences between the QNSE and MYJ PBL schemes for stable conditions, Q. J. R. Meteorol. Soc., 141(691), 2077–2089, doi:10.1002/qj.2503, 2015.

Taylor, A. C., Beare, R. J. and Thomson, D. J.: Simulating dispersion in the evening-transition boundary layer, Boundary-Layer Meteorol., 153(3), 389–407, doi:10.1007/s10546-014-9960-0, 2014.

Teixeira, J., Stevens, B., Bretherton, C. S., Cederwall, R., Klein, S. A., Lundquist, J. K., Doyle, J. D., Golaz, J. C., Holtslag, A. A. M., Randall, D. A., Siebesma, A. P. and Soares, P. M. M.: Parameterization of the atmospheric boundary layer: a view from just above the inversion, Bull. Am. Meteorol. Soc., 89(4), 453–458, doi:10.1175/BAMS-89-4-453, 2008.

Terradellas, E., Morales, G., Cuxart, J. and Yagüe, C.: Wavelet methods: application to the study of the stable atmospheric boundary layer under non-stationary conditions, Dyn. Atmos. Ocean., 34(2-4), 225–244, doi:10.1016/S0377-0265(01)00069-0, 2001.

Tewari, M., Chen, F., Wang, W., Dudhia, J., LeMone, M. A., Mitchell, K., Ek, M., Gayno, G., Wegiel, J. and Cuenca, R. H.: Implementation and verification of the unified NOAH land surface model in the WRF model. In: Proceedings of

the 20th Conference on weather analysis and forecasting/16th Conference on numerical weather prediction, Seattle (WA), USA, paper 14.2a, 2004.

Theeuwes, N. E., Steeneveld, G. J., Ronda, R. J., Heusinkveld, B. G., van Hove, L. W. A. and Holtslag, A. A. M.: Seasonal dependence of the urban heat island on the street canyon aspect ratio, Q. J. R. Meteorol. Soc., 140, 2197–2210, doi: 10.1002/qj.2289, 2014.

Torrence, C. and Compo, G. P.: A practical guide to wavelet analysis, edited by A. Serganov, Bull. Am. Meteorol. Soc., 79(1), 61–78, doi:10.1175/1520-0477(1998)079<0061:APGTWA>2.0.CO;2, 1998.

Udina, M., Soler, M. R., Viana, S. and Yagüe, C.: Model simulation of gravity waves triggered by a density current, Q. J. R. Meteorol. Soc., 139(672), 701–714, doi:10.1002/qj.2004, 2013.

van de Boer, A.: Atmospheric turbulence over crops: confronting theories with observations, PhD thesis, Wageningen University, The Netherlands, 2015.

van de Boer, A., Moene, A. F., Schüttemeyer, D. and Graf, A.: Sensitivity and uncertainty of analytical footprint models according to a combined natural tracer and ensemble approach, Agric. For. Meteorol., 169, 1–11, doi:10.1016/j.agrformet.2012.09.016, 2013.

van den Kroonenberg, A. and Bange, J.: Turbulent flux calculation in the polar stable boundary layer: Multiresolution flux decomposition and wavelet analysis, J. Geophys. Res., 112(D6), D06112, doi:10.1029/2006JD007819, 2007.

van der Velde, I. R., Steeneveld, G. J., Wichers Schreur, B. G. J. and Holtslag, A. A. M.: Modeling and forecasting the onset and duration of severe radiation fog under frost conditions, Mon. Weather Rev., 138(11), 4237–4253, doi:10.1175/2010MWR3427.1, 2010.

Viana, S.: Estudio de los procesos físicos que tienen lugar en la capa límite atmosférica nocturna a partir de campañas experimentales de campo, PhD thesis, Universidad Complutense de Madrid, Spain, 2011.

Viana, S., Yagüe, C. and Maqueda, G.: Propagation and effects of a mesoscale gravity-wave over a weakly-stratified stable boundary layer during SABLES2006 field campaign, Boundary-Layer Meteorol., 133(2), 165–188, doi:10.1007/s10546-009-9420-4, 2009.

Viana, S., Terradellas, E. and Yagüe, C.: Analysis of gravity waves generated at the top of a drainage flow, J. Atmos. Sci., 67(12), 3949–3966, doi:10.1175/2010JAS3508.1, 2010.

Viana, S., Yagüe, C. and Maqueda, G.: Vertical structure of the stable boundary layer detected by RASS-SODAR and in-situ measurements in SABLES 2006 field campaign, Acta Geophys., 60(5), 1261–1286, doi:10.2478/s11600-011-0072-7, 2012.

Vickers, D. and Mahrt, L.: The cospectral gap and turbulent flux calculations, J. Atmos. Ocean. Technol., 20(5), 660–672, doi:10.1175/1520-0426(2003)20<660:TCGATF>2.0.CO;2, 2003.

Vilà-Guerau de Arellano, J., Dosio, A., Vinuesa, J.-F., Holtslag, A. A. M. and Galmarini, S.: The dispersion of chemically reactive species in the atmospheric boundary layer, Meteorol. Atmos. Phys., 87(1-3), doi:10.1007/s00703-003-0059-2, 2004.

Vilà-Guerau de Arellano, J., van Heerwaarden, C. C., van Stratum, B. J. H., and van den Dries, K.: Atmospheric boundary layer: Integrating chemistry and land interactions, Cambridge University Press, New York, 265 pp., 2015.

Vogelezang, D. H. P. and Holtslag, A. A. M.: Evaluation and model impacts of alternative boundary-layer height formulations, Boundary-Layer Meteorol., 81(3-4), 245–269, doi:10.1007/BF02430331, 1996.

Voronovich, V. and Kiely, G.: On the gap in the spectra of surface-layer atmospheric turbulence, Boundary-Layer Meteorol., 122, 67–83, doi:10.1007/s10546-006-9108-y, 2007.

Wang, W., Bruyère, C., Duda, M., Dudhia, J., Gill, D., Lin, H. C., Michalakes, J., Rizvi, S. and Zhang, S.: ARW Version 3 modeling system user's guide, Mesoscale and Microscale Meteorology Division, National Center for Atmospheric Research, http://www2.mmm.ucar.edu/wrf/users/docs/user_guide_V3/ARWUsersGuideV3.pdf, 2015a.

Wang, Y. Q., Zhang, X. Y., Sun, J. Y., Zhang, X. C., Che, H. Z. and Li, Y.: Spatial and temporal variations of the concentrations of PM_{10}, $PM_{2.5}$ and PM_1 in China, Atmos. Chem. Phys. Discuss., 15(11), 15319–15354, doi:10.5194/acpd-15-15319-2015, 2015b.

Warner, T. T., Peterson, R. A. and Treadon, R. E.: A tutorial on lateral boundary conditions as a basic and potentially serious limitation to regional numerical weather prediction, Bull. Am. Meteorol. Soc., 78(11), 2599–2617, doi:10.1175/1520-0477(1997)078<2599:ATOLBC>2.0.CO;2, 1997.

Wilczac, J. M, Oncley, S. P. and Stage, S. A.: Sonic anemometer tilt correction algorithms, Boundary-Layer Meteorol., 99, 127-150, 2001.

Wingo, S. M. and Knupp, K. R.: Multi-platform observations characterizing the afternoon-to-evening transition of the planetary boundary layer in Northern Alabama, USA, Boundary-Layer Meteorol., 155(1), 29–53, doi:10.1007/s10546-014-9988-1, 2015.

Wyngaard, J. C.: Turbulence in the Atmosphere, Cambridge University Press, Cambridge, 393 pp., 2010.

Xie, B., Hunt, J. C. R., Carruthers, D. J., Fung, J. C. H. and Barlow, J. F.: Structure of the planetary boundary layer over Southeast England: Modeling and measurements, J. Geophys. Res. Atmos., 118(14), 7799–7818, doi:10.1002/jgrd.50621, 2013.

Yagüe, C. and Cano, J. L.: Eddy transfer processes in the atmospheric boundary layer, Atmos. Environ., 28(7), 1275–1289, doi:10.1016/1352-2310(94)90274-7, 1994.

Yagüe, C., Viana, S., Maqueda, G., Lazcano, M., Morales, G. and Rees, J. M.: A Study on the nocturnal atmospheric boundary layer: SABLES2006, Física de la Tierra, 19, 37–53, http://revistas.ucm.es/index.php/FITE/article/view/FITE0707110037A/11535, 2007.

Yagüe, C., Sastre, M., Maqueda, G., Viana, S., Ramos, D. and Vindel, J. M.: CIBA2008, an experimental campaign on the atmospheric boundary layer: preliminary nocturnal results, Física de la Tierra, 21, 13–26, http://revistas.ucm.es/index.php/FITE/article/view/FITE0909110013A, 2009.

Zhang, X. Y., Wang, Y. Q., Niu, T., Zhang, X. C., Gong, S. L., Zhang, Y. M. and Sun, J. Y.: Atmospheric aerosol compositions in China: spatial/temporal variability, chemical signature, regional haze distribution and comparisons with global aerosols, Atmos. Chem. Phys., 12(2), 779–799, doi:10.5194/acp-12-779-2012, 2012.

List of publications and conference presentations

Publications (related to this thesis):

- C. Yagüe, **M. Sastre,** G. Maqueda, S. Viana, D. Ramos, J.M. Vindel, G. Morales (2009): CIBA 2008, an experimental campaign on the atmospheric boundary layer: preliminary nocturnal results. *Física de la Tierra,* 21, 13-26. ISSN: 0214-4557. http://revistas.ucm.es/index.php/FITE/article/view/FITE090911001 3A/11392

- **M. Sastre**, C. Yagüe, C. Román-Cascón, G. Maqueda, F. Salamanca, S. Viana (2012): Evening transitions of the atmospheric boundary layer: characterization, case studies and WRF simulations. *Adv. Sci. Res.* 8, 39-44. doi:10.5194/asr-8-39-2012.

- M. Lothon, F. Lohou, D. Pino, F. Couvreux, E.R. Pardyjak, J. Reuder, J. Vilà-Guerau de Arellano, P. Durand, O. Hartogensis, D. Legain, P. Augustin, B. Gioli, D.H. Lenschow, I. Faloona, C. Yagüe, D.C. Alexander, W.M. Angevine, E. Bargain, J. Barrié, E. Bazile, Y. Bezombes, E. Blay-Carreras, A. van de Boer, J.L. Boichard, A. Bourdon, A. Butet, B. Campistron, O. de Coster, J. Cuxart, A. Dabas, C. Darbieu, K. Deboudt, H. Delbarre, S. Derrien, P. Flament, M. Fourmentin, A. Garai, F. Gibert, A. Graf, J. Groebner, F.

Guichard, M.A. Jiménez, M. Jonassen, A. van den Kroonenberg, V. Magliulo, S. Martin, D. Martínez, L. Mastrorillo, A.F. Moene, F. Molinos, E. Moulin, H.P. Pietersen, B. Piguet, E. Pique, C. Román-Cascón, C. Rufin-Soler, F. Saïd, **M. Sastre-Marugán**, Y. Seity, G.J. Steeneveld, P. Toscano, O. Traullé, D. Tzanos, S. Wacker, N. Wildmann, A. Zaldei (2014): The BLLAST field experiment: Boundary-Layer Late Afternoon and Sunset Turbulence. *Atmos. Chem. Phys.*, 14, 10931-10960. doi:10.5194/acp-14-10931-2014

- **M. Sastre**, C. Yagüe, C. Román-Cascón, G. Maqueda (2015): Atmospheric boundary-layer evening transitions: a comparison between two different experimental sites. *Boundary-Lay. Meteorol.* doi:10.1007/s10546-015-0065-1

- **M. Sastre**, G.-J. Steeneveld, C. Yagüe, C. Román-Cascón, G. Maqueda (2015): WRF tests on atmospheric boundary-layer transitions during the BLLAST campaign. *Atmos. Chem. Phys.*, to be submitted.

- **M. Sastre,** C. Yagüe, C. Román-Cascón, G. Maqueda: Observational seasonal study of the atmospheric boundary layer evening transitions. In preparation.

Other publications:

- M.A. Revuelta, **M. Sastre**, A.J. Fernández, L. Martín, R. García, F.J. Gómez-Moreno, B. Artíñano, M. Pujadas and F. Molero (2012): Characterization of the Eyjafjallajökull volcanic plume over the Iberian Peninsula by lidar remote sensing and ground-level data

collection. *Atmos. Environ*, 48, 46-55. doi:10.1016/j.atmosenv.2011.05.033

- C. Román-Cascón, C. Yagüe, **M. Sastre**, G. Maqueda, F. Salamanca, S. Viana (2012): Observations and WRF simulations of fog events at the Spanish Northern Plateau. *Adv. Sci. Res.,* 8, 11-18. doi:10.5194/asr-8-11-2012

- J. Fernández-Gálvez, J.L. Guerrero-Rascado, F. Molero, H. Lyamani, M.A. Revuelta, F. Navas-Guzmán, **M. Sastre**, J.A. Bravo-Aranda, A.J. Fernández, M.J. Granados-Muñoz, F.J. Gómez-Moreno, F.J. Olmo, M. Pujadas, L. Alados-Arboledas (2013): Aerosol size distribution from inversion of solar radiances and measured at ground-level during SPALI10 campaign. *Atmos. Res.*, 127, 130-140. doi:10.1016/j.atmosres.2012.03.015

- C. Román-Cascón, C. Yagüe, L. Mahrt, **M. Sastre**, G.J. Steeneveld, E. Pardyjak, A. van de Boer, O. Hartogensis (2015): Interactions among drainage flows, gravity waves and turbulence: a BLLAST case study. *Atmos. Chem. Phys.*, 15, 9031-9047. doi:10.5194/acp-15-9031-2015

- C. Román-Cascón, C. Yagüe, S. Viana, **M. Sastre**, G. Maqueda, M. Lothon, I. Gómara (2015): Near monochromatic ducted gravity waves associated with a convective system close to the Pyrénées. *Q. J. R. Meteorol. Soc.*, 141, 1320-1332. doi:10.1002/qj.2441

Oral presentations:

- **M. Sastre**, C. Román-Cascón, C. Yagüe, G. Maqueda, S. Viana: Evening transitions from the microbarometers point of view. In: BLLAST Workshop 2012, Florence (Italy), 6-7 February 2012.

- **M. Sastre**, C. Yagüe, C. Román-Cascón, G. Maqueda, S. Viana: Transiciones vespertinas en la capa límite atmosférica durante la campaña BLLAST. In: XXXII Spanish Meteorological Society (AME) Scientific Meeting, Alcobendas (Spain), 28-30 May 2012.

- **M. Sastre**, C. Yagüe, C. Román-Cascón, G. Maqueda, M. Lothon, F. Saïd: Pressure perturbations and multi-scale analysis in the atmospheric boundary layer at the afternoon and evening transition during the BLLAST campaign. In: 20th Symposium on Boundary Layers and Turbulence, Boston (USA), 9-13 July 2012.

- **M. Sastre**, C. Yagüe, C. Román-Cascón, G. Maqueda: Atmospheric Boundary Layer evening transitions: a comparison between two experimental sites (CIBA-Spain and BLLAST-France). In: 12th European Meteorological Society (EMS) Annual Meeting, Łódź (Poland), 10-14 September 2012.

  Award: *Young Scientist Travel Award* (YSTA)

- **M. Sastre**, G.J. Steeneveld, C. Yagüe, C. Román-Cascón, G. Maqueda: Sensitivity of LSM and PBL schemes in WRF simulations of the Atmospheric Boundary Layer during the BLLAST campaign. In: BLLAST Workshop 2013, Bergen (Norway), 14-16 August 2013.

- **M. Sastre**, C. Yagüe, G.J. Steeneveld, C. Román-Cascón, G. Maqueda: Simulaciones de transiciones de la capa límite atmosférica con el modelo WRF: casos de estudio de la campaña BLLAST. In: XXXIII Spanish Meteorological Society (AME) Scientific Meeting, Oviedo (Spain), 7-9 April 2014.

  Award: *Travel grant for young scientists*

- **M. Sastre**, G.J. Steeneveld, C. Yagüe, C. Román-Cascón, G. Maqueda: WRF tests on sensitivity to PBL and LSM schemes during atmospheric transition periods: validation with BLLAST case study. In: European Geosciences Union (EGU) General Assembly 2014, Vienna (Austria), 27 April - 2 May 2014.

- **M. Sastre**, C. Yagüe, C. Román-Cascón, G. Maqueda: Study of the atmospheric boundary layer evening transitions using two different datasets: An observational and numerical approach. In: 21st Symposium on Boundary Layers and Turbulence, Leeds (UK), 9-13 June 2014.

- **M. Sastre**, G.J. Steeneveld, C. Yagüe, C. Román-Cascón, G. Maqueda: Boundary-layer and land-surface schemes in WRF for the evening transition during the BLLAST campaign. In: 14th European Meteorological Society (EMS) Annual Meeting, Prague (Czech Republic), 6-10 October 2014.

- **M. Sastre**, C. Yagüe, C. Román-Cascón, G. Maqueda: A comparison between atmospheric boundary layer evening transitions at two experimental sites. In: BLLAST Workshop 2015, Barcelona (Spain), 2-3 February 2015.

Poster presentations:

- **M. Sastre**, S. Viana, G. Maqueda, C. Yagüe: Study of the evening transition to the nocturnal atmospheric boundary layer: statistical analysis and case studies. In: European Geosciences Union (EGU) General Assembly 2010, Vienna (Austria), 3-7 May 2010.

- **M. Sastre**, F. Salamanca, C. Yagüe, G. Maqueda, C. Román-Cascón, S. Viana: Evening transitions of the atmospheric boundary layer: global characterization and case studies. In: European Meteorological Society (EMS) Annual Meeting 2011, Berlin (Germany), 12-16 September 2011.

- **M. Sastre**, C. Yagüe, C. Román-Cascón, G. Maqueda, S. Viana: Characterization of evening atmospheric boundary layer transitions from a sonic anemometer and an array of microbarometers during the BLLAST field campaign. In: European Geosciences Union (EGU) General Assembly 2012, Vienna (Austria), 22-27 April 2012.

- **M. Sastre**, C. Yagüe, C. Román-Cascón, G. Maqueda, S. Viana: From diurnal to nocturnal boundary layer: the afternoon and evening transition. In: Buys Ballot Research School (BBOS) Autumn Symposium 2012, Nijmegen (The Netherlands), 24-26 October 2012.

- **M. Sastre**, G.J. Steeneveld, C. Yagüe, C. Román-Cascón, G. Maqueda, A. van de Boer: WRF simulations of the atmospheric boundary layer evening transitions during the BLLAST field

campaign. In: European Geosciences Union (EGU) General Assembly 2013, Vienna (Austria), 7-12 April 2013.

- M.A. Jiménez, W.M. Angevine, E. Bazile, F. Couvreux, J. Cuxart, D. Pino, **M. Sastre**: An intercomparison of mesoscale simulations during the Boundary Layer Late Afternoon and Sunset Turbulence (BLLAST) experimental field campaign. In: European Geosciences Union (EGU) General Assembly 2014, Vienna (Austria), 27 April - 2 May 2014.

- **M. Sastre**, G.J. Steeneveld, C. Yagüe, C. Román-Cascón, G. Maqueda: WRF sensitivity to boundary-layer and land-surface schemes during the evening transition: validation with BLLAST case study. In: 21st Symposium on Boundary Layers and Turbulence, Leeds (UK), 9-13 June 2014.

  Award: *Best Student Poster Presentation*

- **M. Sastre**, C. Yagüe, C. Román-Cascón, G. Maqueda, J.A. Arrillaga: The atmospheric boundary layer evening transitions: an observational and numerical study from two different datasets. In: European Geosciences Union (EGU) General Assembly 2015, Vienna (Austria), 12-17 April 2015.